THE OHIO STATE UNIVERSITY

Revolutionizing Turbine Cooling with Micro-Architectures Enabled by Direct Metal Laser Sintering

The Ohio State University
Aerospace Research Center

J.P. Bons, A. Ameri, J. Gregory, R. Lundgreen,
R. Prenter, A. Hossain, L. Agricola

(2 Nov 2016 – NETL UTSR Workshop)

ARC

THE OHIO STATE UNIVERSITY

Research Team

TEAM LEAD
Dr. Jeffrey Bons
Focus: Experimental Fluid Mechanics and Heat Transfer

Co-PI
Dr. Ali Ameri
Focus: Computational Fluid Dynamics and Heat Transfer

Co-PI
Dr. Jim Gregory
Focus: Experimental Fluid Mechanics, Fluidic Oscillator Development

Ryan Lundgreen
Postdoc

Robin Prenter
PhD Candidate

Arif Hossain
PhD Candidate

Lucas Agricola
PhD Candidate

Objectives

- Explore innovative cooling architectures enabled by additive manufacturing techniques for improved cooling performance and reduced coolant waste.
- Leverage DMLS to better distribute coolant through microchannels, as well as to integrate inherently unstable flow devices to enhance internal and external heat transfer.
- Demonstrate these technologies
    1. at large scale and low speed.
    2. at relevant Mach numbers in a high-speed cascade.
    3. finally, at high speed and high temperature.
- Complement experiments with CFD modeling to explore a broader design space and extrapolate to more complex operating conditions.

Direct Metal Laser Sintering

QUOTES FROM 2015 UTSR WORKSHOP at Georgia Tech

"To take advantage of additive manufacturing, you need to start with the design." - Bill Brindley, Pratt & Whitney

"DMLS enables novel designs." - Karl Wygant, Samsung Techwin America

"Challenges become opportunities!" – David Teraji, Solar Turbines

"Additive manufacturing moving from nicety to necessity." – Boeing

"Manufacturing as an enabler rather than as a burden." - Sanjay Sampath, Stony Brook University

"Ability to make macroscale parts with microscale features." Suman Das, Georgia Tech

Cooling Designs Enabled by DMLS

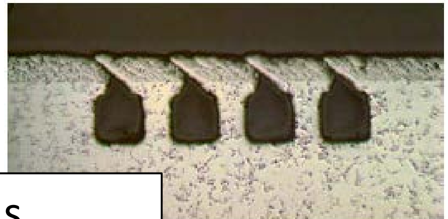

Microchannels provide unparalleled coverage.
Bunker (IGTI 2013)

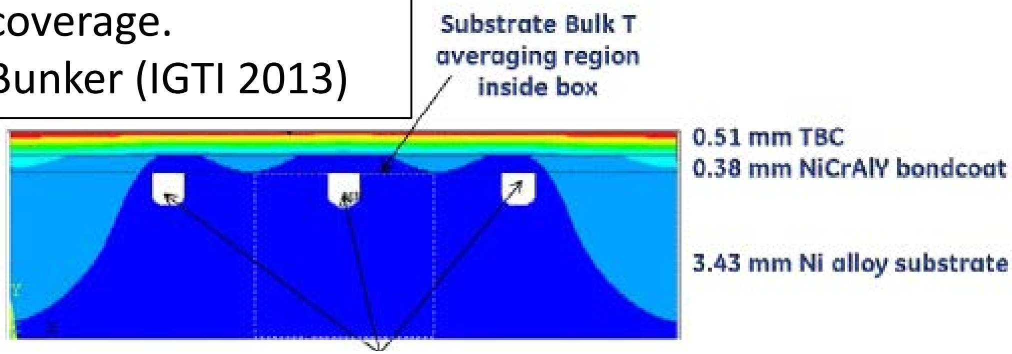

Sweeping Fluidic Oscillators for…
- Film Cooling (Thurman et al. , IGTI2015)
- Unsteady Impingement Jets (Camci & Herr, JHT 1999)

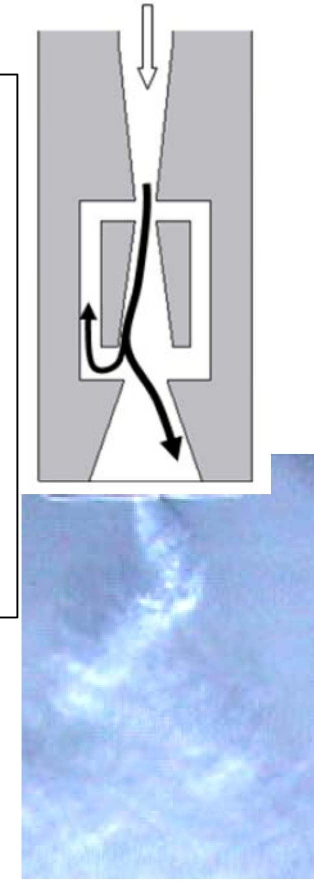

Reverse Film Cooling (Li et al., Energy and Power 2013)

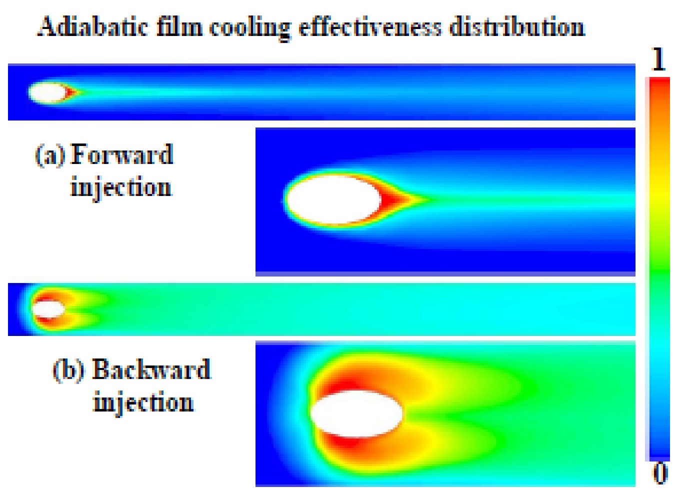

Integration of Promising Designs in NGV

Reverse Cooling on PS:

- Fed by upstream microchannel
- Better surface coverage with lower massflow?

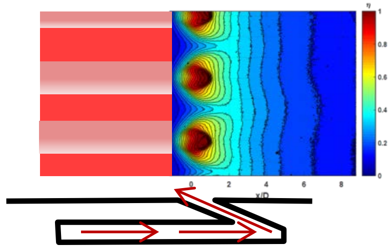

Fluidic Oscillator Impingement Cooling on LE:

- Eliminate showerhead
- Lower massflow required?
- Microchannel exhaust

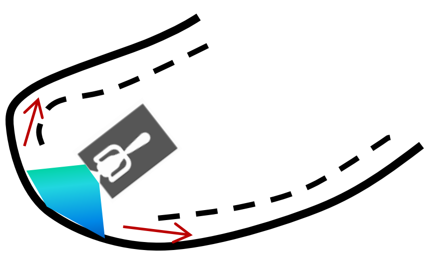

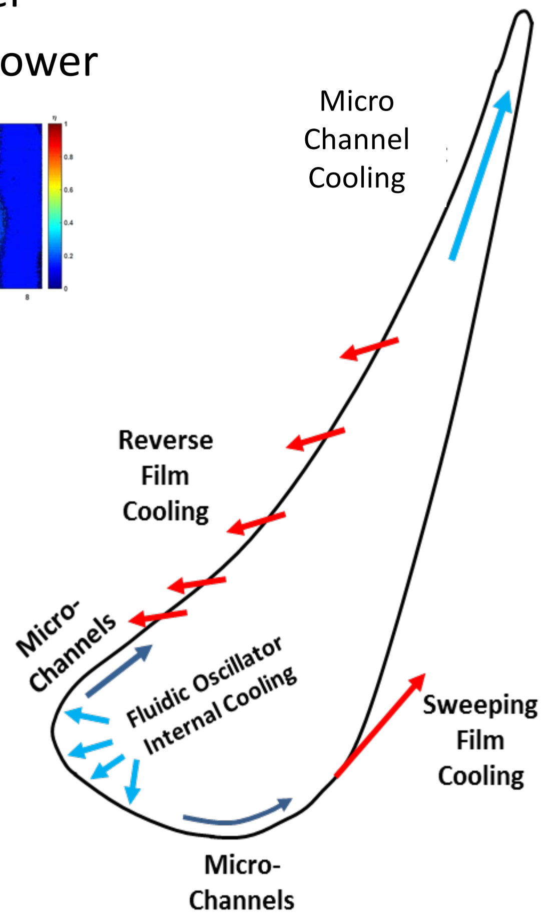

Microchannels in TE:

- Improved coverage with lower massflow required?
- Weight savings with skin cooling?

Sweeping Fluidic Oscillator Film Cooling:

- Improved coverage with lower massflow required?

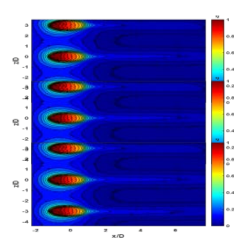

vs.

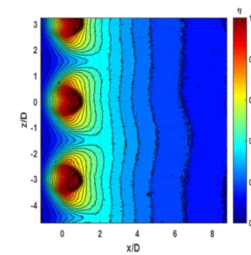

vs.

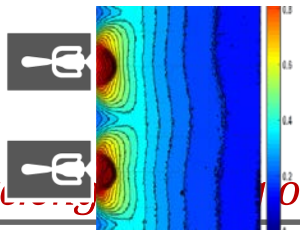

Turbine Heat Transfer Facilities

- For innovative concepts to be viable, must be vetted in facilities that simulate the real operating environment
- Graduated complexity
  - Low speed, large scale
  - High speed, smaller scale
  - High speed, high temp (T_w/T_b), small scale

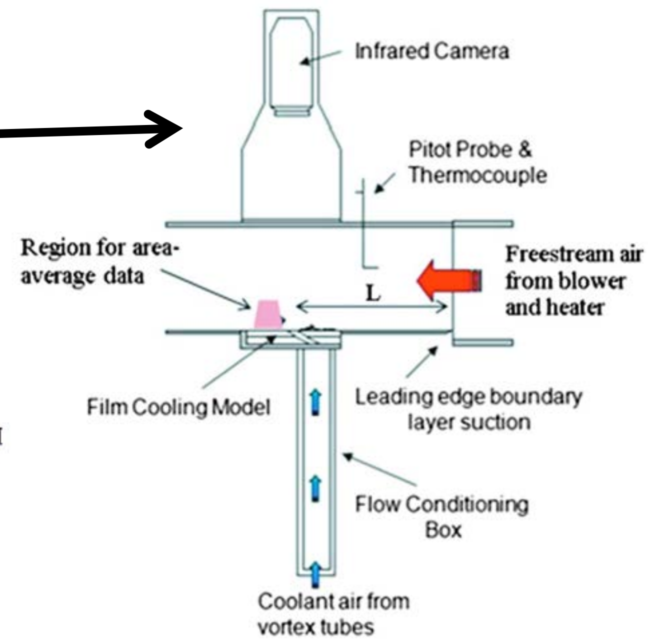

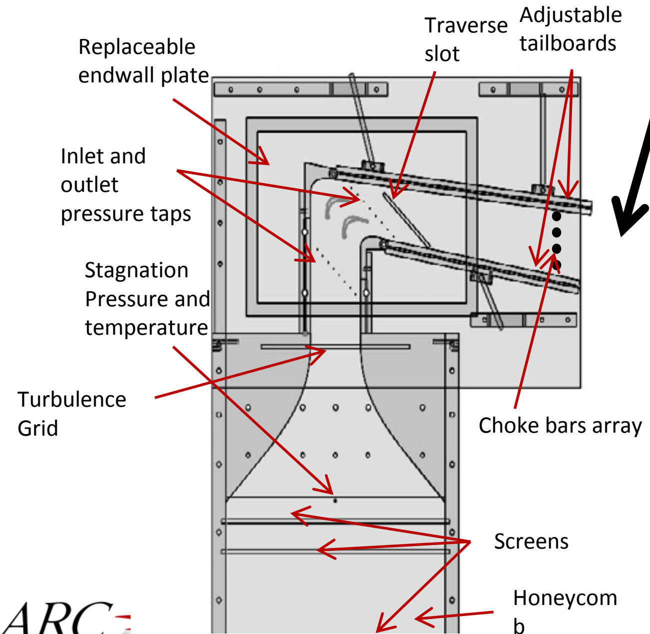

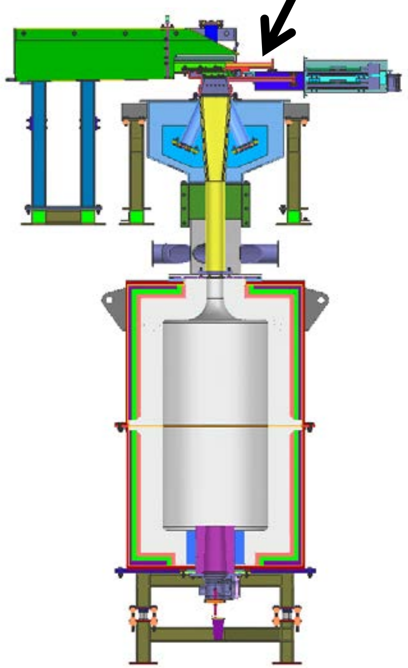

Gantt Chart

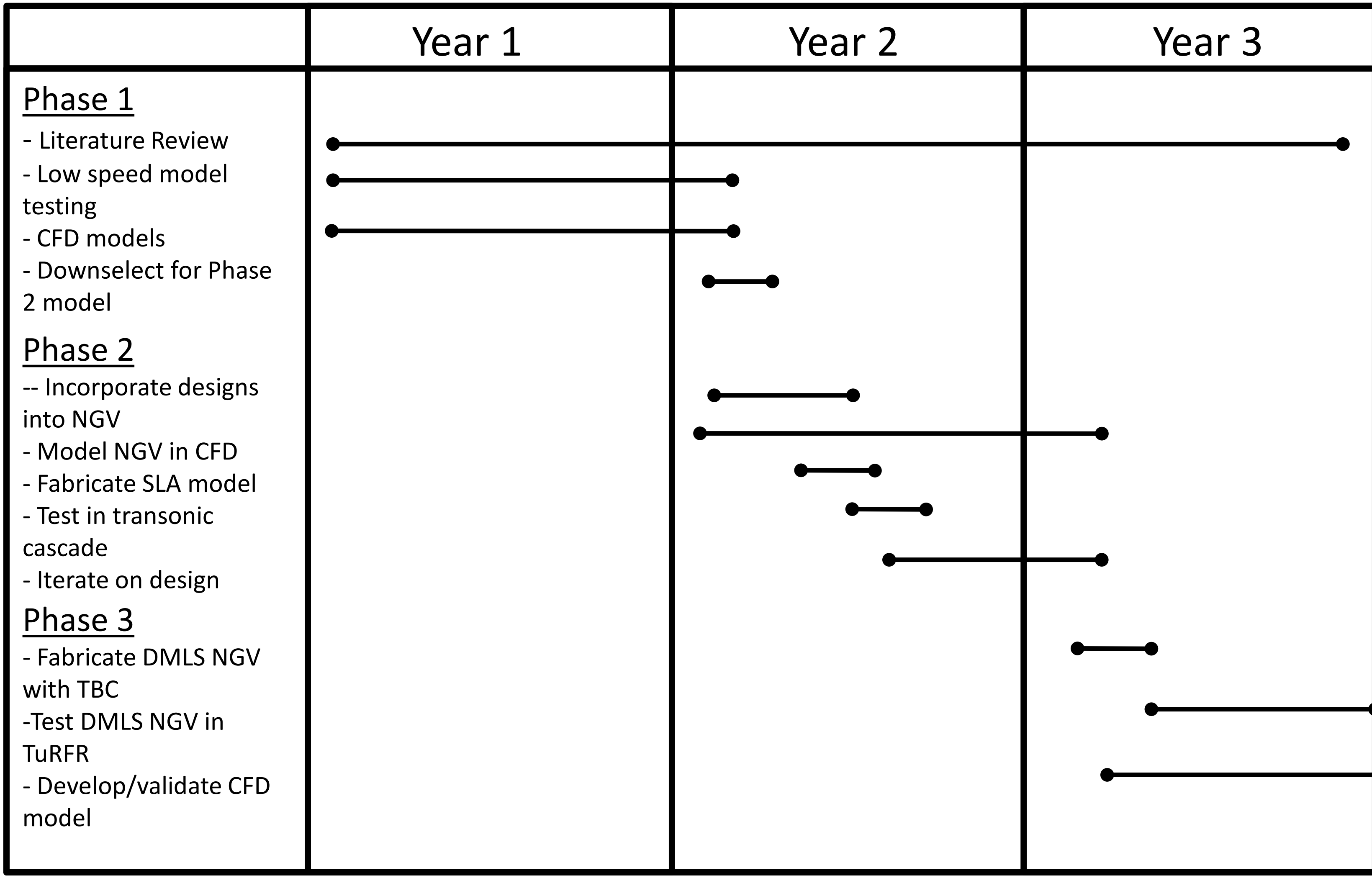
Year 1
Year 2
Year 3
Phase 1
- Literature Review
- Low speed model testing
- CFD models
- Downselect for Phase 2 model
Phase 2
-- Incorporate designs into NGV
- Model NGV in CFD
- Fabricate SLA model
- Test in transonic cascade
- Iterate on design
Phase 3
- Fabricate DMLS NGV with TBC
-Test DMLS NGV in TuRFR
- Develop/validate CFD model

PHASE 1: Concept Exploration

- Use available literature to identify most **promising cooling designs**:
  - Pulsed fluidic oscillators for internal cooling of leading edges
  - Sweeping fluidic oscillators for external film cooling
  - Reverse flow film cooling from microchannel circuits for pressure surface
  - Microcooling circuits replace trailing edge cooling
- **Low-speed wind tunnel testing** with scaled geometry
  - Characterize cooling effectiveness and heat transfer
  - Test variants of geometry to determine optimum
  - Test sensitivity of each design to manufacturing tolerances
- Develop **computational models** of each cooling design
  - Generate flow solutions for each initial geometry
  - Validate solutions with experimental data from initial geometry
  - Explore design space and aid in optimization of geometry for each design
- Determine **most promising and feasible technologies** for Phase 2 based on experimental and computational results

Fluidic Oscillator Characterization

Design Variables:
Aspect Ratio
Surface Roughness

Fluidic Oscillator Characterization

- Jet attached to the main channel wall due to Coanda effect.
- Part of the flow comes back through feedback channel.
- The extra mass feeds the separation bubble that pushes the jet to the other wall.

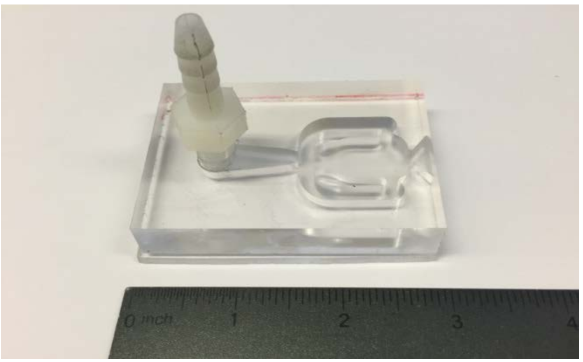

CNC machined part

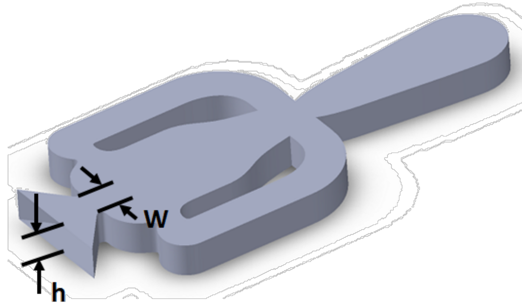

$$Aspect\ ratio\ (AR) = \frac{Throat\ width\ (W)}{Throat\ height\ (h)}$$

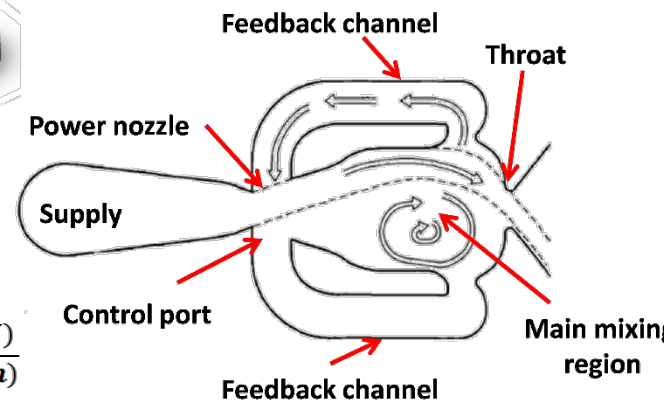

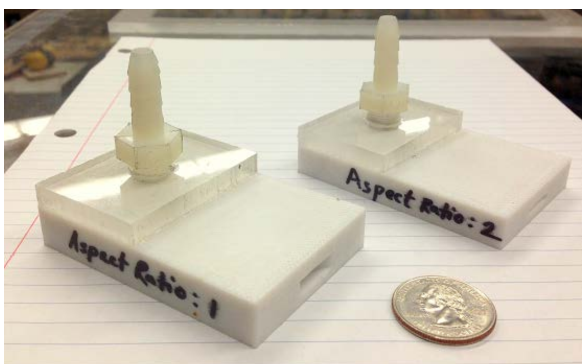

FDM (3D printed part)

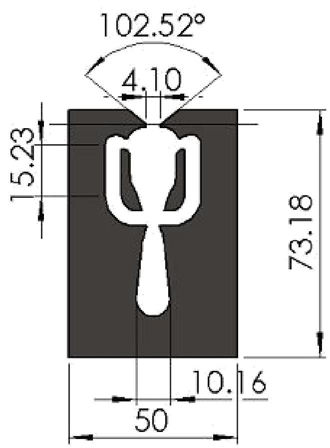

All dimensions are in mm

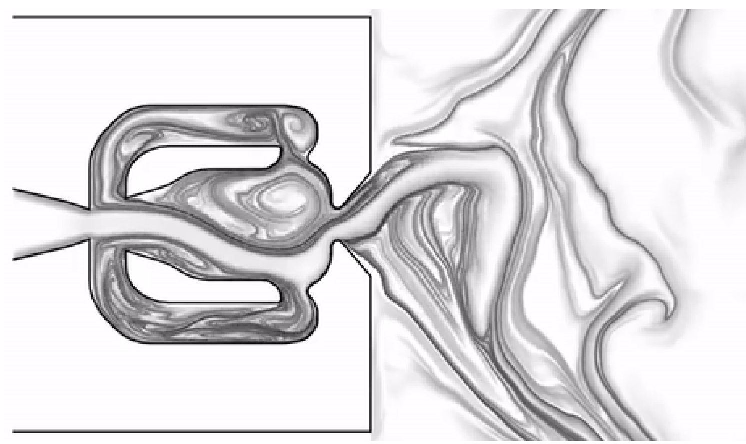

Lagrangian coherent structures in the flow field of a fluidic oscillator, **Ostermann et al (2015)**

Fluidic Oscillator Characterization

- **Schlieren** for unsteady jet motion
- A **microphone** to measure the fluctuating pressure field.
- **Hot wire** to measure spreading angle.

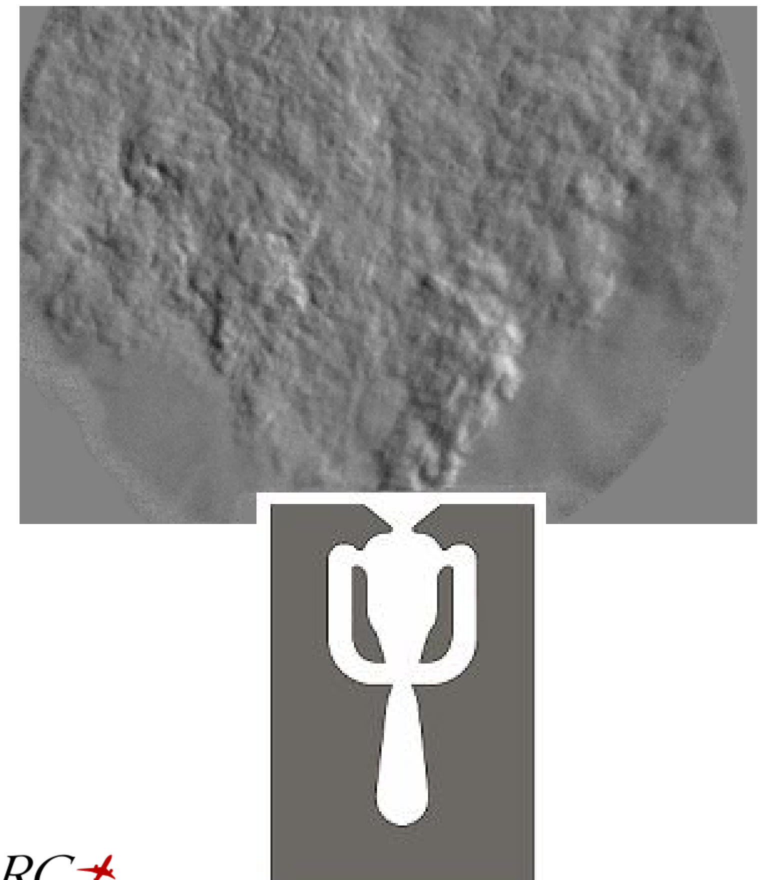

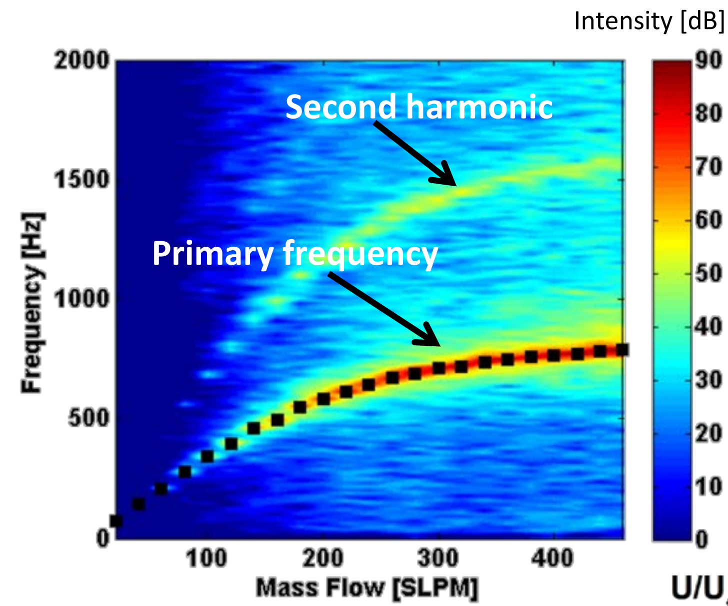

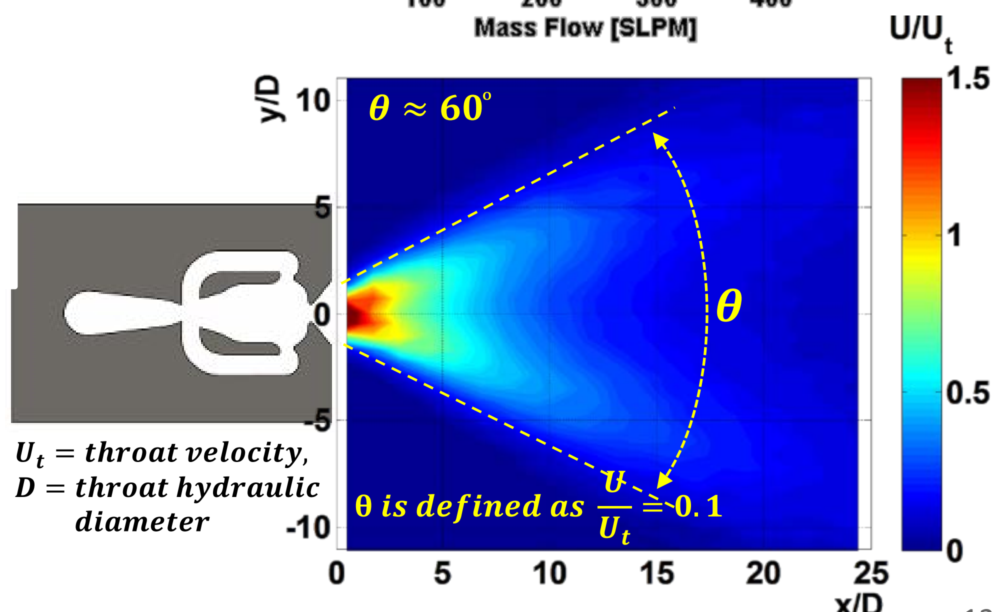

Fluidic Oscillator Frequency Response

- Two different 3D printing technique have been used.
  - Fused deposition modeling (FDM)
  - Polyjet.

- Material : ABS Plus(FDM), ULTEM*9085 (Polyjet)
- Aspect ratio : 0.125,0.25,0.5,1,2

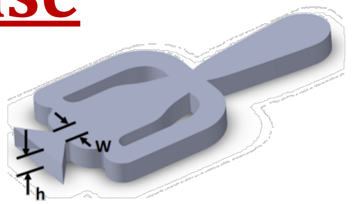

$$Aspect\ ratio\ (AR) = \frac{Throat\ width\ (W)}{Throat\ height\ (h)}$$

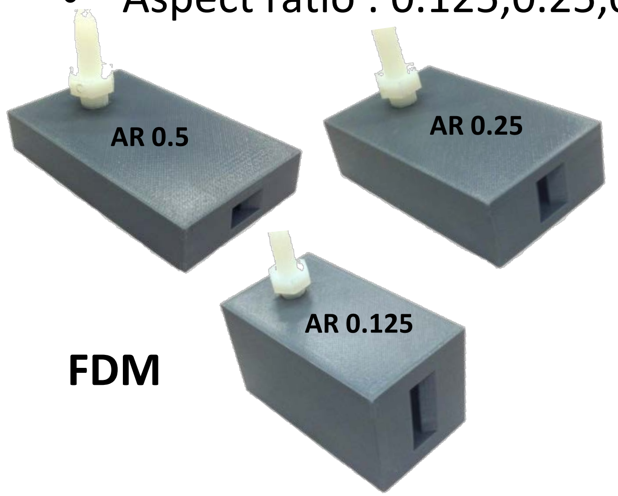

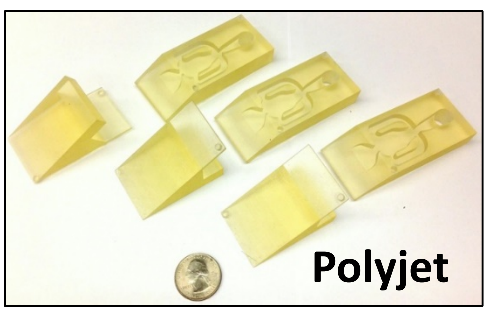

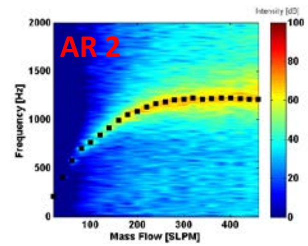

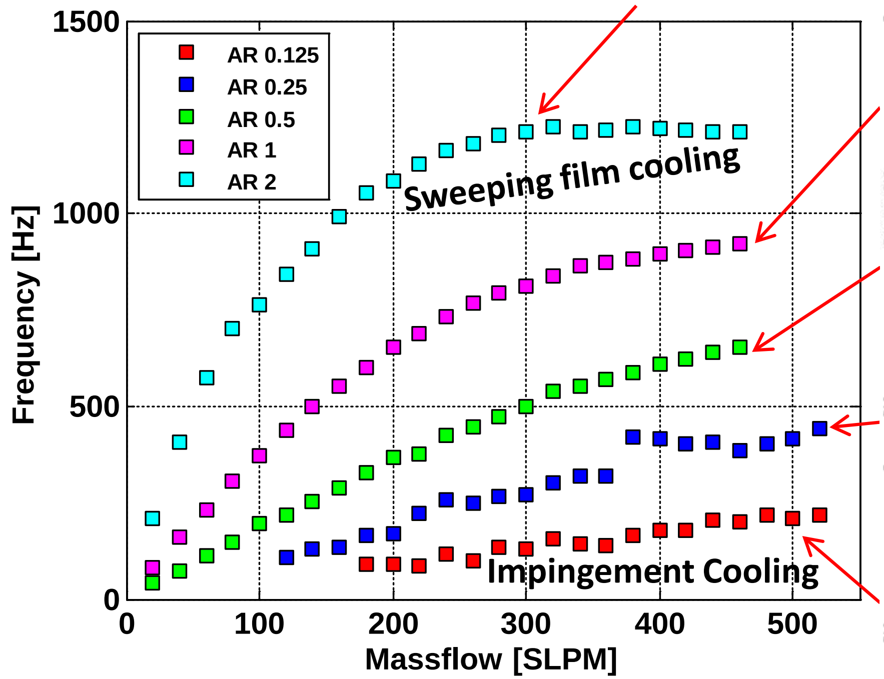

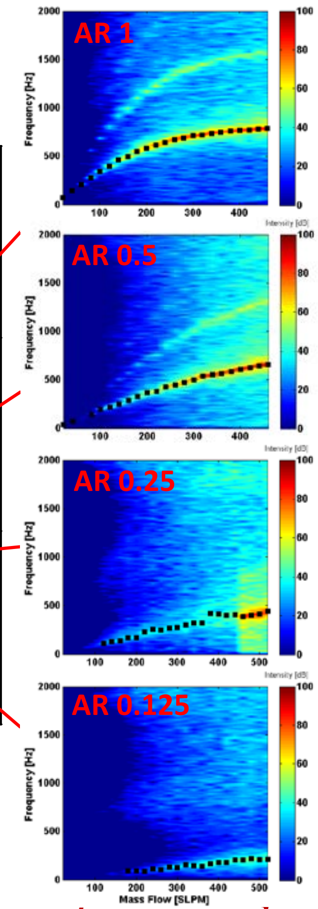

Fluidic Oscillator Frequency Response

- High density ABS.
- Resolution: 0.010”
- Identical build direction.

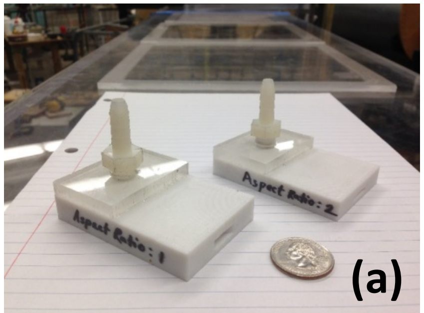

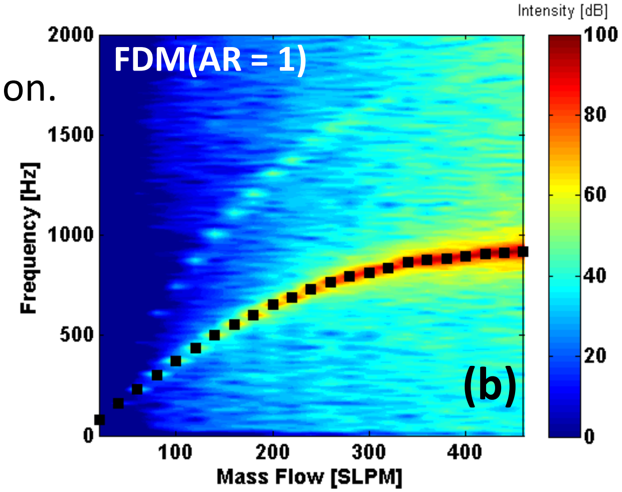

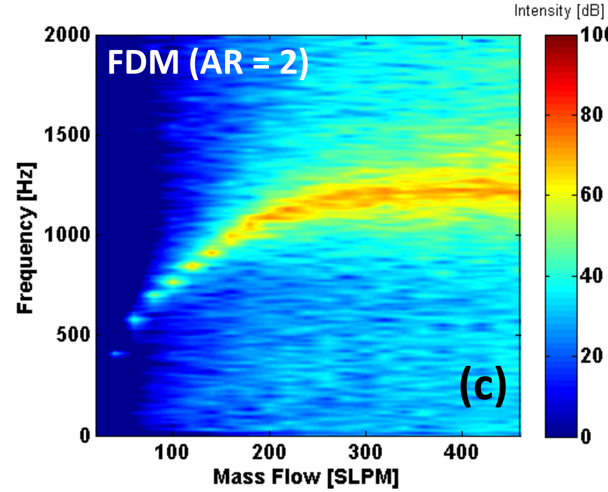

- Low density ABS.
- Resolution: 0.013”
- Different build direction

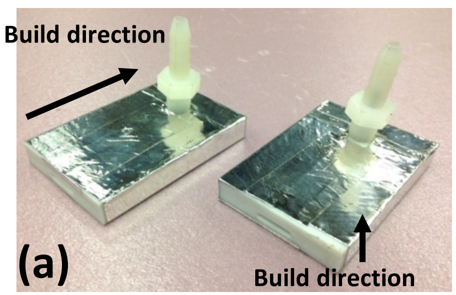

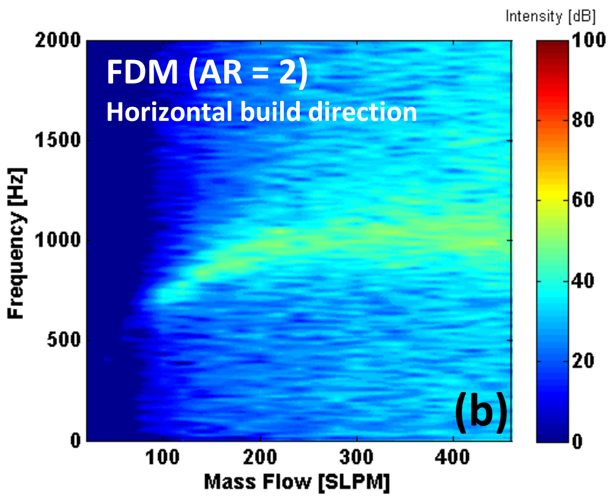

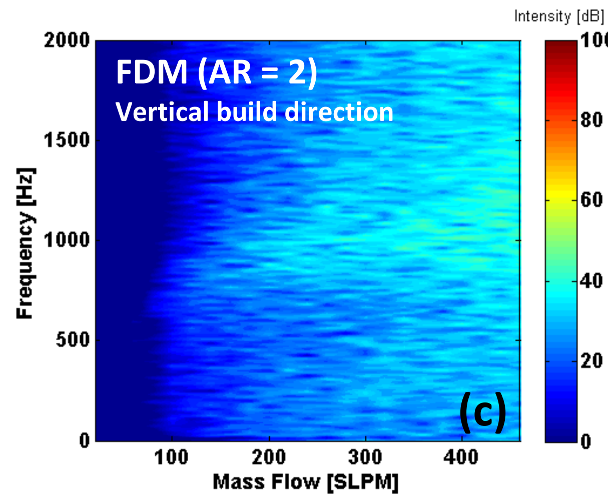

Roughness affects both frequency and spreading of the jet

THE OHIO STATE UNIVERSITY

Effect of Roughness

- Grit 100 sand paper has been characterized by Confocal microscopy.
- Range : -81 to 164 µm

$$Ra = \frac{1}{n}\sum_{i=1}^{n}\left|z_{surf,i} - z_{mean,i}\right| = 25.28\mu m$$

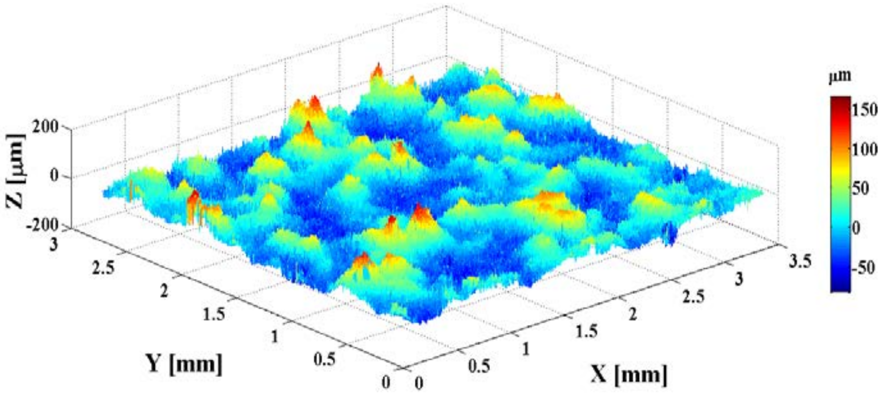

Confocal laser scanning (CLSM) data for a grit 100 sand paper

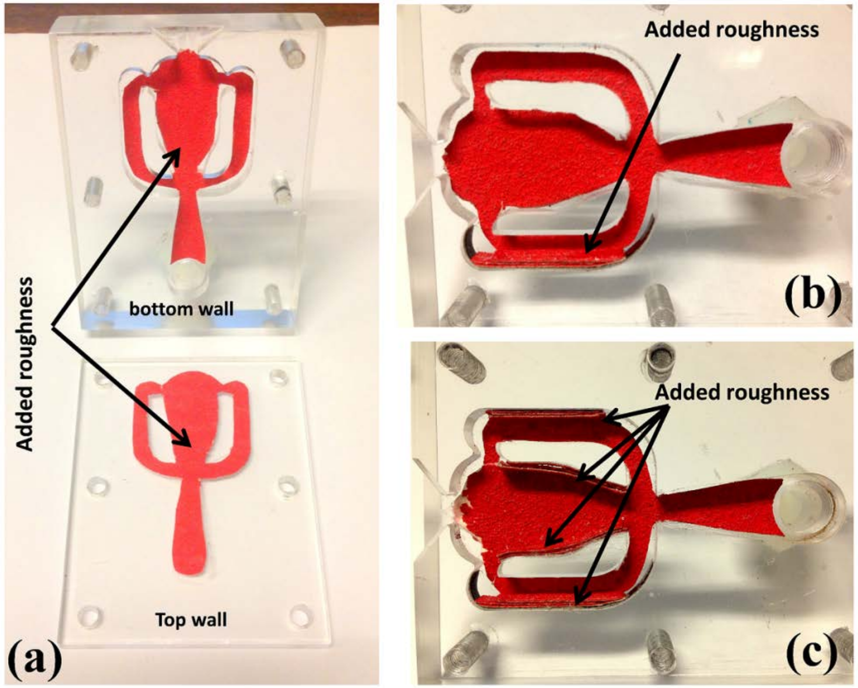

Different test configurations with added roughness

Roughness configurations for different test runs

Test case	Top wall	Bottom wall	Feedback channel	Mixing Channel
Case 1	Rough	Rough		
Case 2	Rough	Rough	Rough	
Case 3	Rough	Rough		Rough
Case 4	Rough	Rough	Rough	Rough

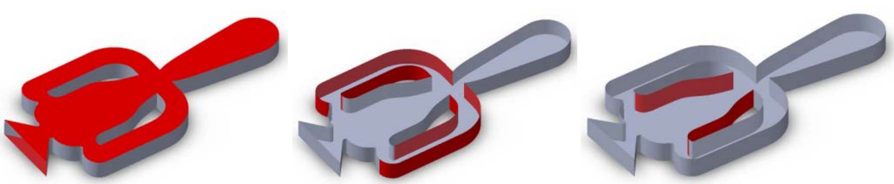

(a) rough top & bottom wall (b) rough feedback channel (c) rough mixing channel

Schematics of different roughness configuration where rough walls are colored in red.

Effect of Roughness (Frequency Response)

- Weak frequency peak was observed for rough case.
- No oscillation was detected at higher mass flow (Case 4).

Test case	Top wall	Bottom wall	Feedback channel	Mixing Channel
Case 1	Rough	Rough		
Case 4	Rough	Rough	Rough	Rough

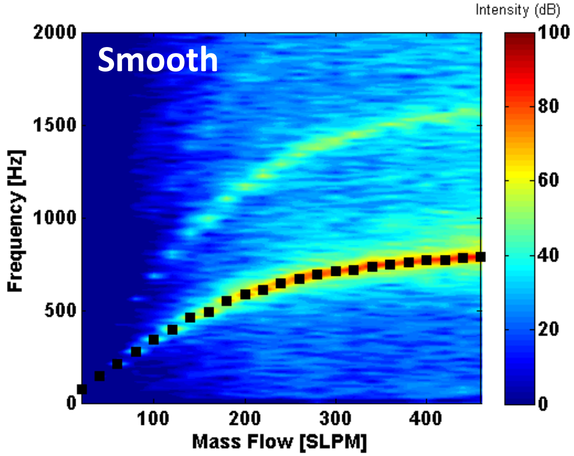

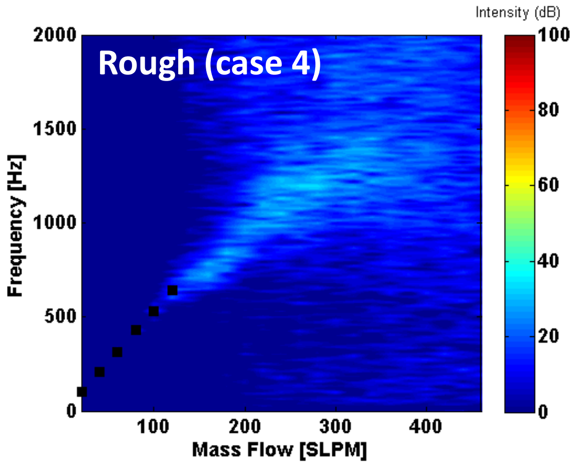

Frequency response of fluidic device (a) Smooth case, (b) rough top-bottom-mixing walls (test case 4)

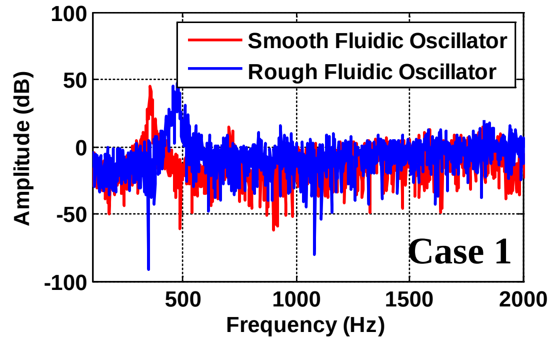

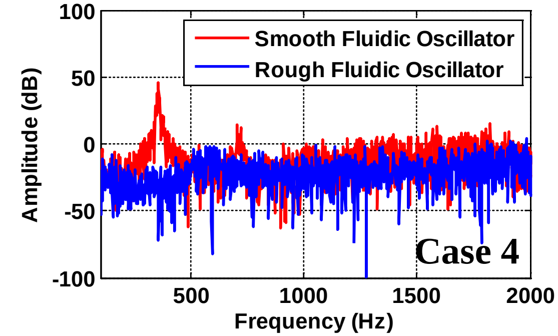

Oscillation frequency of different roughness configurations at $\dot{m} = 100\ SLPM$

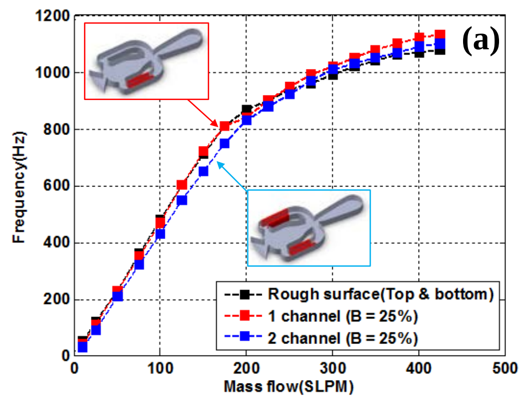

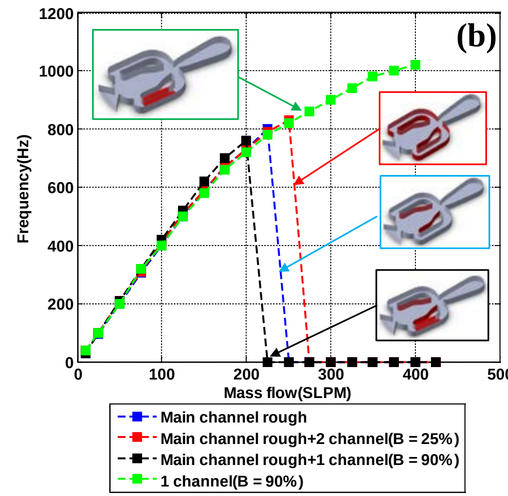

Oscillation frequency at different roughness configurations

Effect of Roughness (Schlieren Imaging)

- Frame rate: 3200 fps.
- Exposure time: 10ms.

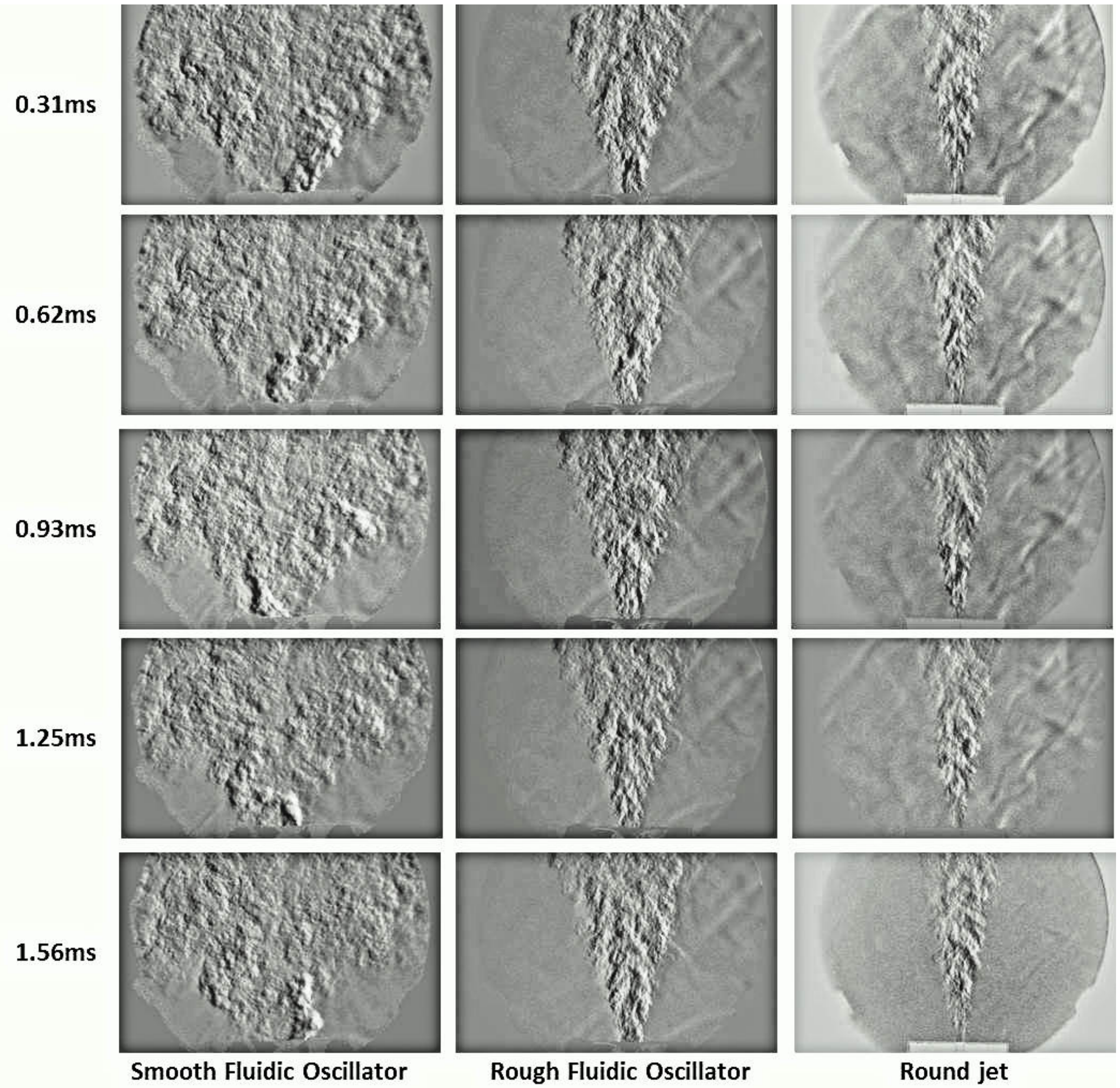

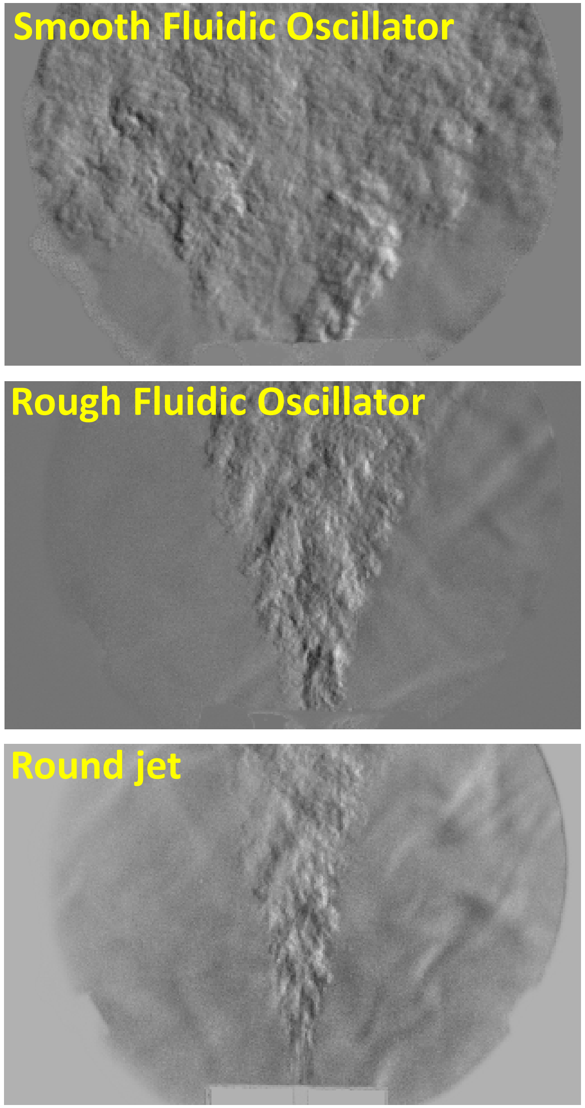

Fluidic Oscillator CFD study (Grid generation)

Boundary conditions

- Mass flow inlet.
- Pressure outlet.

Model description

- URANS k-ω SST model
- 2nd order in time.

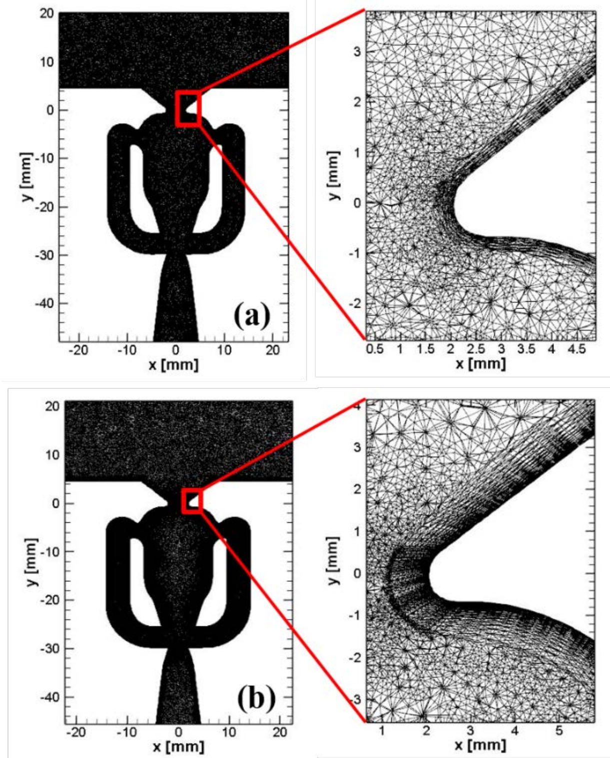

Grid independence study (a) coarse grid with 0.6 million cells, (b) fine grid with 1.3 million cells

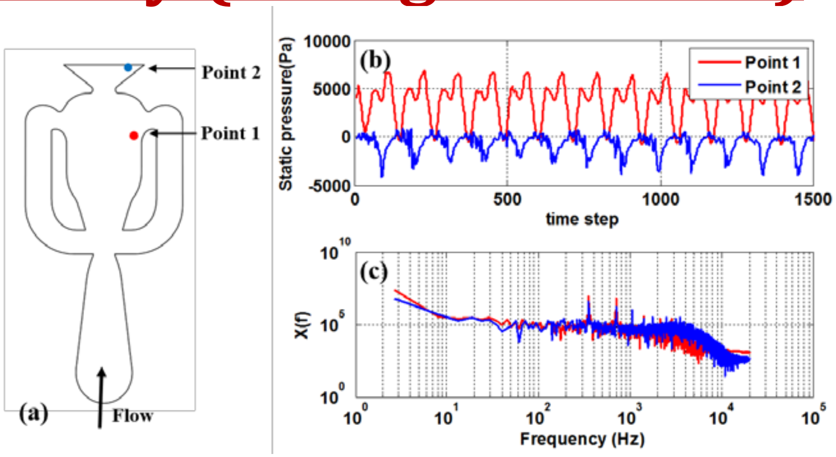

Oscillation frequency calculation from CFD at $\dot{m} = 100\ slpm$, (a) Static pressure monitor locations, (b) Static pressure variation (c) FFT of the static pressure

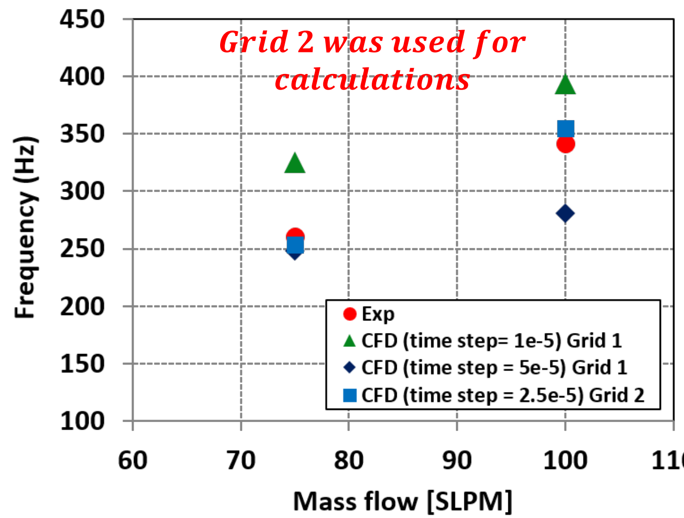

Estimated oscillation frequency for different grids and comparison with experimental data

Fluidic Oscillator CFD study (Model Validation)

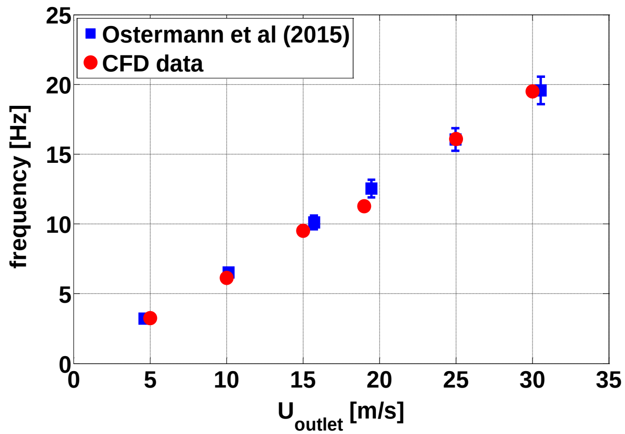

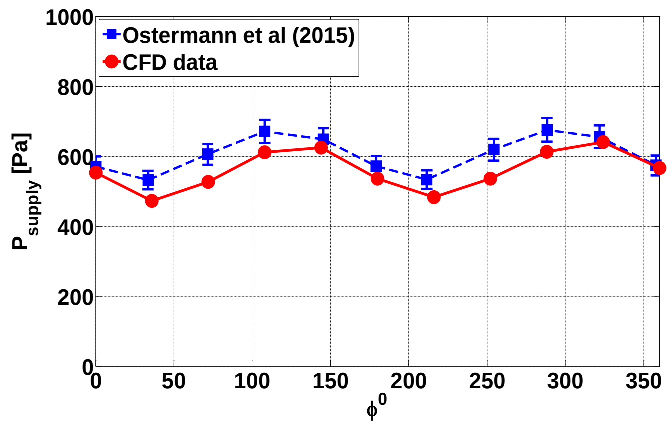

Comparison of oscillating frequency (left) and supply pressure (right) with experimental data

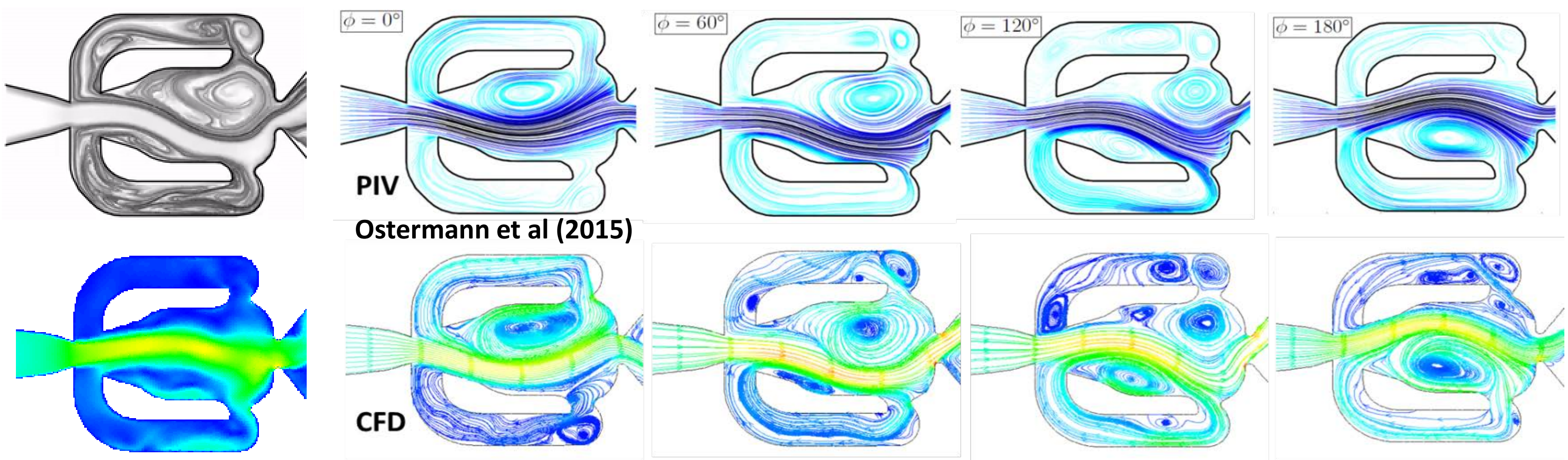

Comparison of streamlines on a bisecting plane from experiment (top) taken from and CFD (bottom), over a half period.

Ref: Ostermann, F., Woszidlo, R., Nayeri. C.N., Paschereit, C.O., "Experimental comparison between the flow field of two common fluidic oscillator designs," 53rd AIAA Aerospace Science Meeting, Jan 2015, AIAA 2015-0781

Fluidic Oscillator Impingement Heat Transfer

Fluidic Oscillator Impingement: Motivation

- Camci (2002) found fluidic oscillators provide a "highly elevated stagnation line Nusselt number", where the impingement zone area coverage is "significantly enhanced"

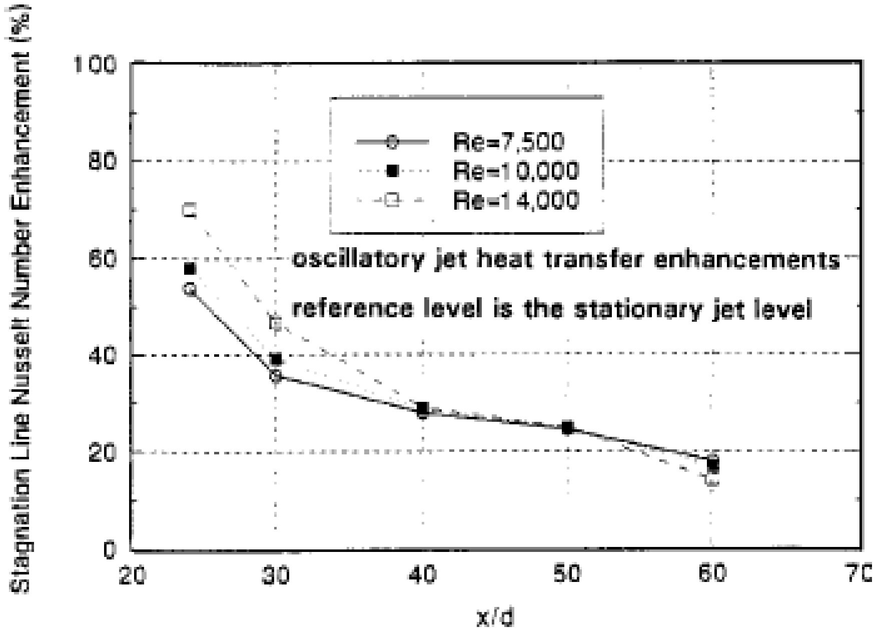

Camci, C., Herr, F., "Forced Convection Heat Transfer Enhancement Using a Self-Oscillating Impinging Planar Jet," *J. Heat Trans.* 2002 Vol. 124, pp. 770-782.

- Fluidic oscillators at lower x/D values could provide a wider, more uniform impingement zone than straight jets in leading edge impingement cooling

Fluidic Oscillator Impingement: IR Thermography Test Setup

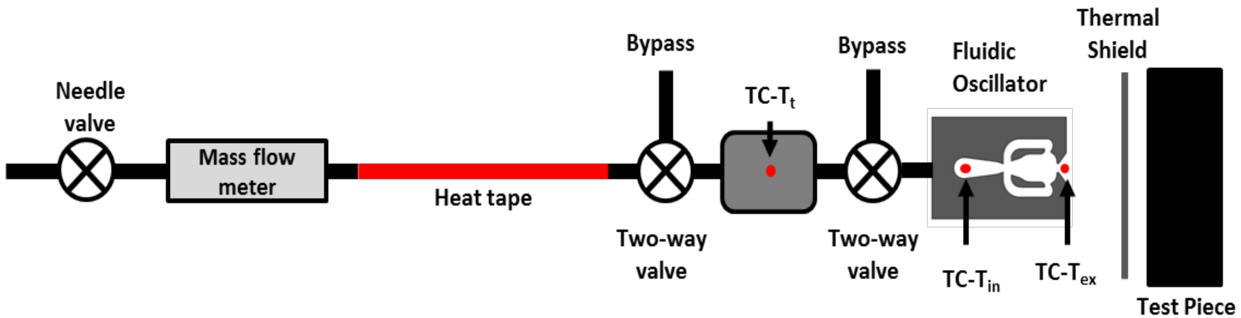

Schematic of Impingement Heat Transfer Test Setup

Transient IR Thermography Test Batch				
Device	z/D	$\dot{m}$ [SLPM]	T_t [°F]	Re_D
Fluidic Osc.	4	70	150	22,600
Round Jet	4	70	150	33,200
Fluidic Osc.	8	70	150	22,600
Round Jet	8	70	150	33,200

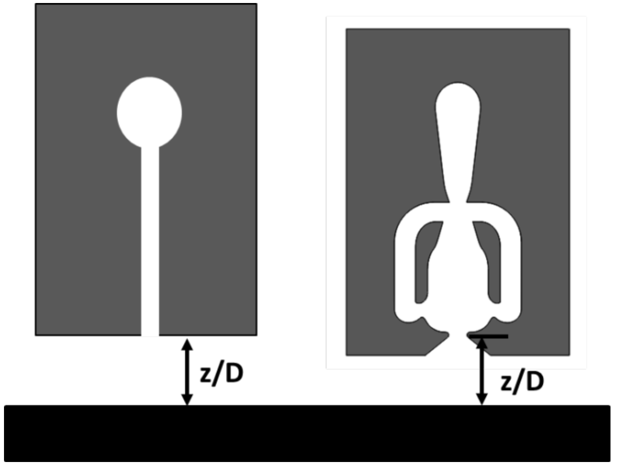

Fluidic Oscillator Impingement: IR Thermography Open Test Analysis

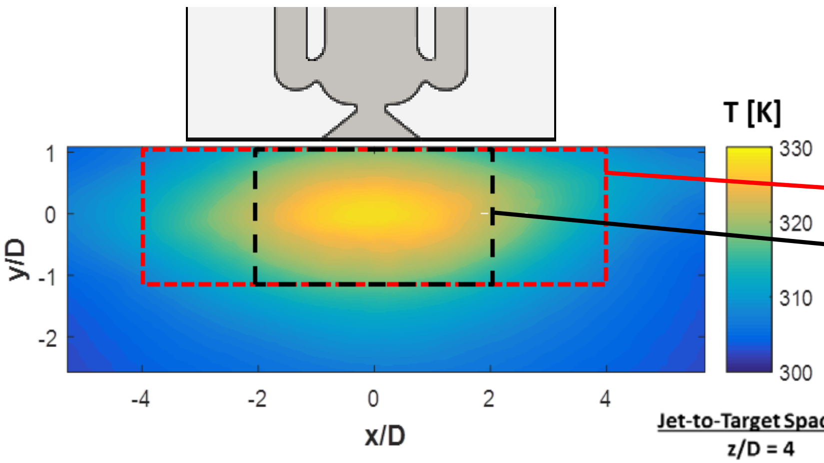

Jet-to-Target Spacing:
z/D = 4

Averaging Area:
X: -2:2D
Y: -1:1D

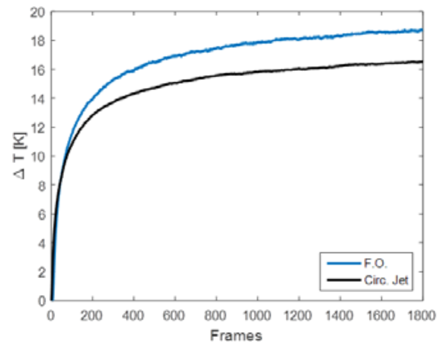

Averaging Area:
X: -4:4D
Y: -1:1D

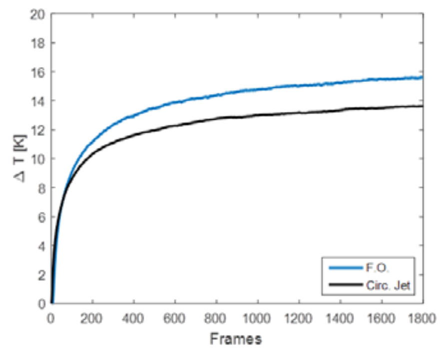

Jet-to-Target Spacing:
z/D = 8

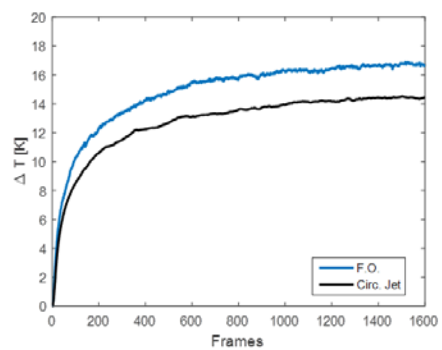

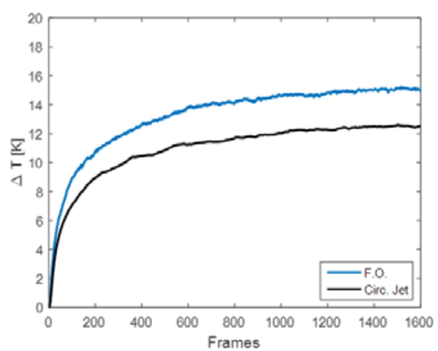

Fluidic Oscillator Impingement: Transient h Analysis

$$\frac{\partial^2 T}{\partial x^2} = \frac{1}{\alpha}\frac{\partial T}{\partial t}$$

1D heat equation

$$\frac{\partial^2 T}{\partial \eta^2} = -2\eta\frac{\partial T}{\partial \eta} \qquad \eta \equiv \frac{x}{(4\alpha t)^{1/2}}$$

Boundary conditions (semi-infinite solid)

$T(x,0) = T_{init}$ and $\lim\limits_{x\to\infty} T(x,t) = T_{init}$

$$\frac{T(x,t) - T_{init}}{T_s - T_{init}} = erf\left(\frac{x}{2\sqrt{\alpha t}}\right)$$

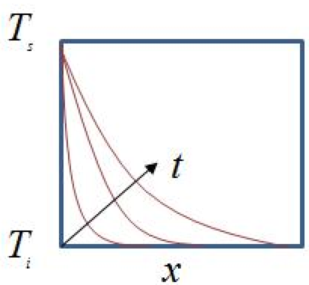

Boundary condition (step change in T_surface)

$$T(0,t) = T_s$$

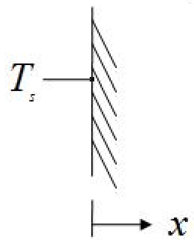

$$q''_{s,cond}(t) = -\kappa\left.\frac{dT}{dx}\right|_{x=0} = \frac{\kappa}{\sqrt{\pi\alpha}}\frac{(T_s - T_{init})}{\sqrt{t}}$$

Duhamel's Superposition

$$q''_{s,cond}(t) = \frac{\kappa}{\sqrt{\pi\alpha}}\sum_{i=1}^{n}\frac{T_s(\tau_i) - T_s(\tau_{i-1})}{\frac{1}{2}\left[\sqrt{t-\tau_i} - \sqrt{t-\tau_{i-1}}\right]}$$

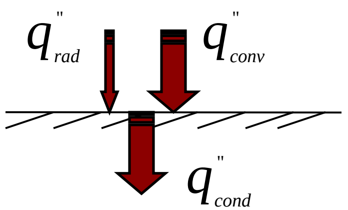

$$q''_{cond} = q''_{rad} + q''_{conv}$$

$$q''_{conv} = h(T_\infty - T_s)$$

$$\boxed{h_n = \frac{1}{T_\infty - T_{s\,n}}\left[\frac{2\kappa}{\sqrt{\pi\alpha}}\sum_{m=1}^{n}\frac{T_{s\,m}(\tau_i) - T_{s\,m-1}(\tau_{i-1})}{\sqrt{t_n - \tau_i} + \sqrt{t_n - \tau_{i-1}}}\right]}$$

Fluidic Oscillator Impingement: IR Thermography Open Test Analysis

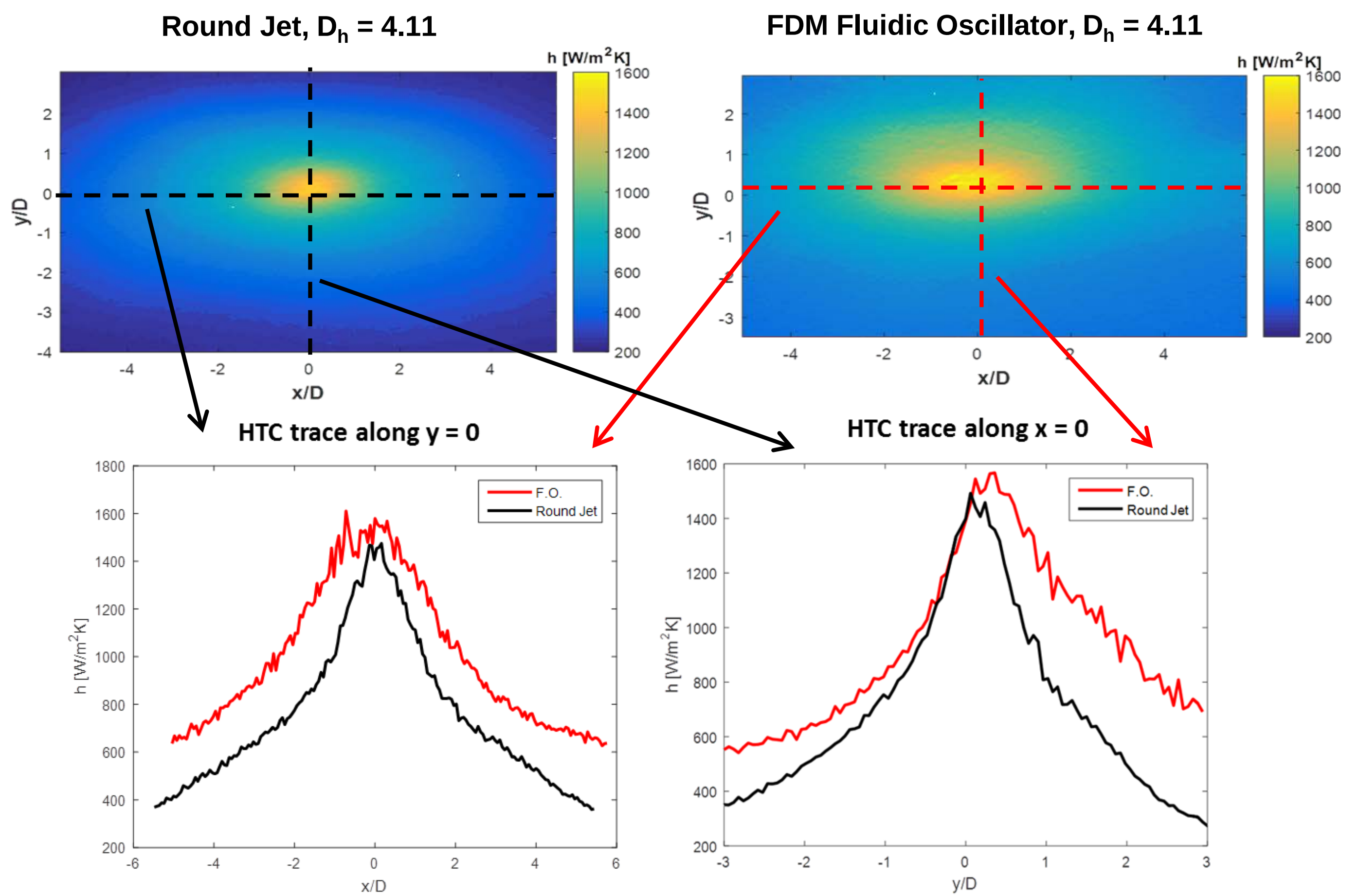

z/D = 8

- Fluidic oscillator achieves a higher, more uniform heat transfer coefficient

Fluidic Oscillator Impingement: IR Thermography Thermal Enclosure Test Setup

Engine Conditions:
Cold Jet, Cold Entrainment

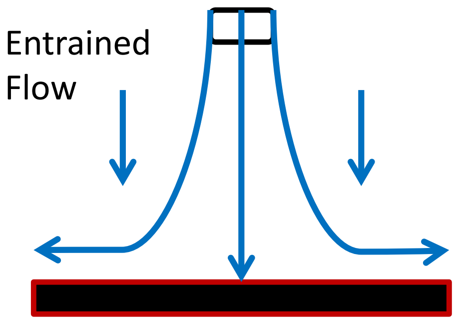

Open Test Conditions:
Hot Jet, Cold Entrainment

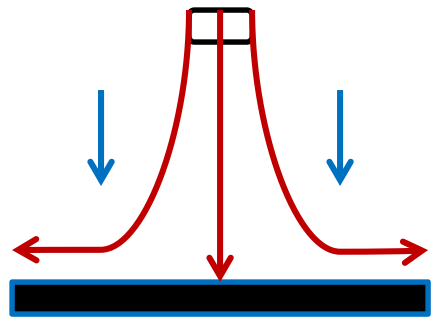

Thermal Enclosure Test Conditions:
Hot Jet, Hot Entrainment

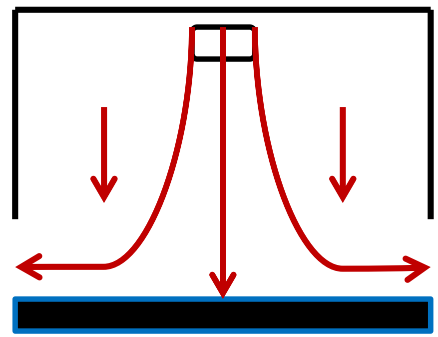

Fluidic Oscillator Test Batch		
AR	D_h (mm)	Manufacturing Technique
0.5	4.11	CNC
1	4.11	CNC, FDM
2	4.11	CNC
1	2.06	CNC, DMLS
1	1.37	DMLS

Thermal Enclosure Test Setup

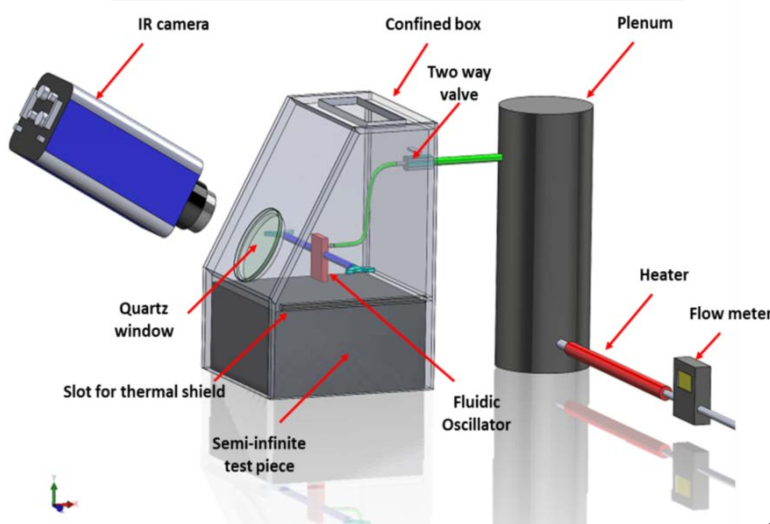

Fluidic Oscillator Impingement: IR Thermography Thermal Enclosure Test

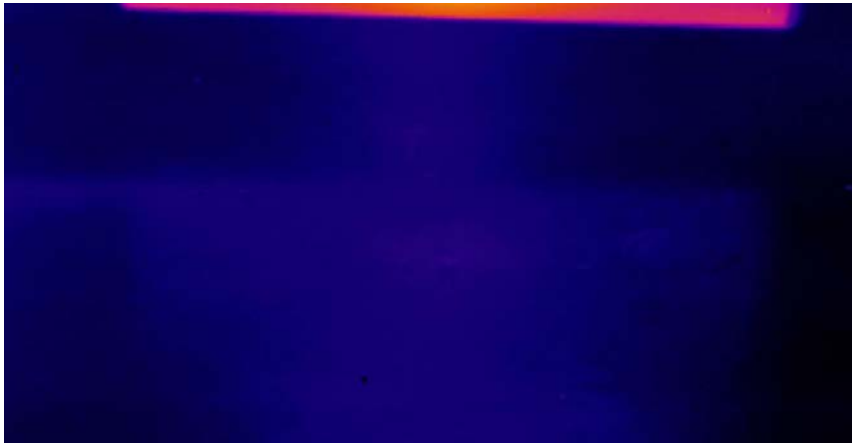

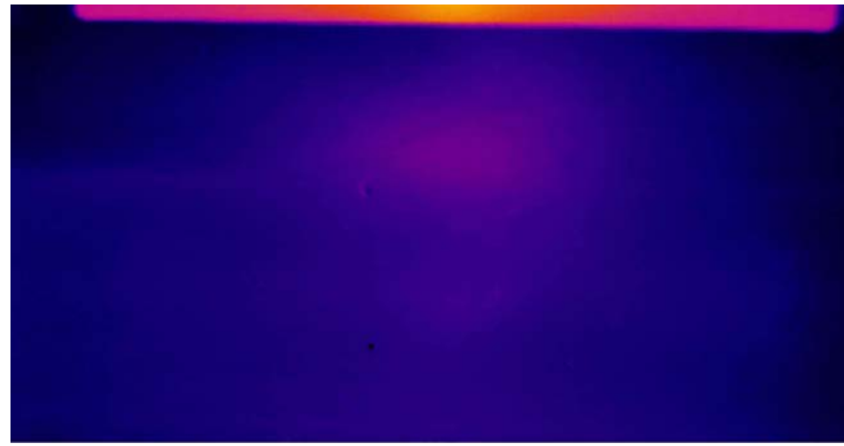

CNC Fluidic Oscillator, AR = 1, d_h = 4.11 mm

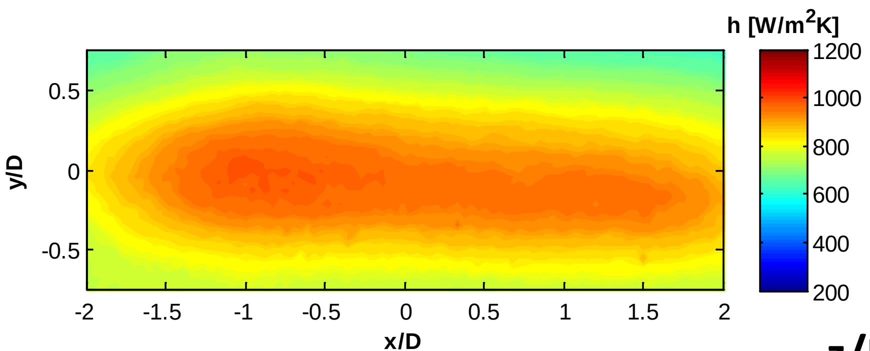

FDM Fluidic Oscillator, AR = 1, d_h = 4.11 mm

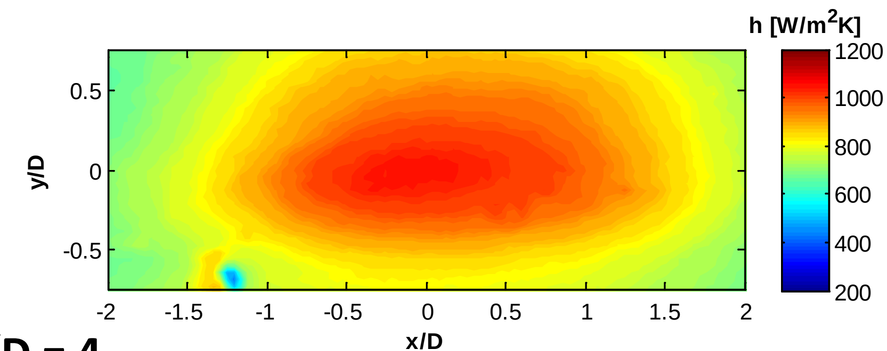

z/D = 4

- Smooth CNC part has greater spreading angle than “rough” FDM part
- Asymmetry in fluidic oscillator flow field is commonly observed

Fluidic Oscillator Impingement: Heat Flux Gauge *h* Analysis

- Transient heat transfer calculations are more commonly used for steady systems
- Heat flux gauges
  - Validate the transient method
  - Resolve oscillations with high frequency response

- New test plate accommodates IR and HFGs
- HFGs provide q, T_s
- T_∞ taken from plenum or box quiescent air

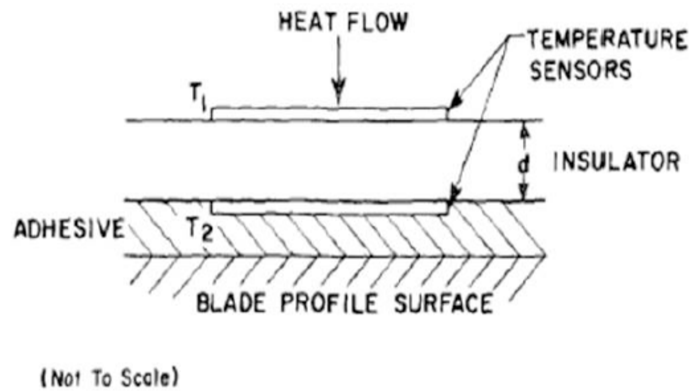

$$q''_{conv} = h(T_\infty - T_s)$$

Epstein, A.H., Guenette, G.R., Norton, R.J.G., and Yuzhang, C., 1985, "High Frequency Response Heat-Flux Gauge," Review of Scientific Instruments, 75(4): pp. 639-649.

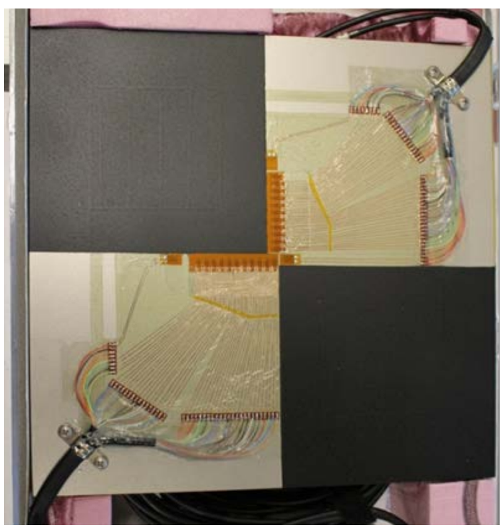

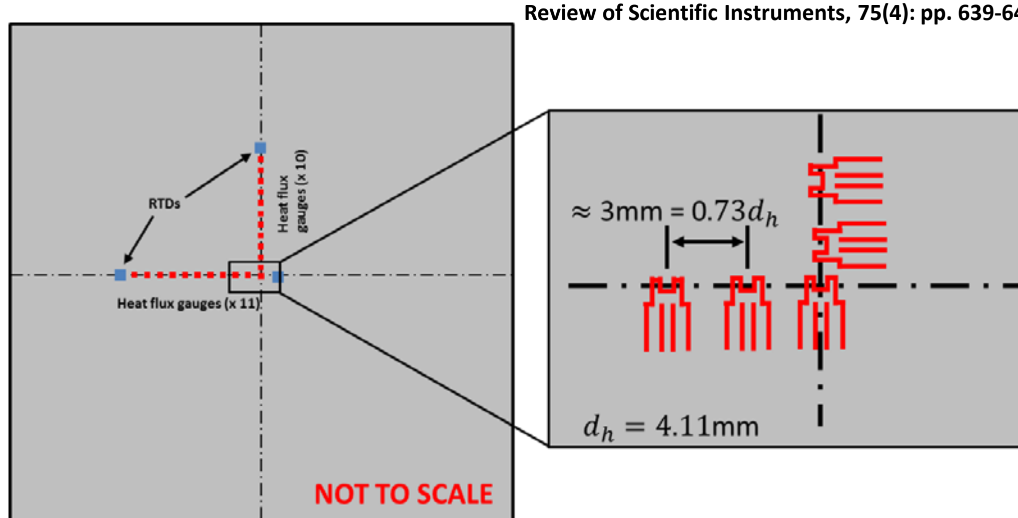

Fluidic Oscillator Impingement: CFD Summary

- Jet impingement heat transfer – Fluidic Oscillator vs. Steady Round Jet
  - Three z/D positions: 4, 6, and 8
  - Five mass flow rates: 10, 25, 50, 75, and 100 SLPM

Fluidic Oscillator

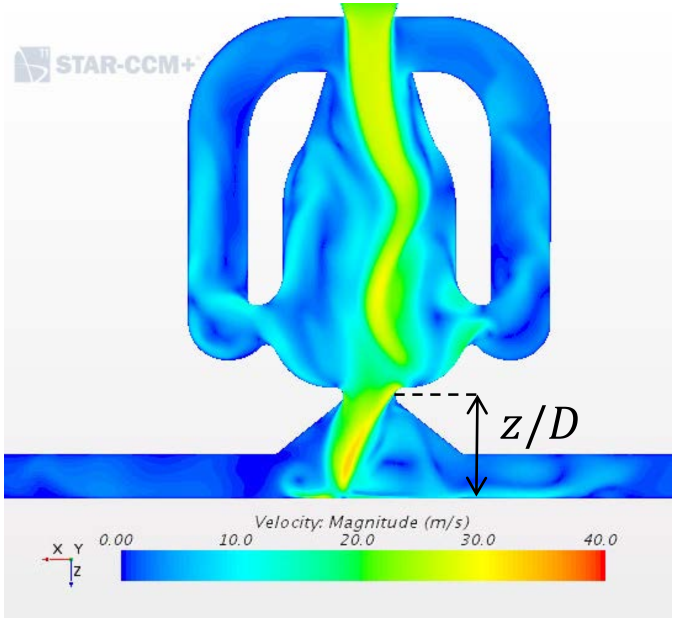

Steady Circular Jet

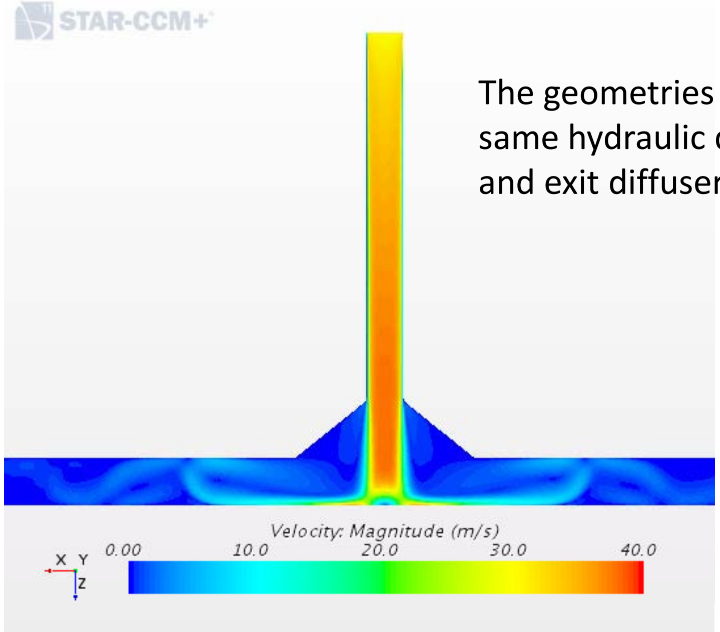

The geometries have the same hydraulic diameter and exit diffuser geometry.

Fluidic Oscillator Impingement: CFD Domain

- Mesh size: 2-8 million polyhedral cells
- Boundary conditions:
  - Mass flow inlet
  - Pressure outlet
  - Constant temperature impingement plate
  - Symmetry boundary at the center of the oscillator
  - Other walls are adiabatic
- Turbulence modeled with the $v^2 f$ model
- Second order in time and space URANS with nominal $2\mu s$ time steps

Aspect ratio = 2

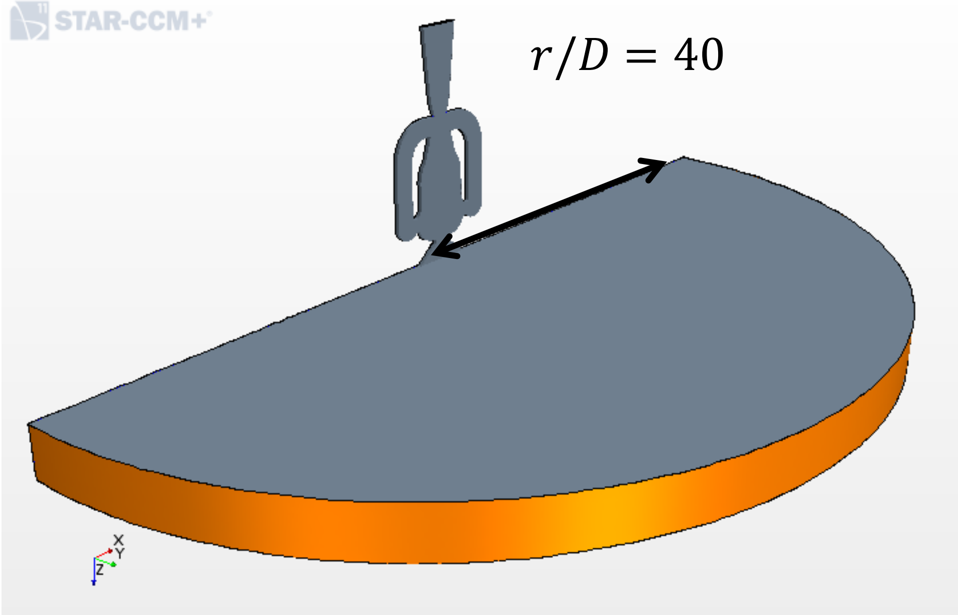

Fluidic Oscillator Impingement: CFD Validation

- The steady jet average Nu up to $r/D = 6$ matches within 10% of the Nu correlation at all flow rates.
- Grid independence was measured by looking at meshes ranging from 2 million to 16 million cells. An intermediate grid (m2) was determined sufficient for this study.
- The v^2f turbulence model was selected in order to best model the impingement heat transfer, though some accuracy of the fluidic oscillator fluid mechanics was sacrificed.

$$Nu = \frac{q''D}{k(T_{ref} - T_{wall})}$$

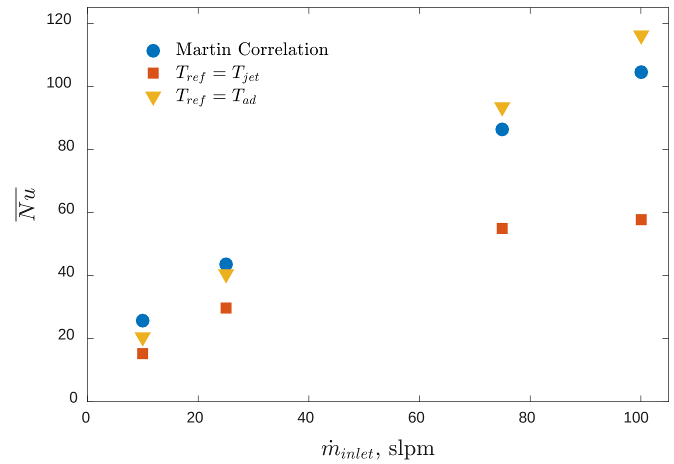

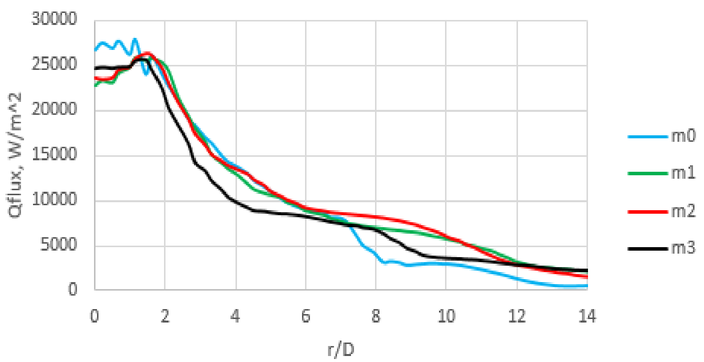

m0: 2 million cells **m2: 9 million cells**
m1: 9 million cells **m3: 16 million cells**

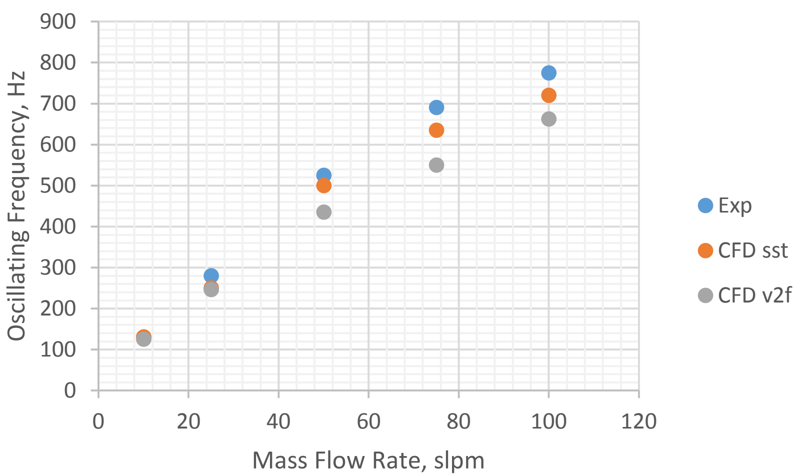

Fluidic Oscillator Impingement: CFD Results @ $z/D = 4$

- Even though the mass flow rate and the hydraulic diameters were matched, the jet Re is significantly different between the two geometries.

The throat of an oscillator with an aspect ratio of 2 and a round hole with matching D_h

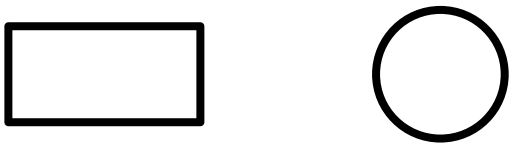

If hydraulic diameters are matched, the round hole will have 30% less area than the rectangular F.O. throat for $AR = 2$.

$$\dot{m} = \rho V A \qquad Re_{D_h} = \frac{\rho V D_h}{\mu}$$

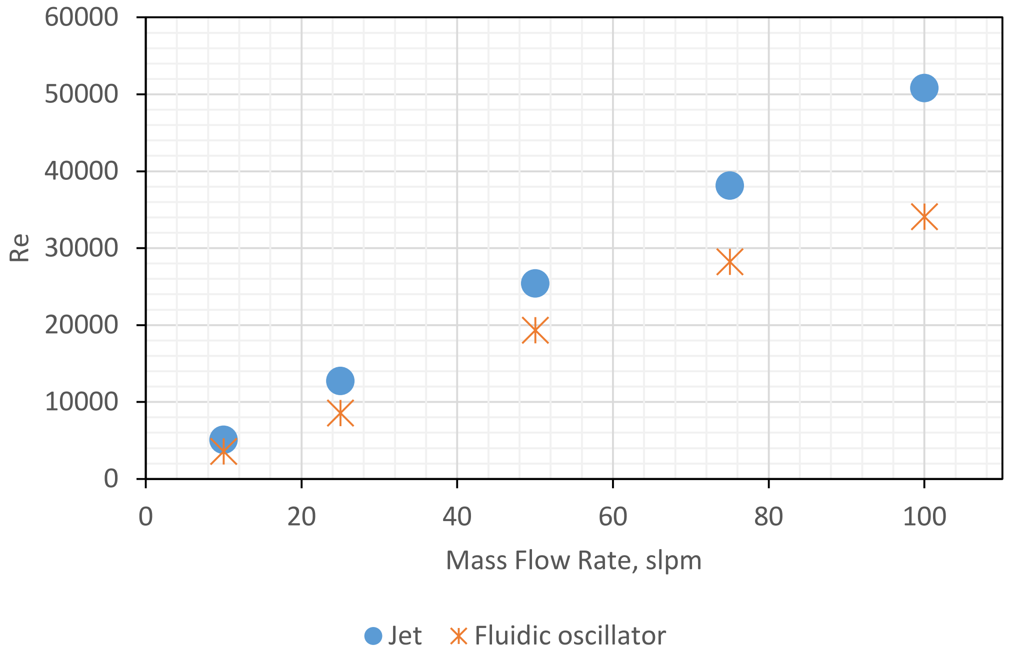

Fluidic Oscillator Impingement: CFD Results @ $z/D = 4$

*Steady = Steady round jet

- In the stagnation region, the Nu for the fluidic oscillator is nominally 50% below the steady jet
- Nu peaks near $r/D = 2$ for the oscillator and then drops more gradually than the steady jet

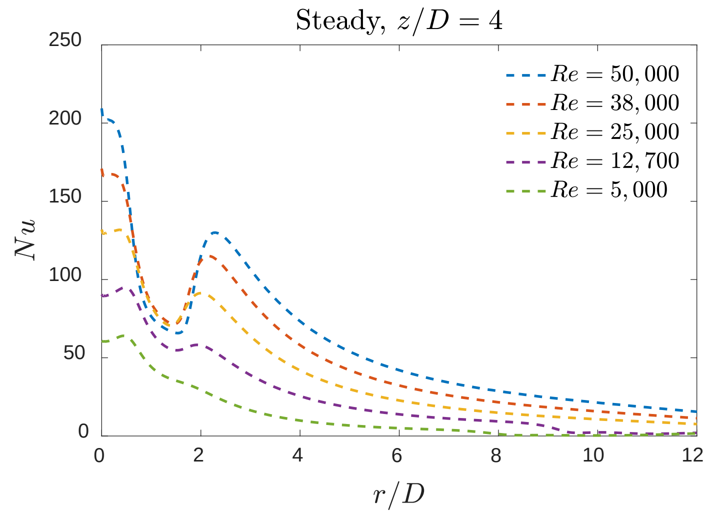

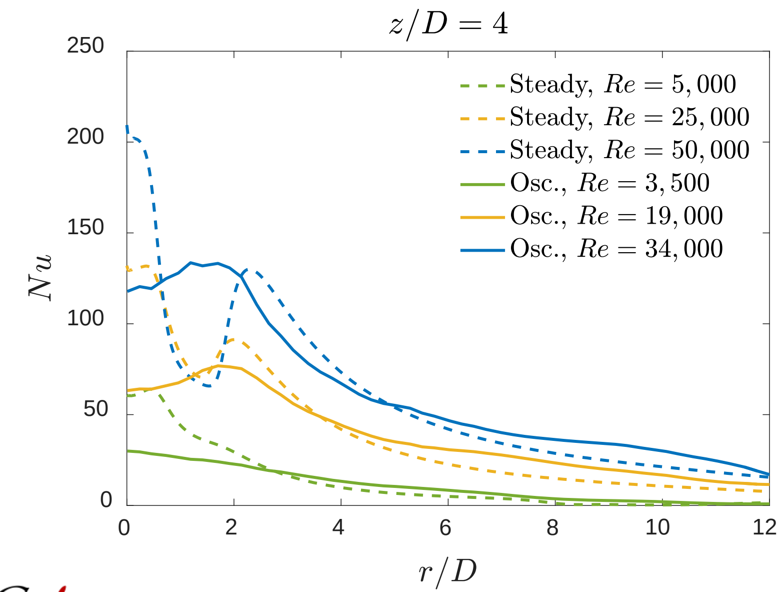

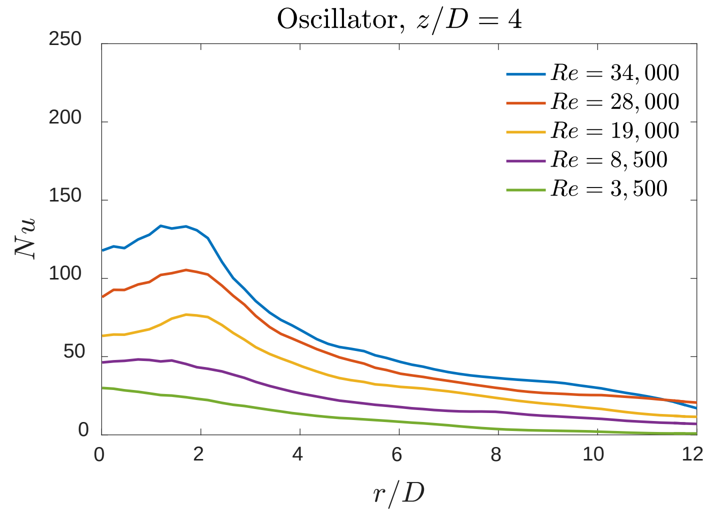

Fluidic Oscillator Impingement: CFD Results @ $z/D = 4$

- Dividing Nu by $Re^{0.72}$ collapses the data sets for r/D >2.
- The fluidic oscillator Nu is higher than the round jet by **30%** at r/D=3 and **70%** at r/D=6, which creates a more uniform Nu over a larger r/D

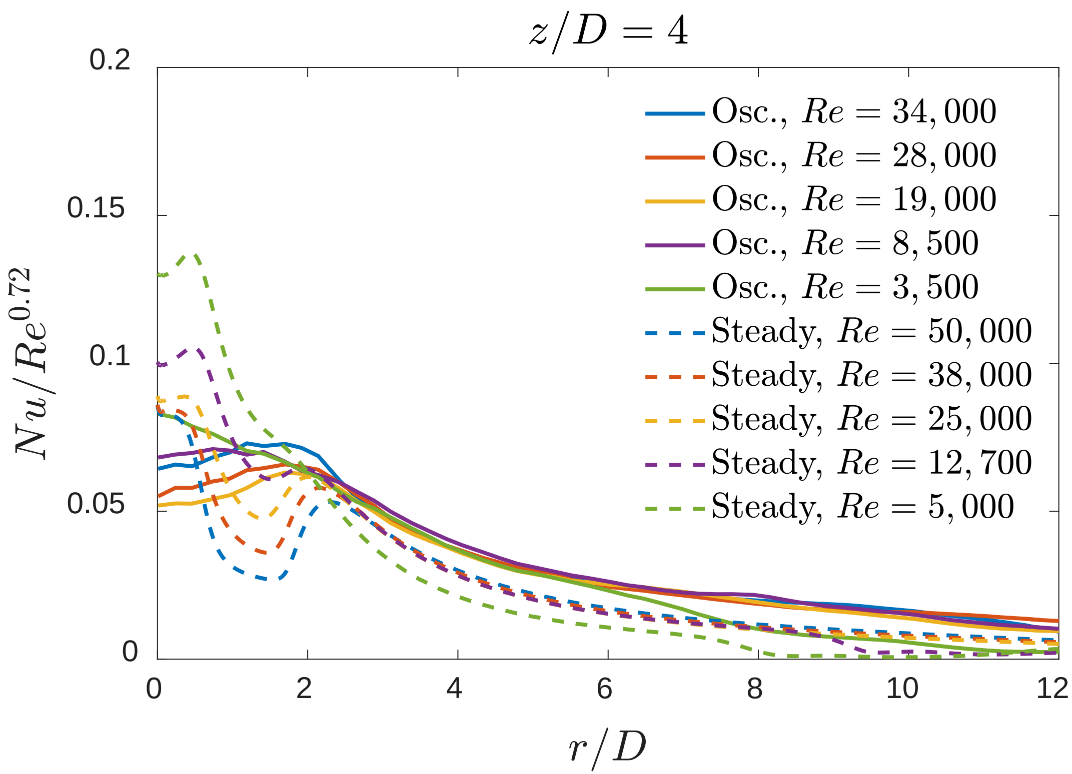

Fluidic Oscillator Impingement: CFD Results

- Results at $z/D = 6$ and 8 have a similar trend.
- Nu is higher for the steady jet in the stagnation region.
- Nu is higher for the fluidic oscillator at larger r/D values.

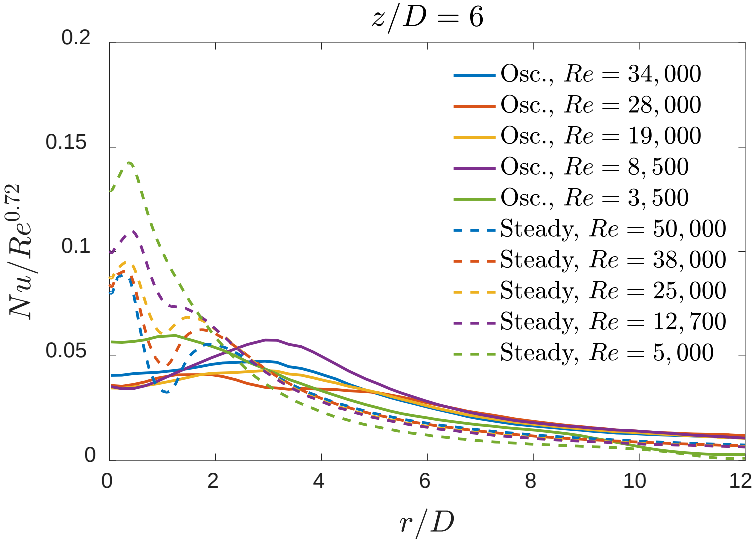

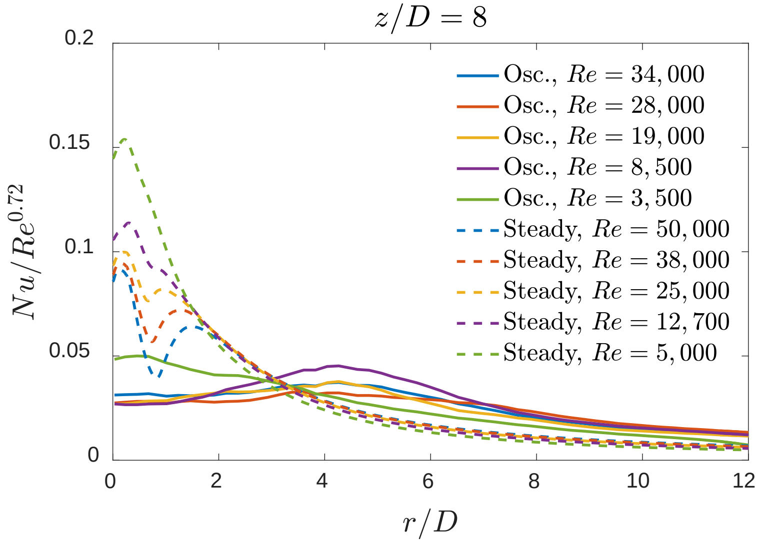

Fluidic Oscillator Impingement: CFD Results

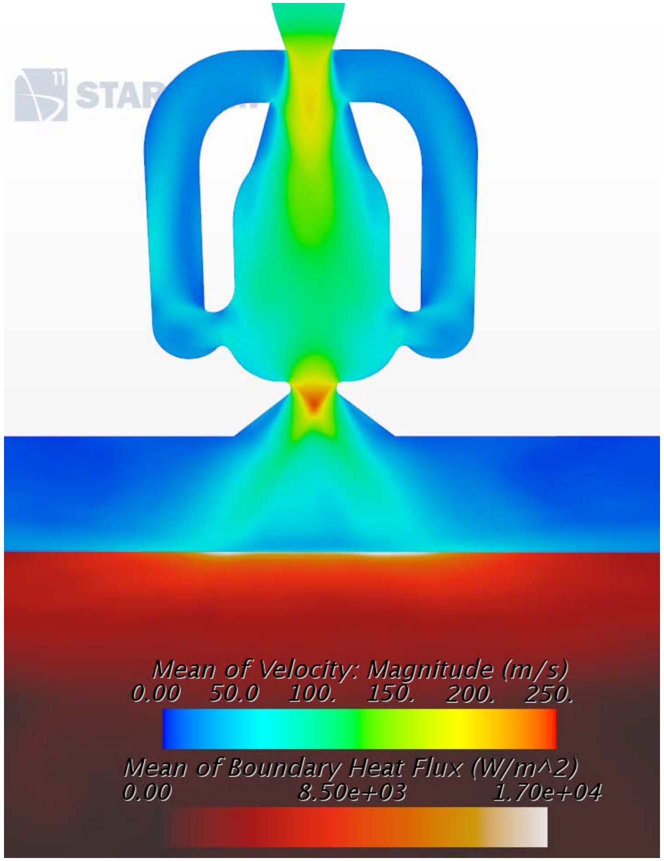

Time-averaged

Fluidic Oscillator
Sweeping Film Cooling

Fluidic Oscillator film cooling study by Thurman et al.

Sweeping Fluidic Oscillators

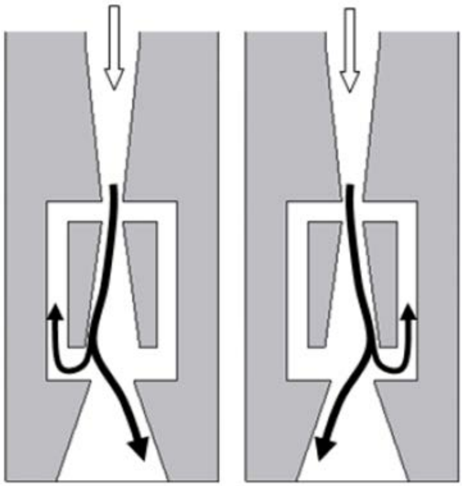

Thurman et al. (IGTI2015) experimentally studied application to film cooling.

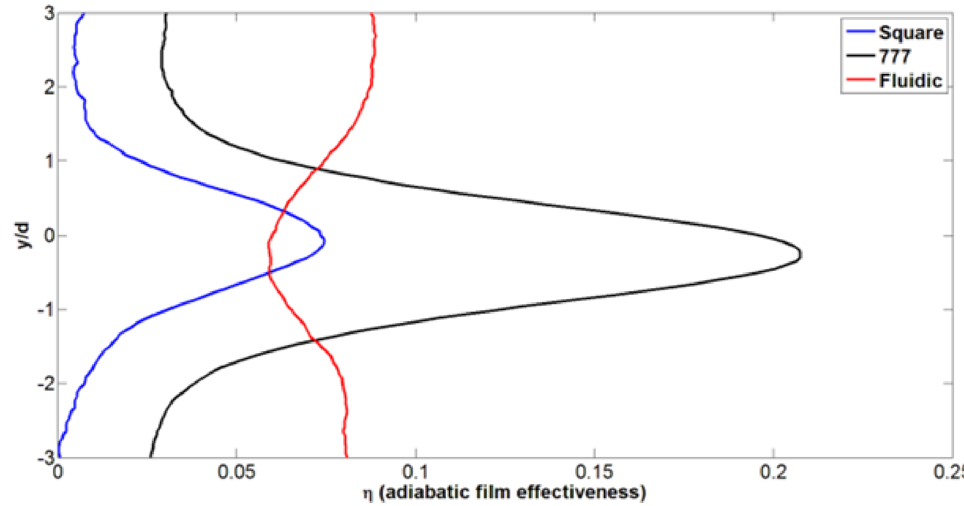

Sweeping film cooling yields higher midpitch film effectiveness. More uniform coverage.

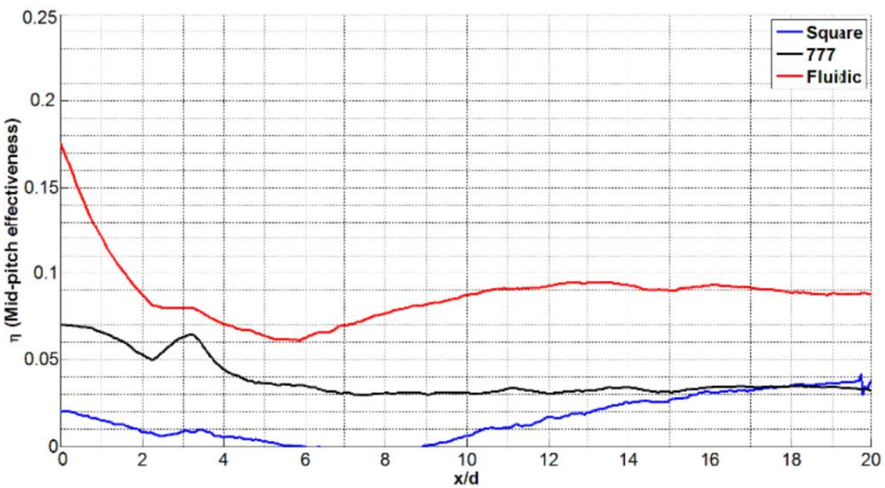

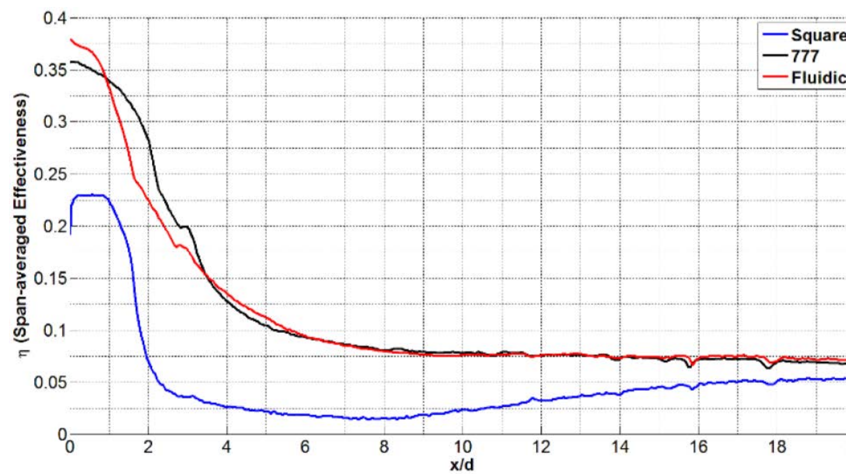

Experimental Setup

- Open circuit wind tunnel was used.
- Test modules were printed with polyjet technique.

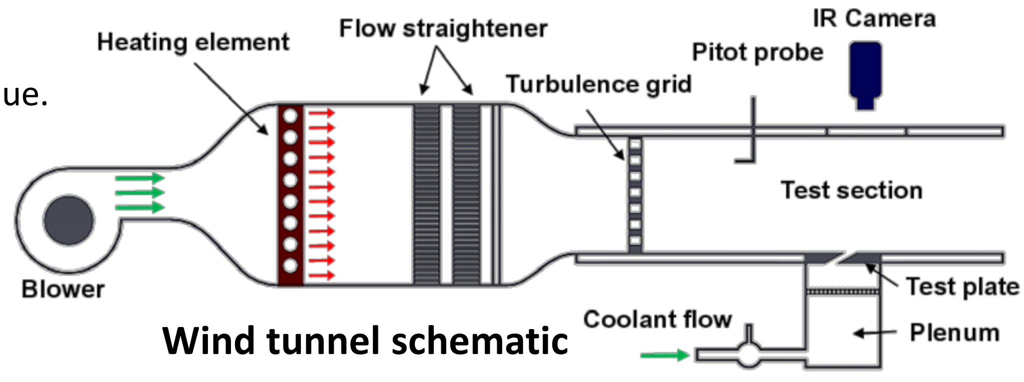

Wind tunnel schematic

Test plate development process

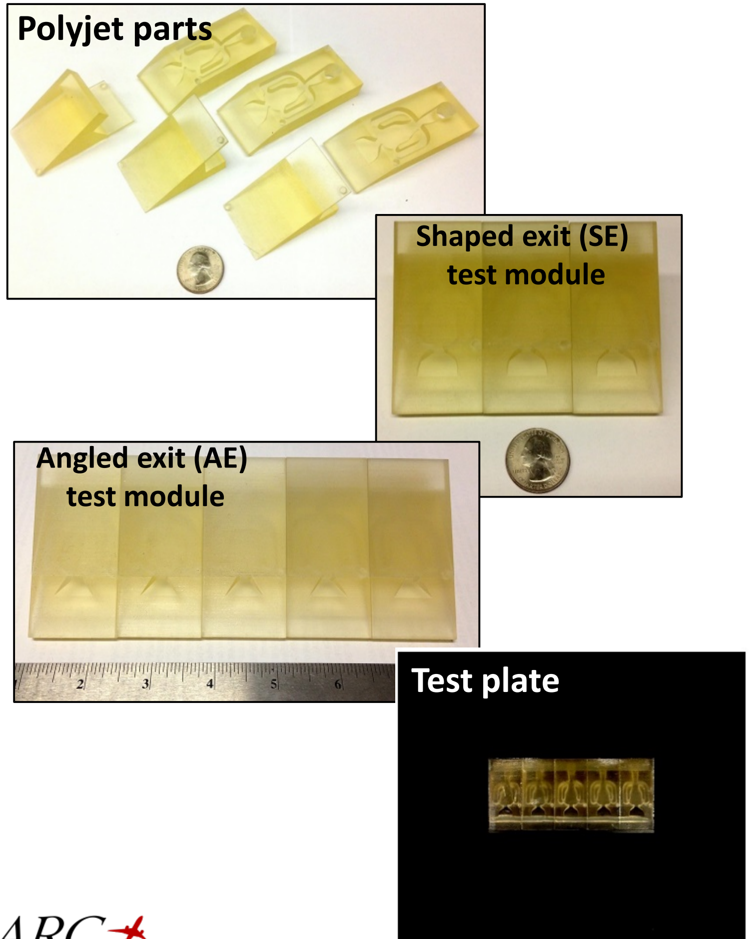

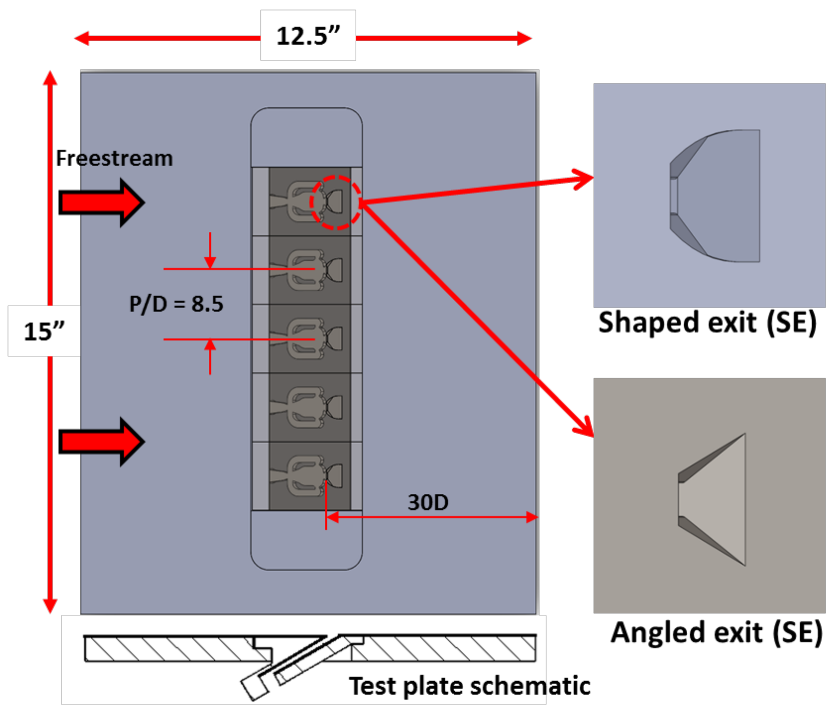

Cooling Hole Geometry

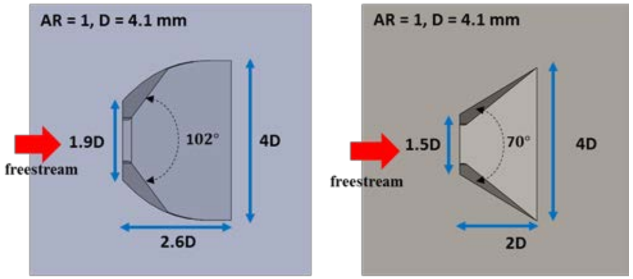

(a) Shaped exit (b) Angled exit

Frequency response

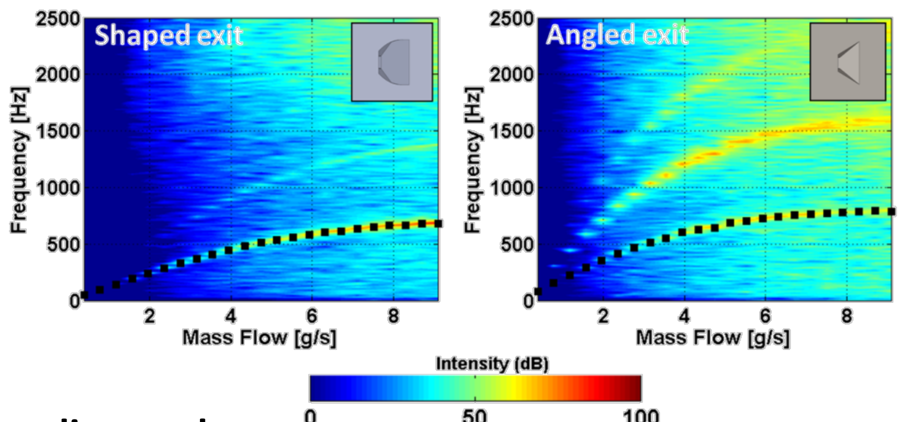

Spreading angle

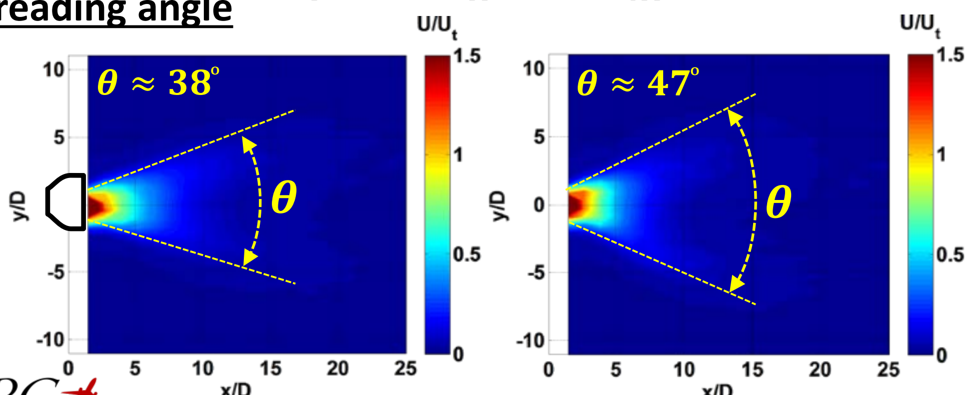

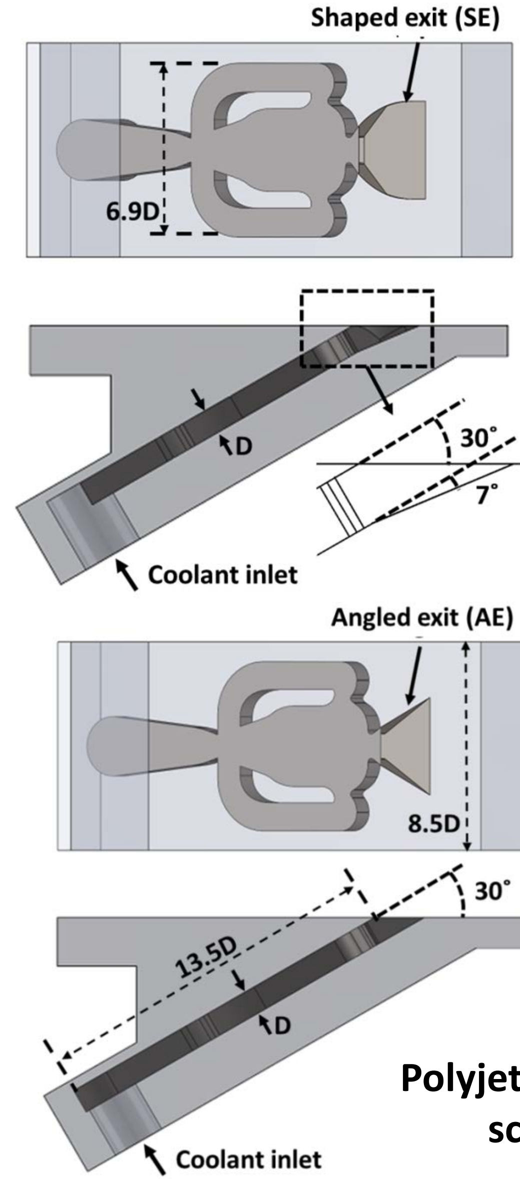

Polyjet test module schematic

Test Conditions

Freestream velocity	U_∞	10.4 m/s
Exit geometry		Shaped, Angled
Blowing ratio	$U_c\rho_c/U_\infty\rho_\infty$	0.98, 1.97, 2.94, 3.96
Freestream temp	T_∞	95 ˚F
Coolant temp	T_c	75 ˚F
Freestream turbulence	Tu	0.4%, 10.1%
Hole Reynolds number	Re_D	2900
Density ratio,	ρ_c/ρ_∞	1.05

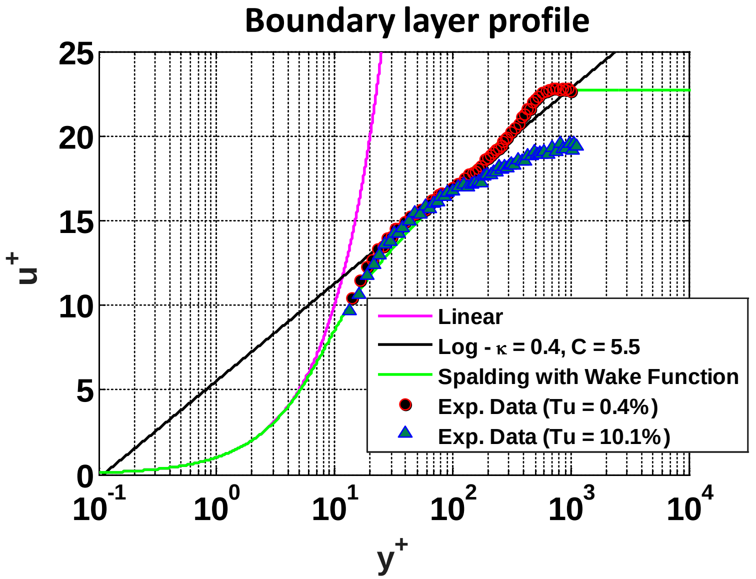

Infrared camera:

- Cedip SILVER 480M
- Resolution: 320x256 pixel
- Sensor: Indium Antimonide (InSb) sensor
- Accuracy: ± 1°C
- Sensitivity: ± 0.02°C
- Max frame rate: 270Hz
- Intergation time : 1000µs

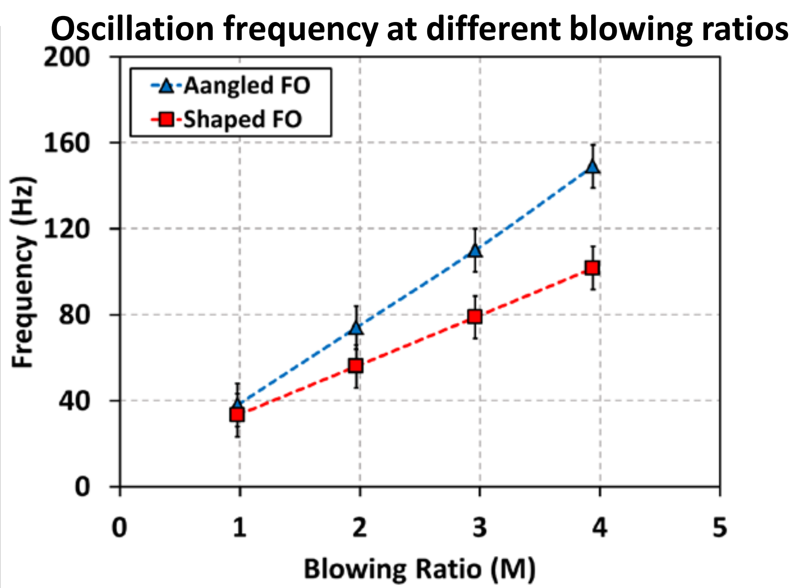

Film Effectiveness Results

$$\eta = \frac{T_\infty - T_w}{T_\infty - T_c}$$

$T_\infty = freestream\ temperature$
$T_c = Coolant\ temperature$

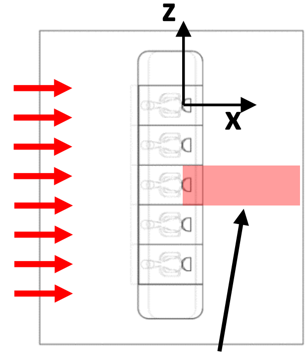

Measurement location

Adiabatic effectiveness (Tu = 0.4%)

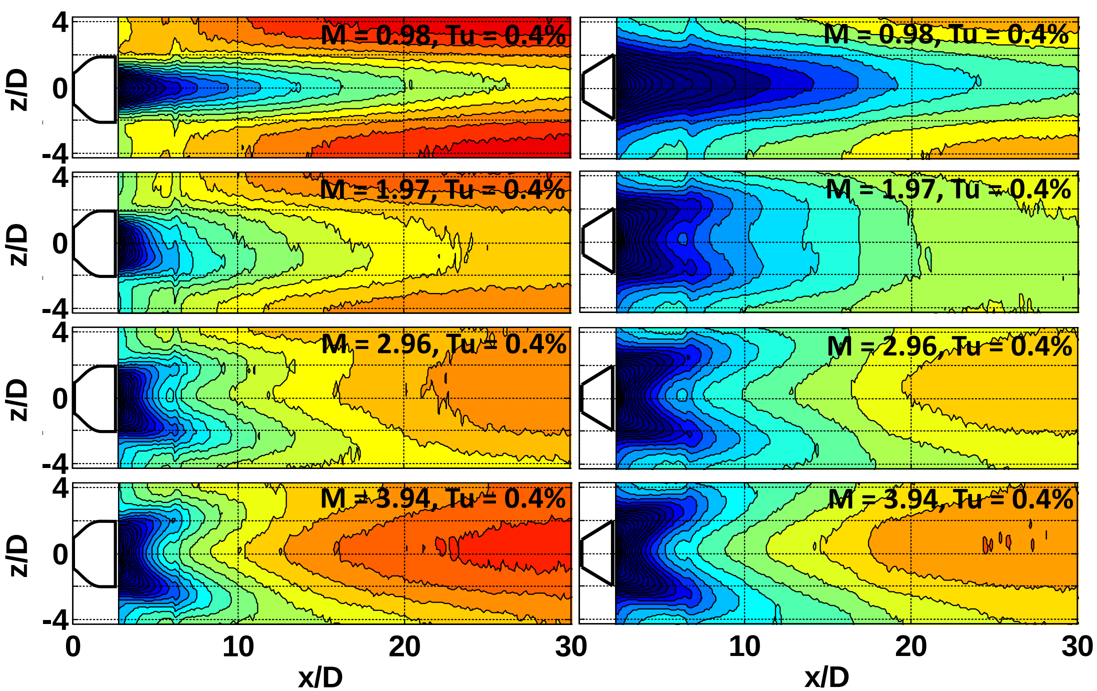

$$\eta = \frac{T_\infty - T_w}{T_\infty - T_c}$$

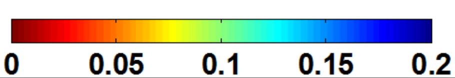

Span averaged effectiveness

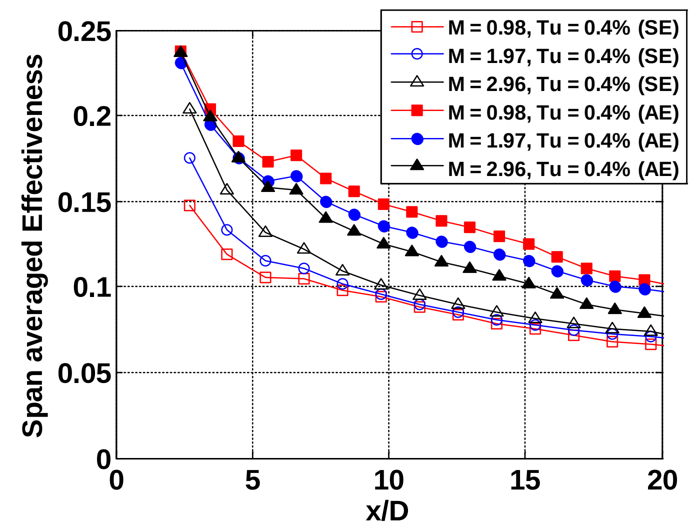

Film effectiveness at x/D = 10

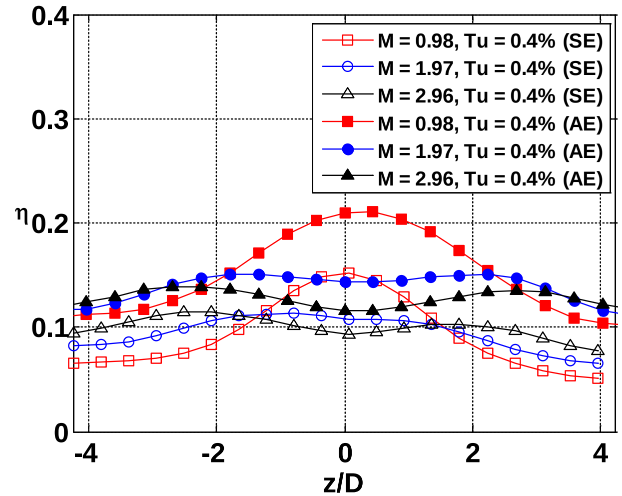

Film Effectiveness Results

$$\eta = \frac{T_\infty - T_w}{T_\infty - T_c}$$

$T_\infty = freestream\ temperature$
$T_c = Coolant\ temperature$

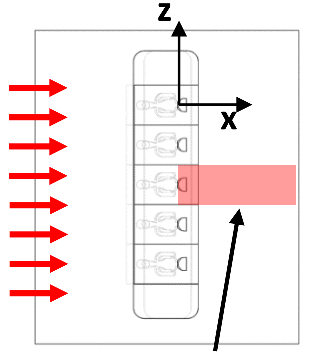

Measurement location

Adiabatic effectiveness (Tu = 10.1%)

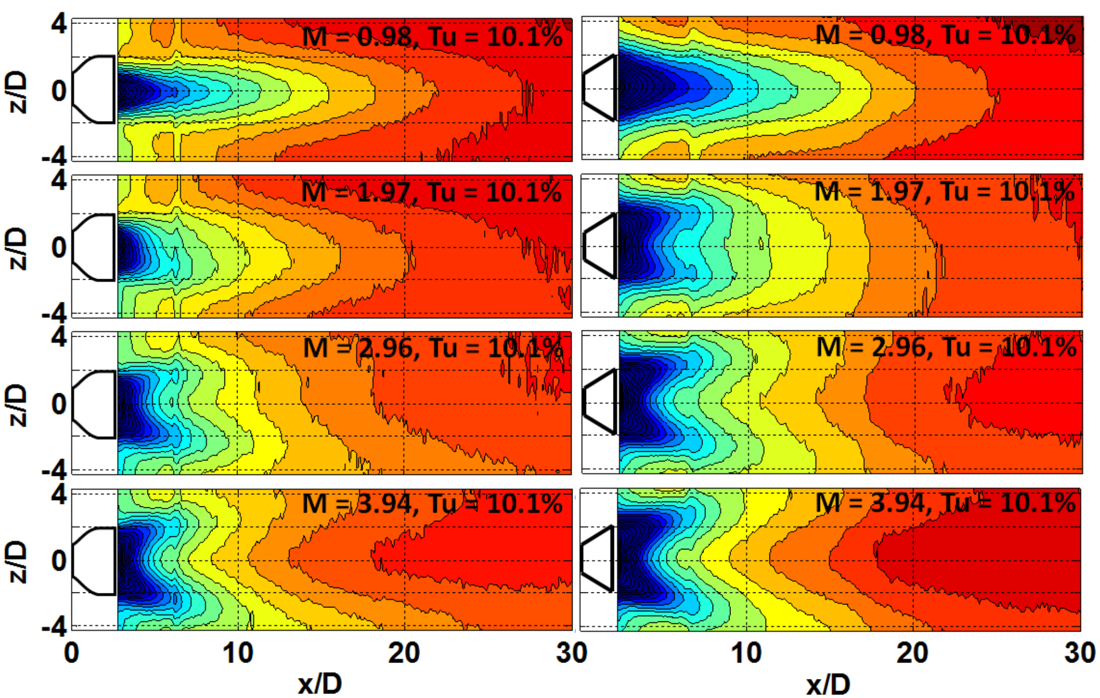

$$\eta = \frac{T_\infty - T_w}{T_\infty - T_c}$$

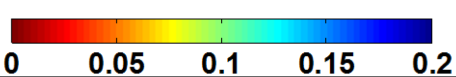

Span averaged effectiveness

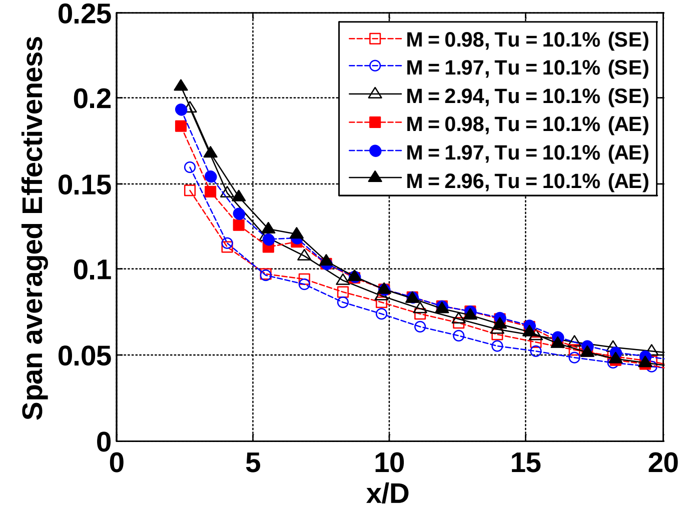

Film effectiveness at x/D = 10

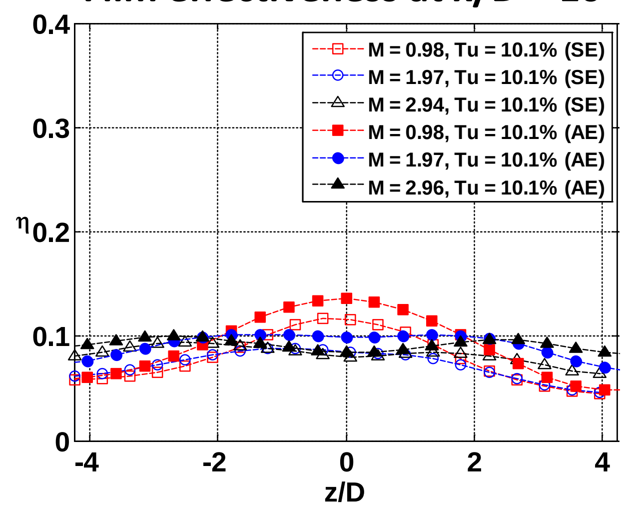

Film Effectiveness Comparison

- Fluidic oscillator with angled exit exhibits higher effectiveness compared to the shaped exit test piece.
- A uniform lateral effectiveness was observed far downstream of the hole (x/D = 10).

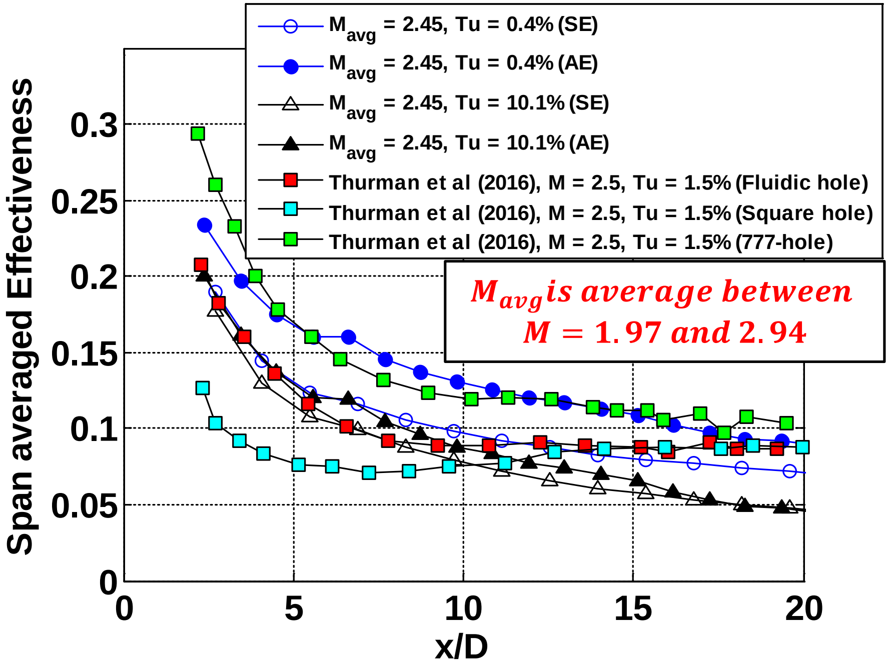

Film effectiveness at x/D = 10

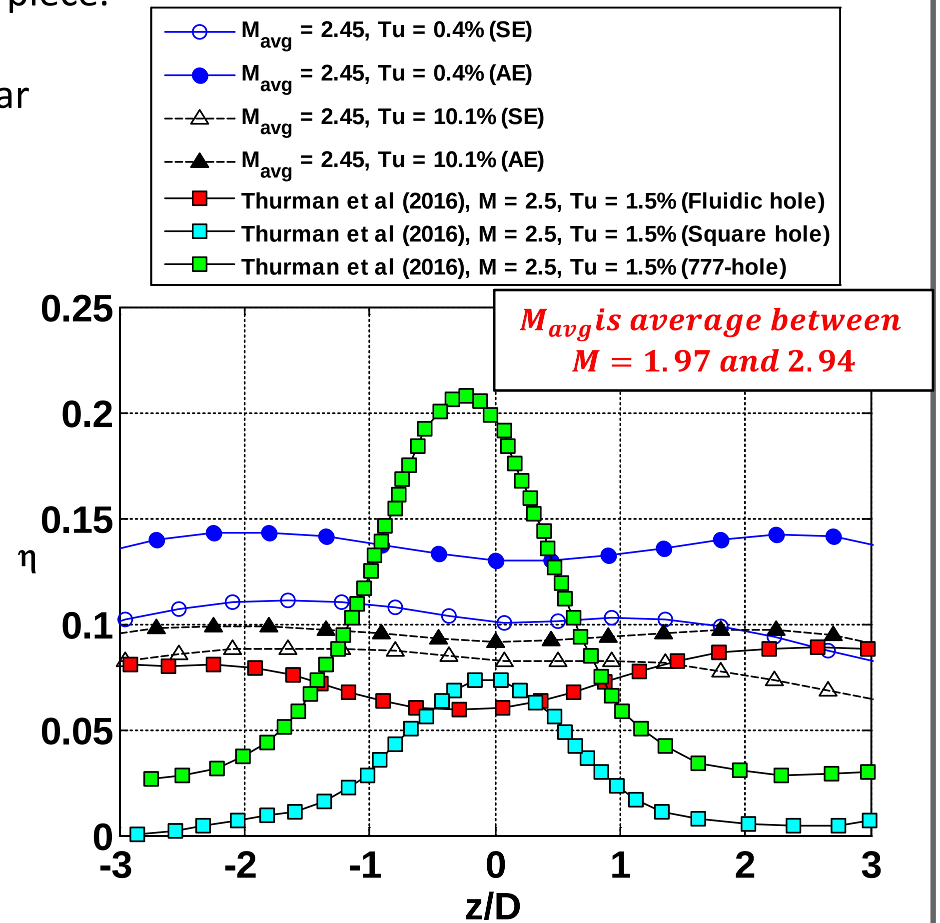

Ref: Thurman, D., Poinsatte, P., Ameri, A., Culley, D., Raghu, S., Shyam, V., 2016, “Investigation of Spiral and Sweeping Holes,” ASME J. Turbomach., 138, pp. 091007-11

Thermal Field (Tu = 0.4%, x/D = 6)

- Angled exit hole exhibits larger spreading than the shaped exit case.
- Maximum jet penetration height is 2.25D at the blowing ratio of 2.94.
- Jet liftoff was also observed at higher blowing ratios

$$\theta = \frac{T_\infty - T_w}{T_\infty - T_c}$$

$T_\infty = freestream\ temperature$
$T_c = Coolant\ temperature$

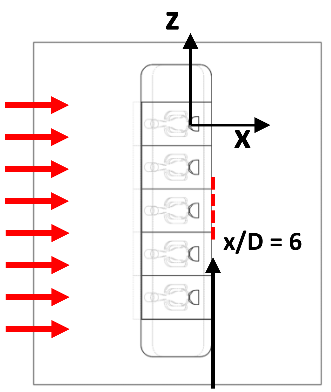

Measurement location

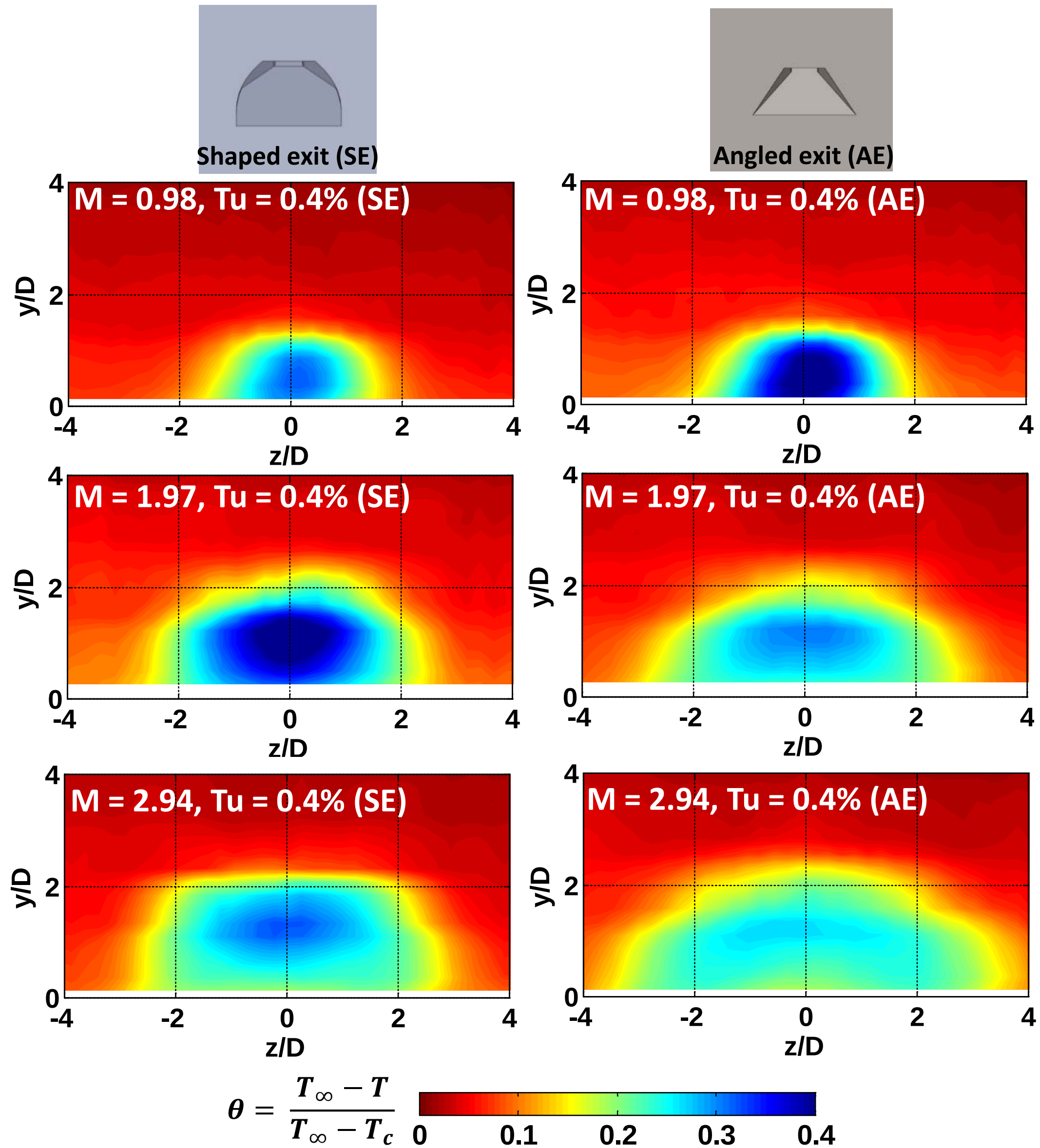

Thermal Field (Tu = 0.4,10.1%, x/D = 6)

- Significant mixing was observed.
- Maximum jet penetration height did not change significantly.
- Larger lateral spreading was observed for high turbulence case.

$$\theta = \frac{T_\infty - T_w}{T_\infty - T_c}$$

$T_\infty = freestream\ temperature$
$T_c = Coolant\ temperature$

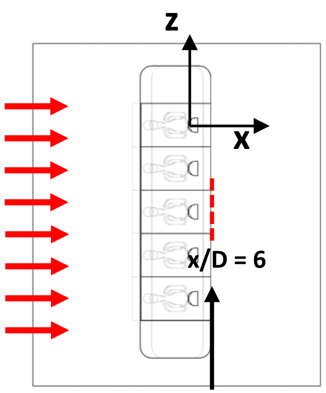

Measurement location

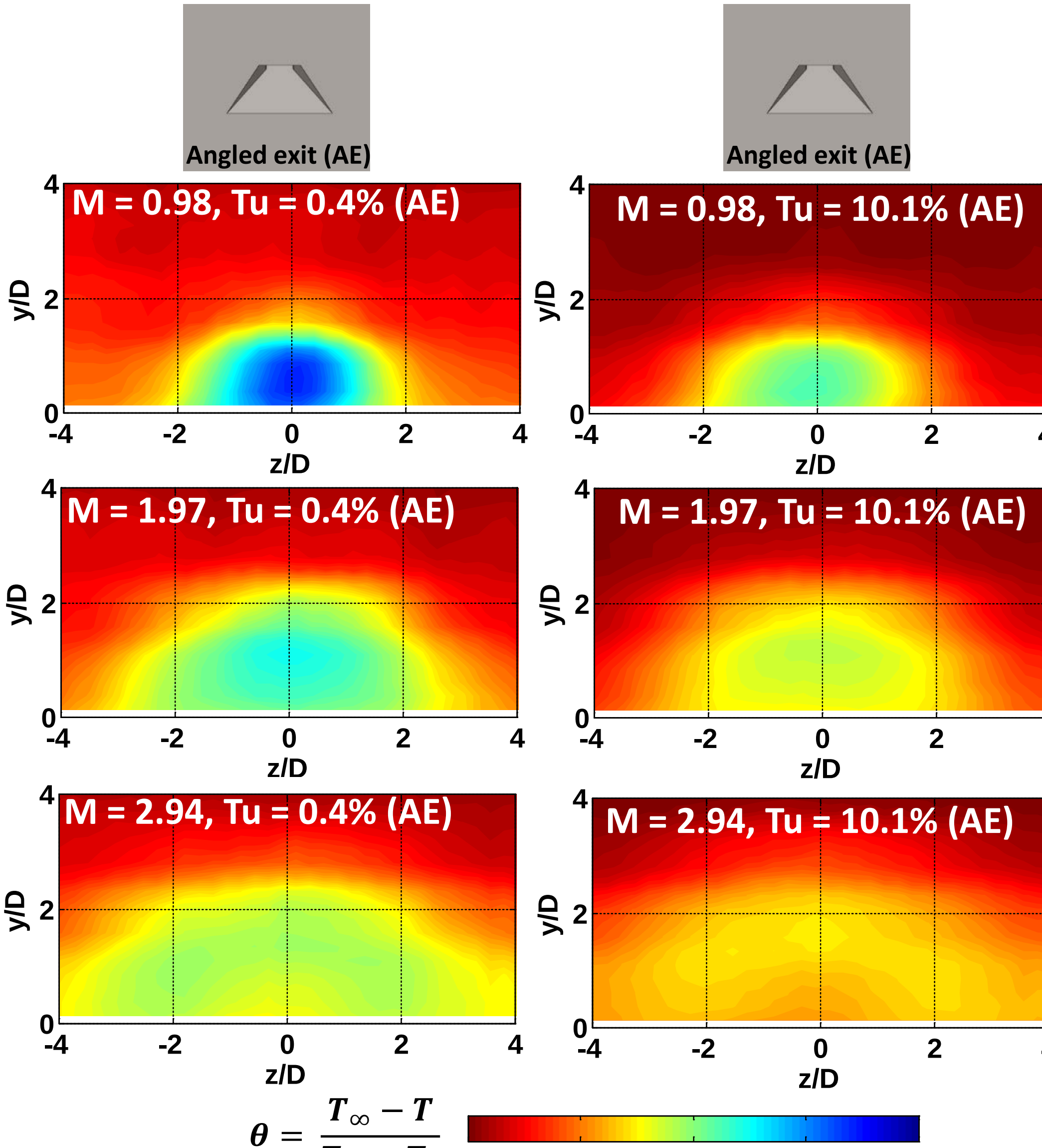

$$\theta = \frac{T_\infty - T}{T_\infty - T_c}$$

Film Cooling CFD Study (Grid Generation)

Grid description

	Cell (ml)	M_dot (g/s)	Time/step (sec)	Time steps
Grid 1	2.31	0.394	5e-5	4000
Grid 2	6.18	0.394	5e-5	1500
Grid 3	8.14	0.394	5e-5	1800

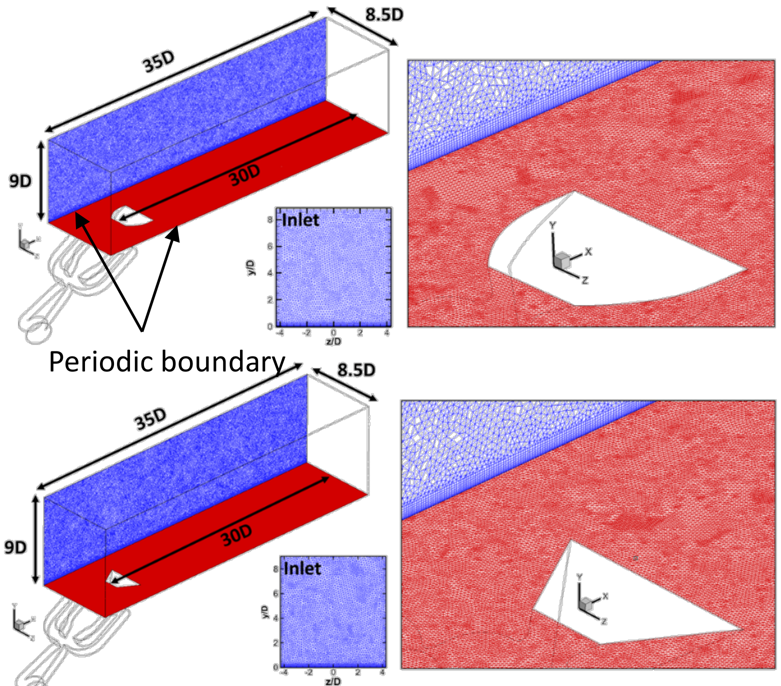

Boundary conditions

- Blowing ratio , M = 1.97
- Mass flow inlet for fluidic oscillator
- Outlet : outflow boundary condition.
- Adiabatic wall.

Grid 2 was used for further calculations

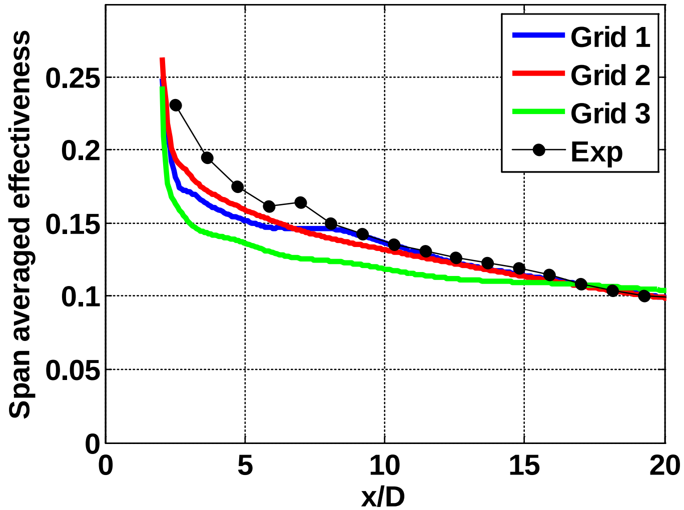

Model description

- URANS k-ω SST model
- 2nd order in time.

ARC

Adiabatic Film Effectiveness and Thermal Field (CFD)

- CFD predicted higher oscillation frequency for the angled exit case which was validated by experimental data.

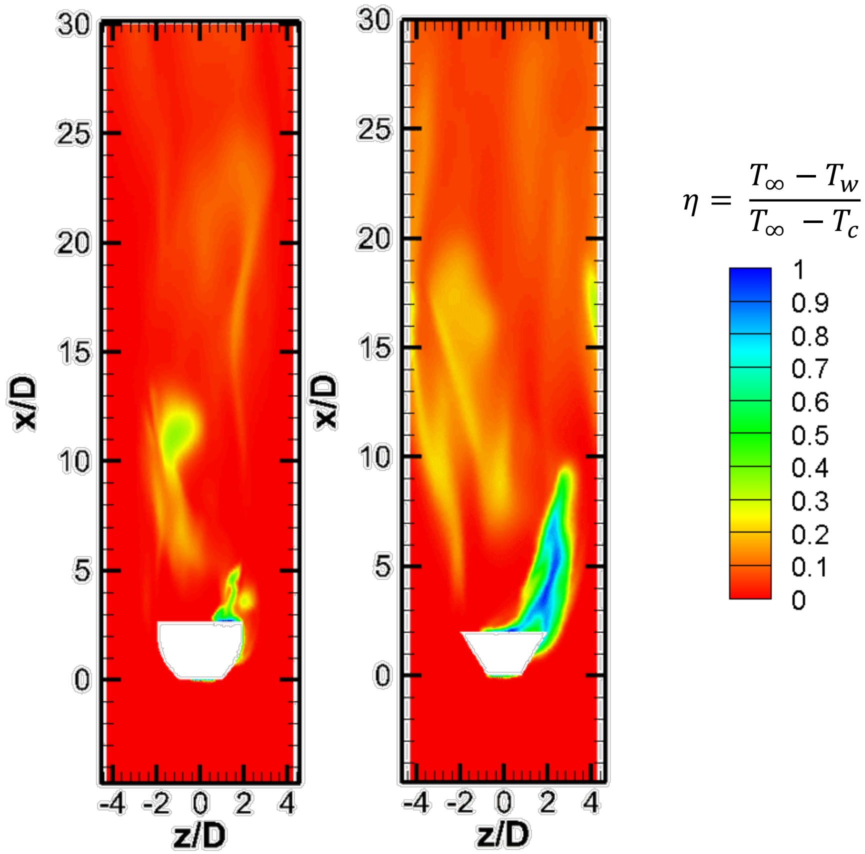

Shaped exit (SE) | Angled exit (AE)

Shaped exit (SE)

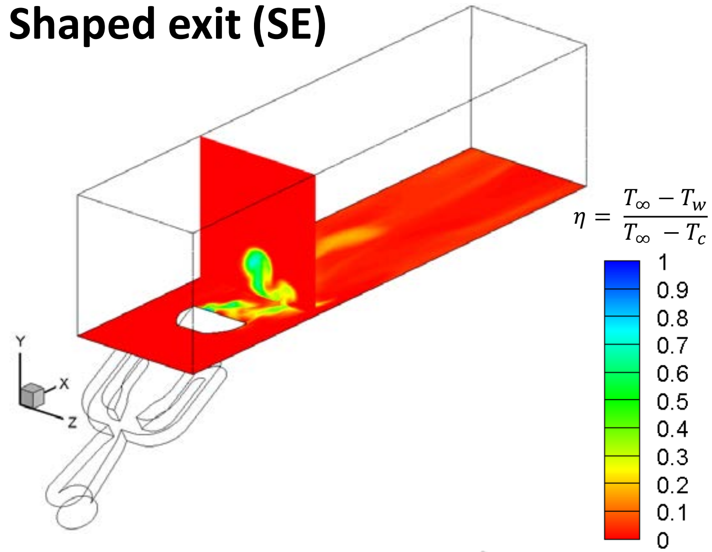

Angled exit (AE)

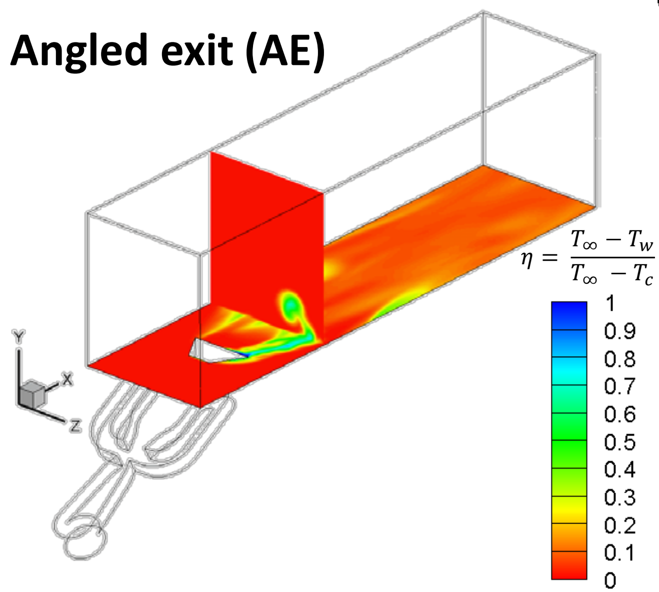

Exp. vs CFD (Thermal field)

- CFD accurately predicted the jet penetration and jet spreading.
- CFD also predicted two distinct peaks which was not observed in the experimental data.

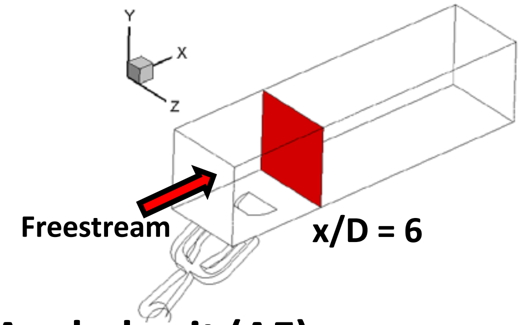

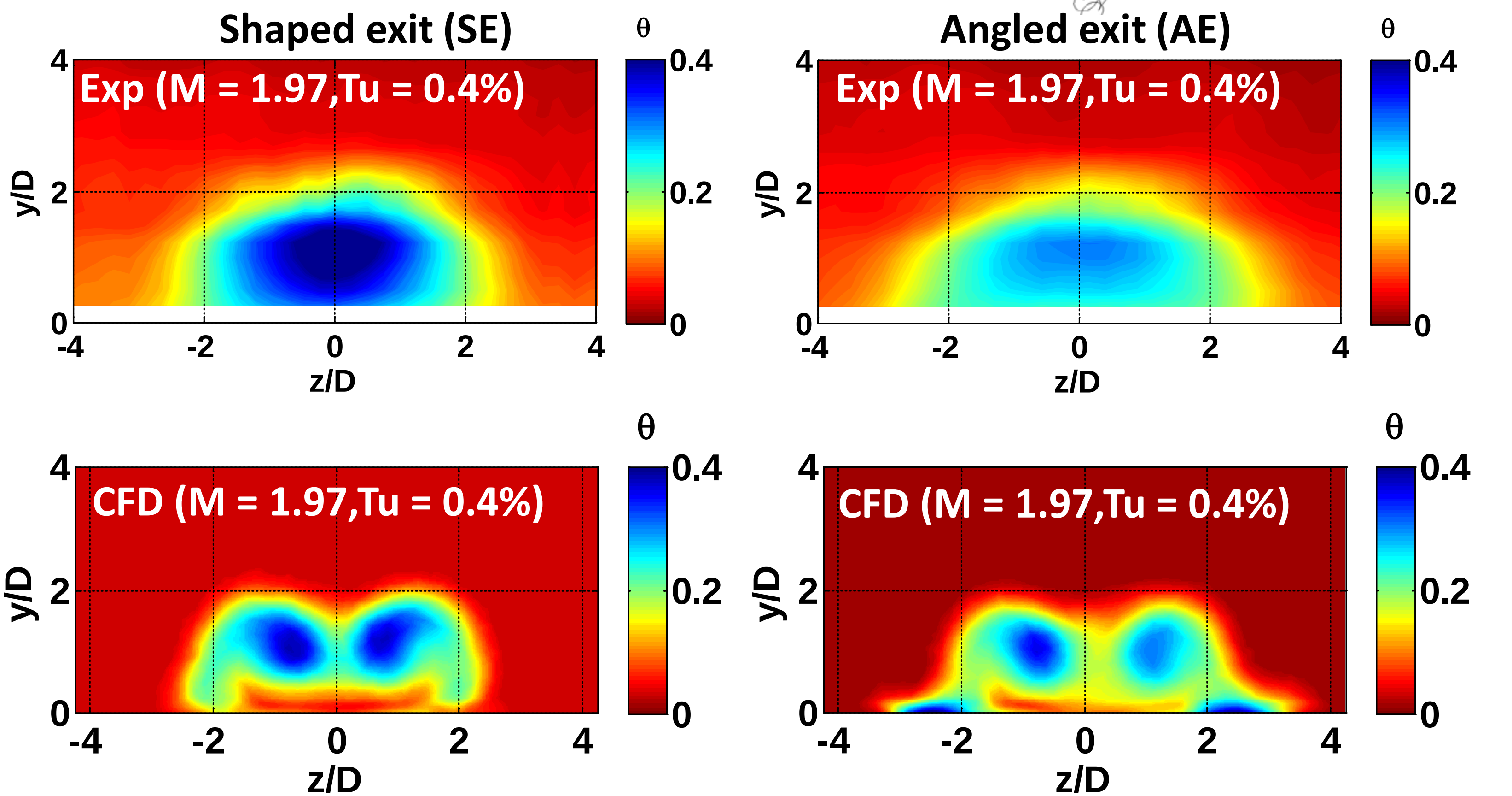

CFD Result (Streamwise vortices)

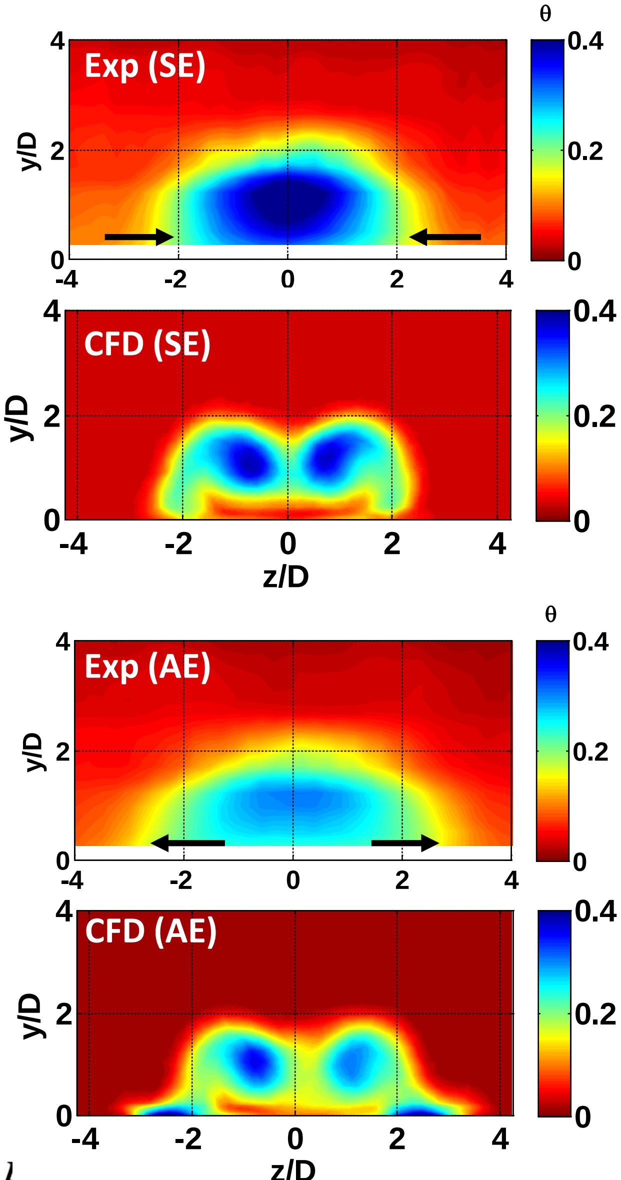

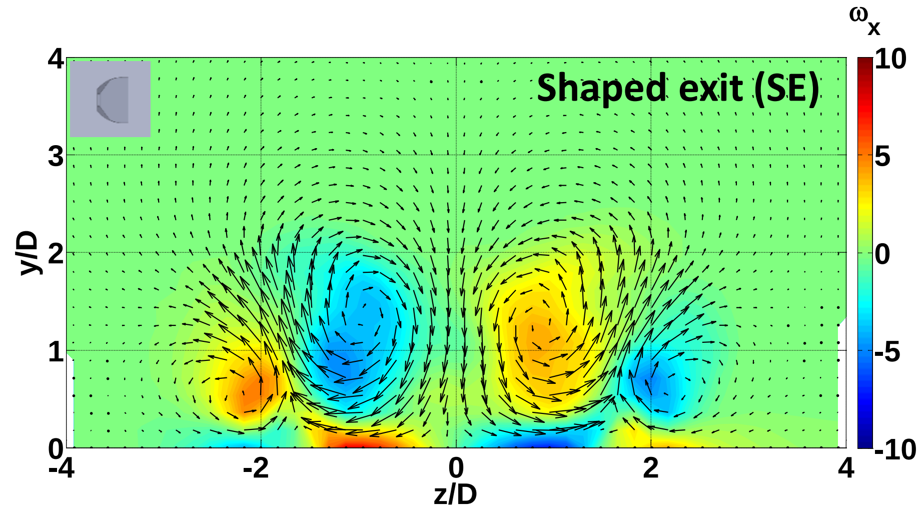

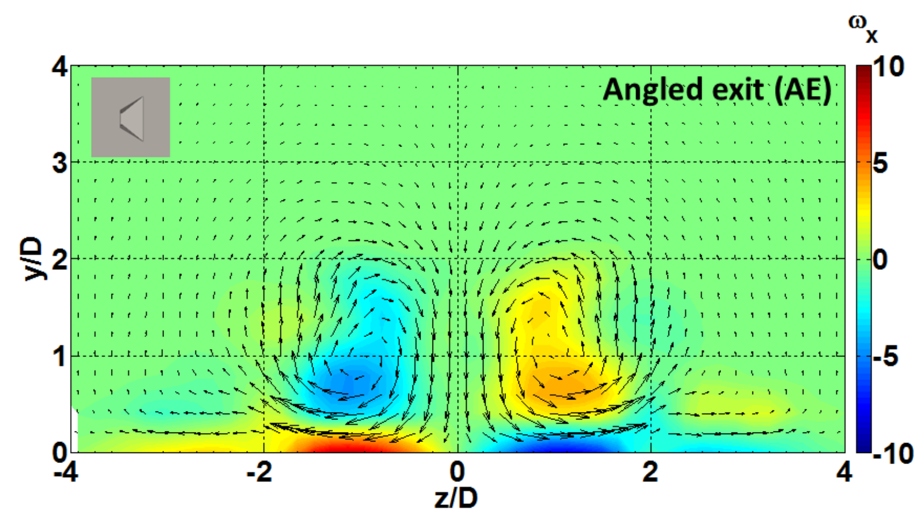

CFD Result (Streamwise vortices)

Instantaneous

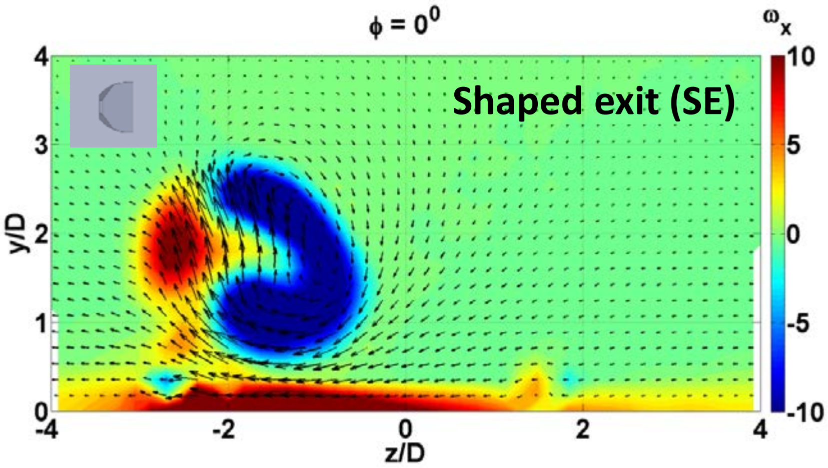

Time Averaged

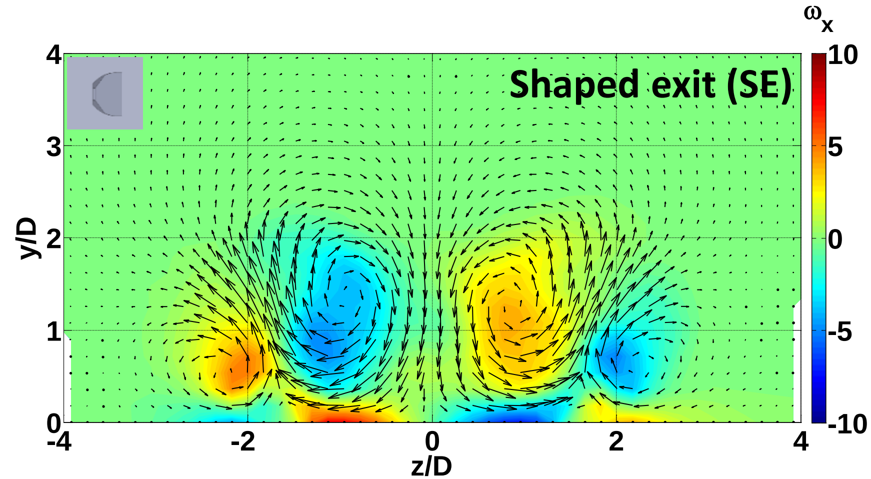

$\emptyset = Phase\ angle$

Instantaneous

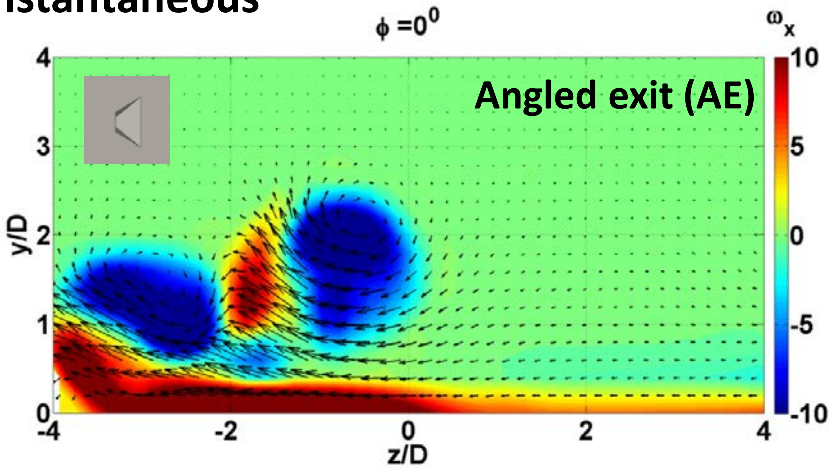

Time Averaged

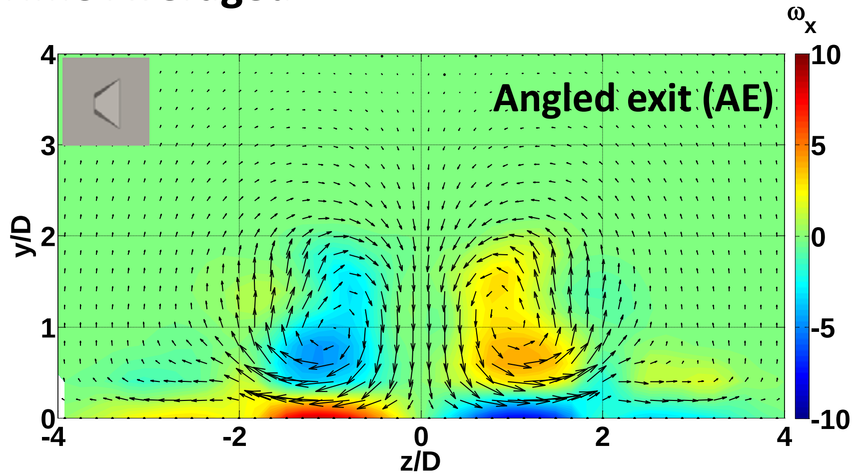

Thermal field (Exp vs. CFD)

- Experiment was conducted with rough polyjet part while CFD calculation was done with a smooth fluidic device.

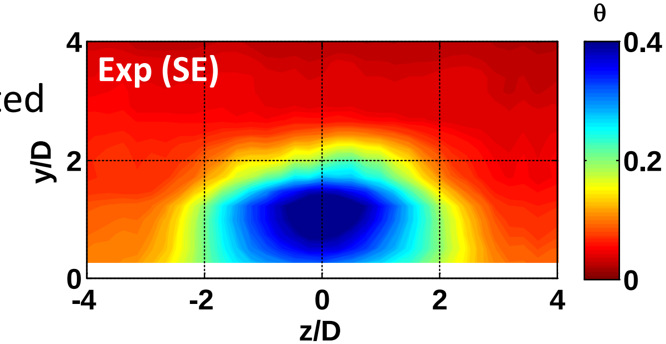

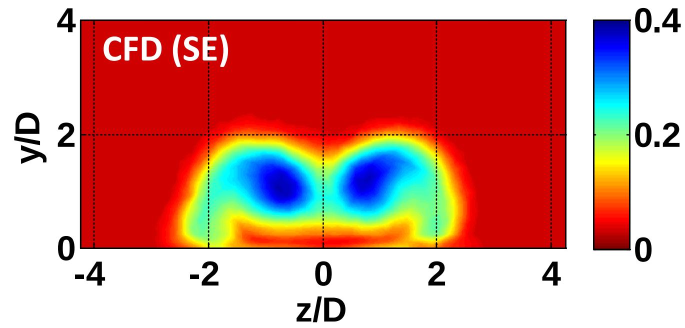

- Roughness limits the spreading of the jet.

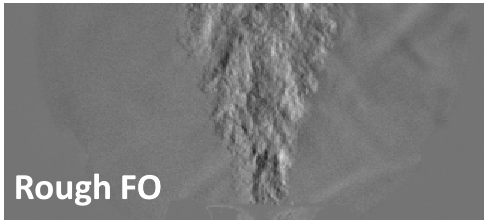

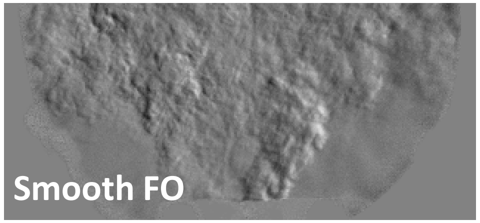

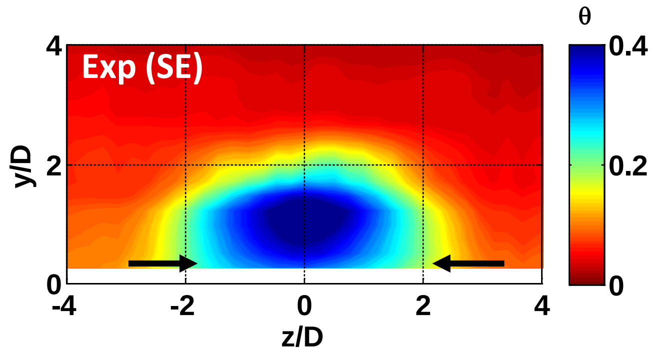

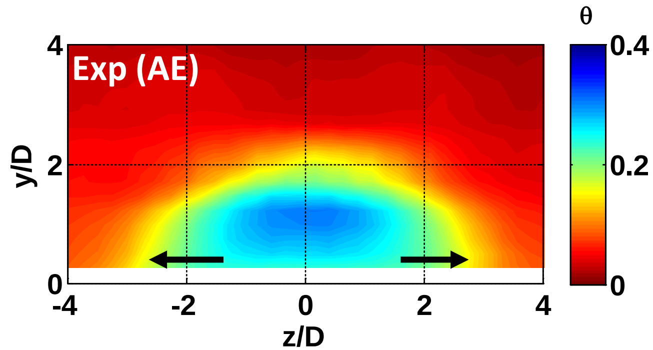

- Spreading of the jet of the two fluidic oscillator varies with the exit geometry.

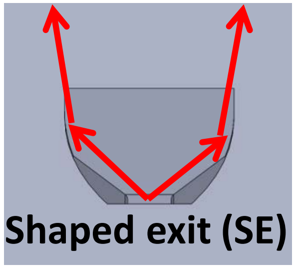

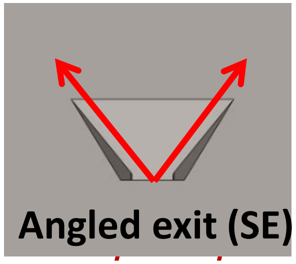

Reverse Film Cooling

Reverse Film Cooling: Motivation and Background

- Reverse film cooling consists of film cooling holes oriented to inject coolant upstream

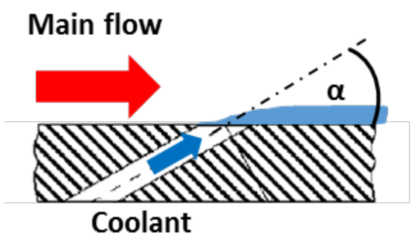

Conventional

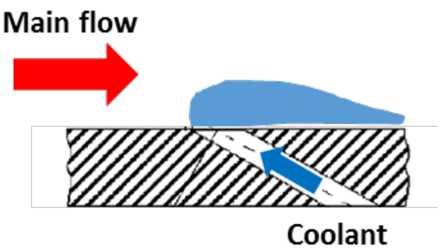

Reverse

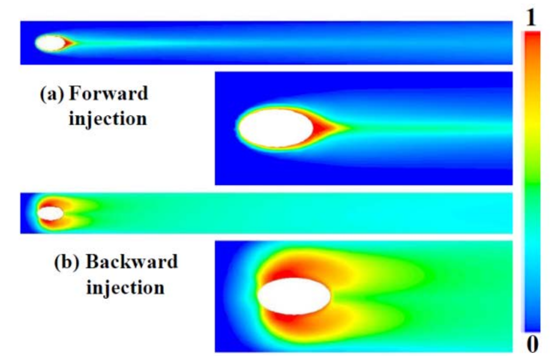

Film cooling effectiveness from CFD comparing conventional and reverse configurations (Li et al., 2013)

- This configuration has not been extensively studied, the studies that have been conducted show that the reverse configuration produces a uniform effectiveness distribution downstream

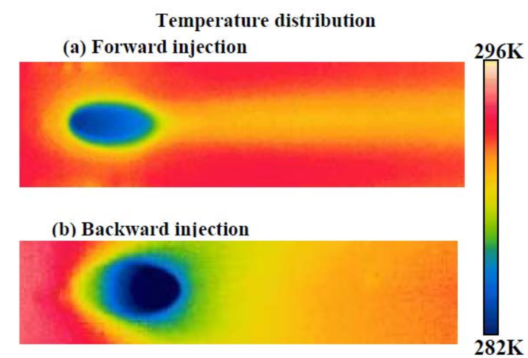

IR Images of temperature distribution comparing conventional and reverse configurations (Li et al., 2013)

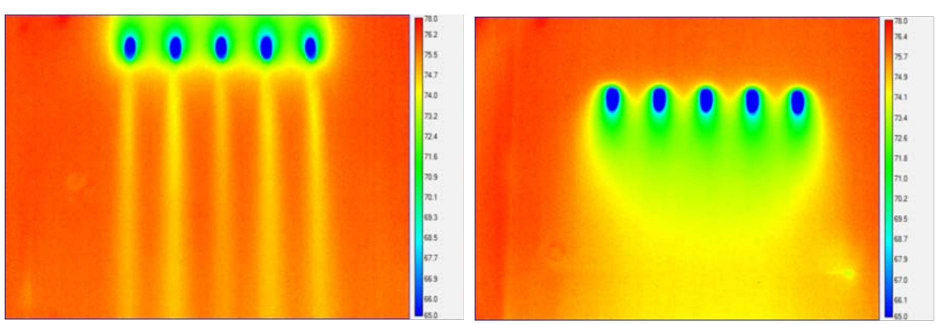

Raw IR measurements of (a) downstream blowing and (b) upstream (reverse) blowing (Ameri and Shyam disclosure, unpublished).

Reverse Film Cooling: Test Plate

- Flat plate test piece with six "short" (L/D = 2) cylindrical film cooling holes.
- Fabricated using stereolithography out of Somos 18420 plastic.

Material Properties – Somos 18420 Plastic	
Density, ρ	1194 kg/m^3
Specific heat, c_p	1325 J/kgK
Thermal conductivity, k	0.231 W/mK

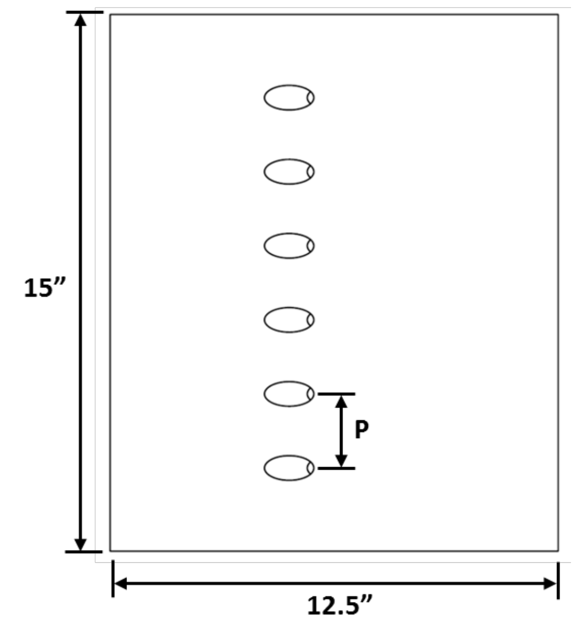

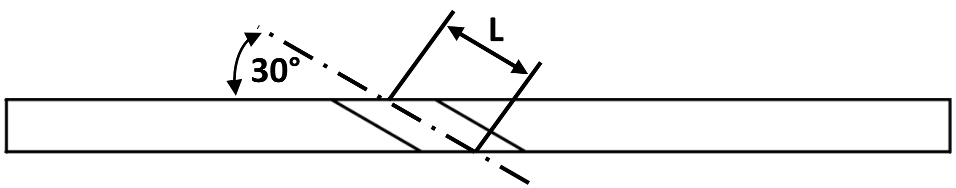

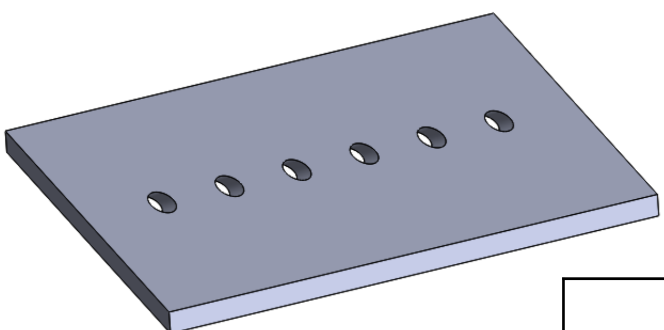

D	L/D	P/D	α
17.5 mm	2	3	30°

Reverse Film Cooling: Test Conditions

- Flat plate film cooling experiments conducted in a low speed, open loop wind tunnel
- Freestream is heated to achieve temperature difference
- Low and high freestream turbulence conditions tested (Tu = 0.4% and 10.1%)
- Several blowing ratios tested at density ratio of approximately 1

Test Conditions	
U_∞	10 m/s
T_∞	93 °F (307 K)
T_c	55 – 65 °F (286 – 291 K)
$M = (\rho_c u_c)/(\rho_\infty u_\infty)$	0.25, 0.5, 0.75, 1.0
$DR = \rho_c/\rho_\infty$	1.055 – 1.073
Re_D	10,500

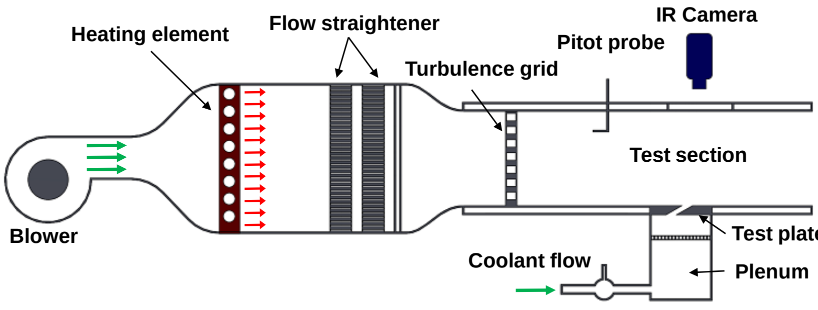

Schematic of low speed wind tunnel setup

Boundary layer profiles for low and high FST conditions

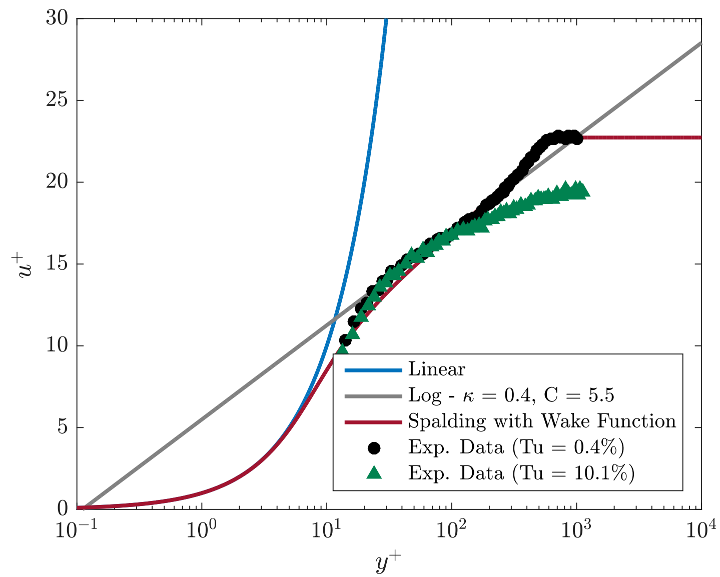

Reverse Film Cooling: Flow Visualization

- Coolant seeded with olive oil
- Images acquired at 5Hz
- Qualitative flow visualization
- Several interesting flow features result from the reverse jet in cross flow interaction

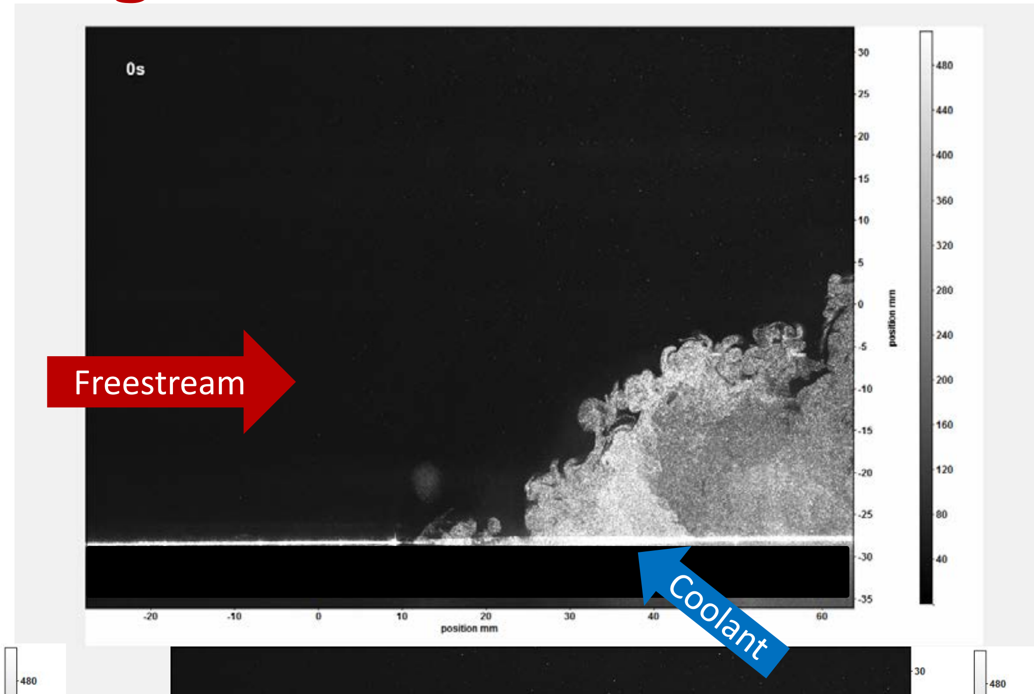

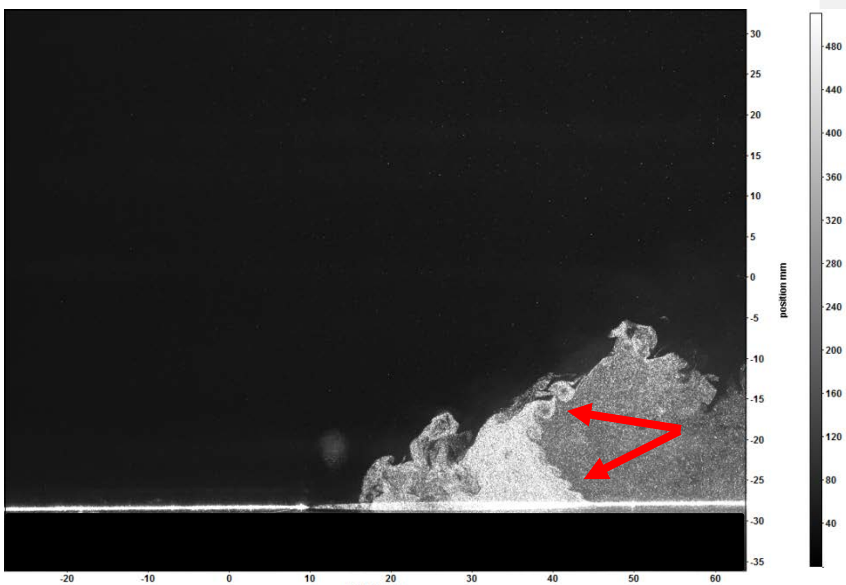

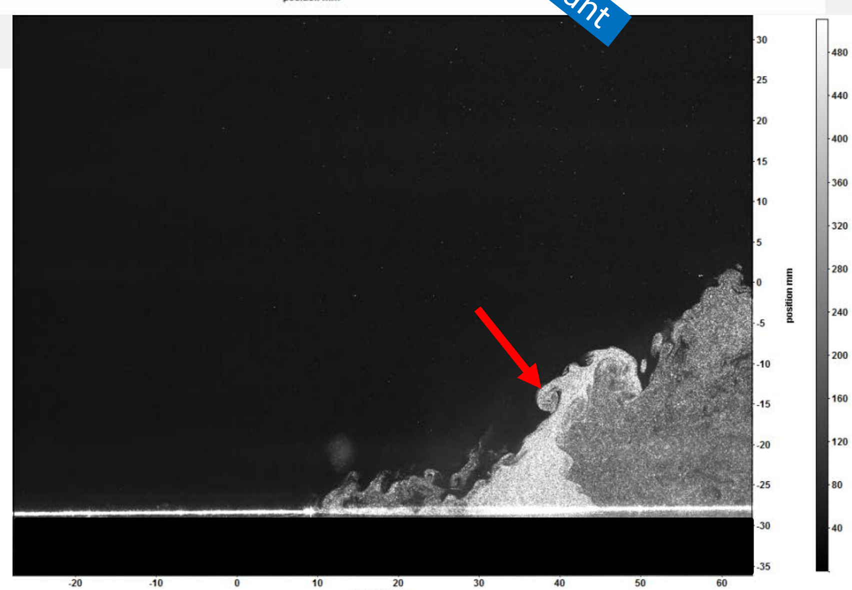

Reverse Film Cooling: Particle Image Velocimetry

- Planar PIV performed in a bisecting plane down the hole centerline (z = 0)

- Freestream and coolant seeded with atomized olive oil. Coolant seeder mass flow rate measured/controlled to ensure accurate blowing ratio

- PIV details:
  - LaVision Imager Intense CCD camera
  - Nd:YAG Laser 532nm
  - 32x32 and 16x16 window sweeps to determine correlation and velocity vectors
  - Each image pair separated by 80μs to achieve pixel shift ~ 8 pixels
  - 500 image pairs for each case

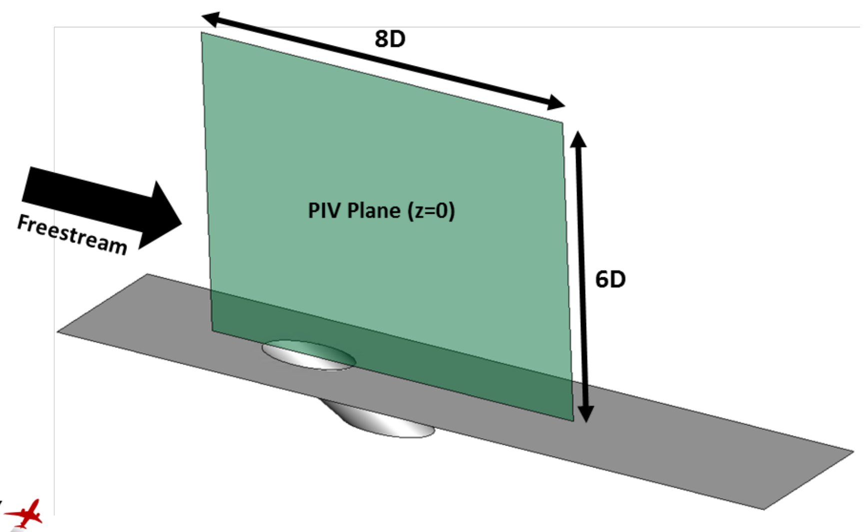

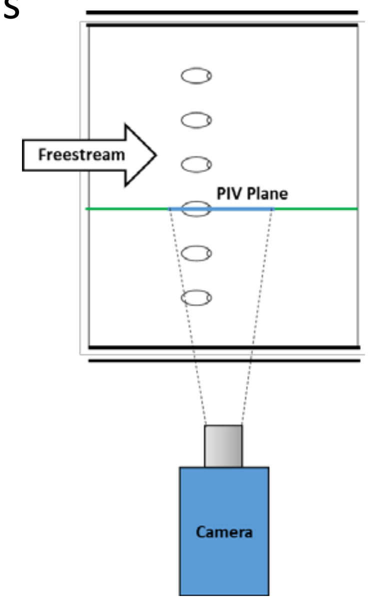

Reverse Film Cooling: Particle Image Velocimetry

- Centerline flow field shows several features:
  - Vertical-redirection and acceleration of the freestream
  - “Jetting” occurs at leeward edge of hole exit
  - Jet penetration increasing with blowing ratio
  - Recirculation zone downstream of the hole exit, which grows with blowing ratio
- Converged vectors in the near hole region for M = 1 case challenging due to high velocities in the “jetting” flow.

$U = \sqrt{u^2 + v^2}$

M = 0.25

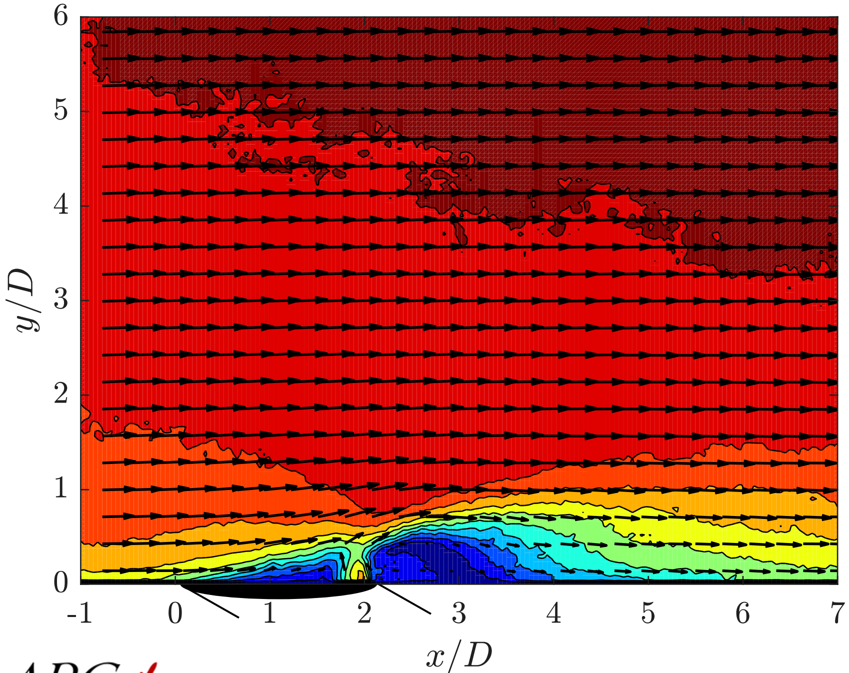

M = 0.5

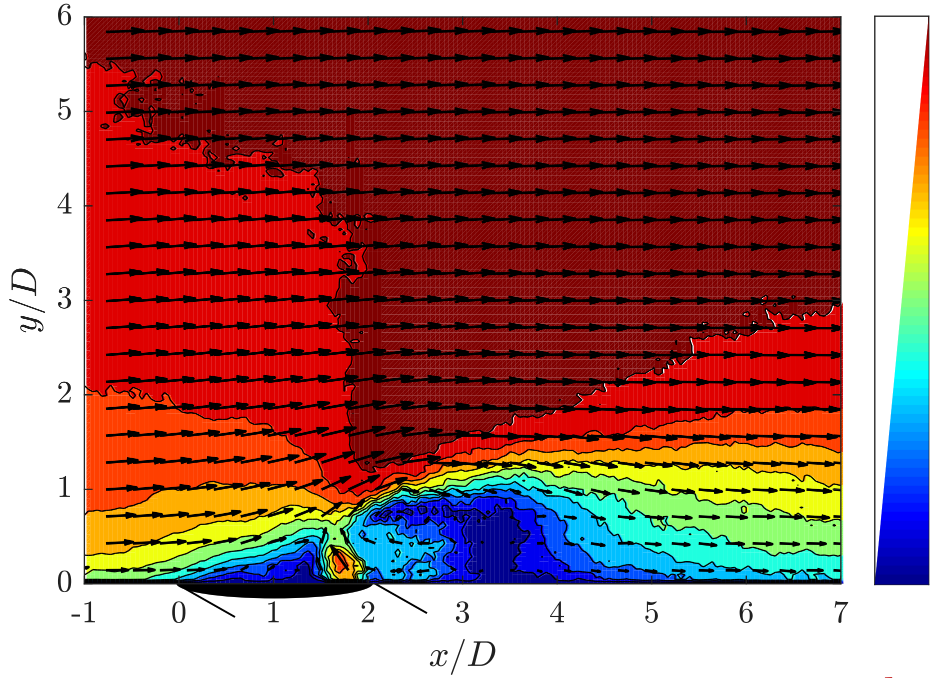

Reverse Film Cooling: Film Cooling Effectiveness

- Film cooling effectiveness obtained using steady-state infrared measurements
- Effectiveness defined as $\eta = \frac{T_\infty - T}{T_\infty - T_c}$
  - Note: this is not the conventional η_{aw} in the near hole region, due to conduction from the upstream injection

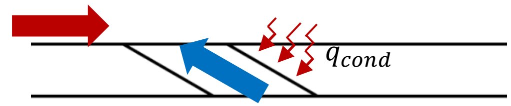

- Lobes of high effectiveness apparent either side of the hole exit, and advance upstream with increasing blowing ratio
- Downstream of the holes the effectiveness becomes very uniform in the lateral direction
- Increased freestream turbulence leads to slightly decreased effectiveness

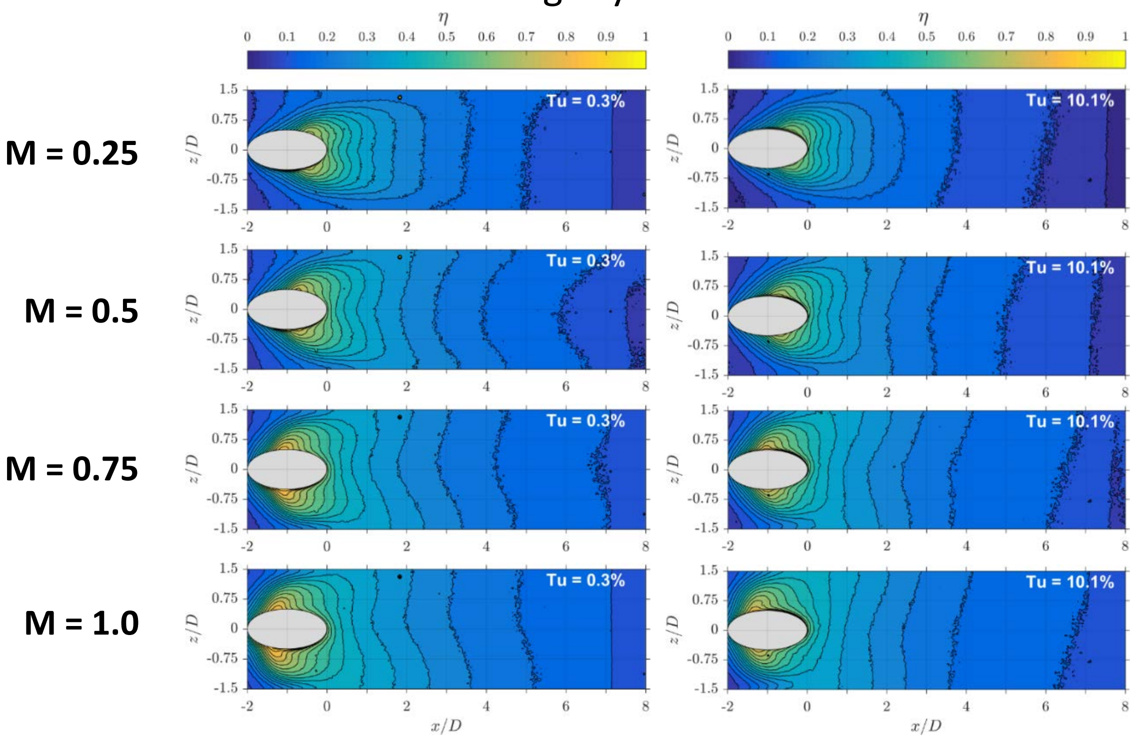

Reverse Film Cooling: Film Cooling Effectiveness

Centerline Traces

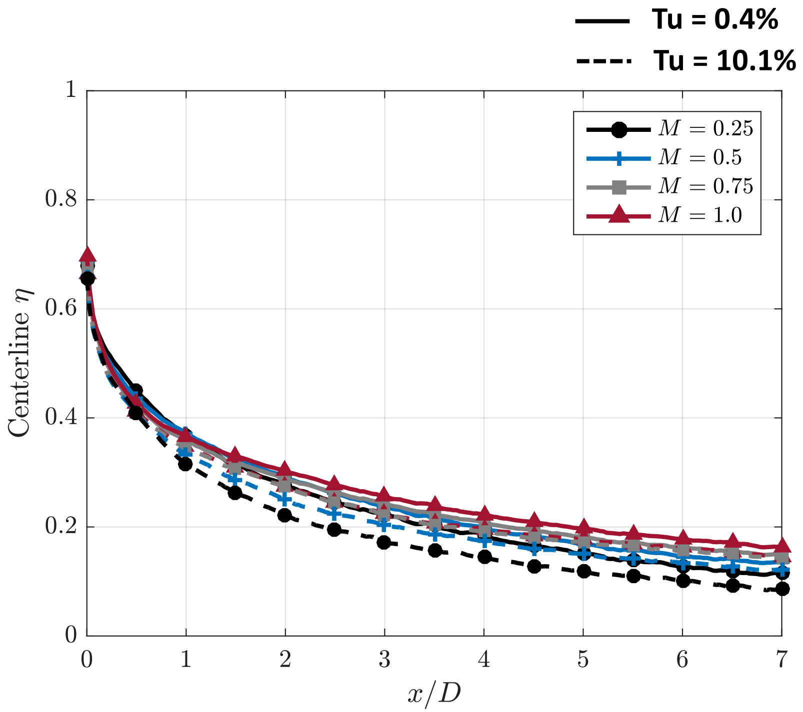

Lateral Traces at x/D = 4

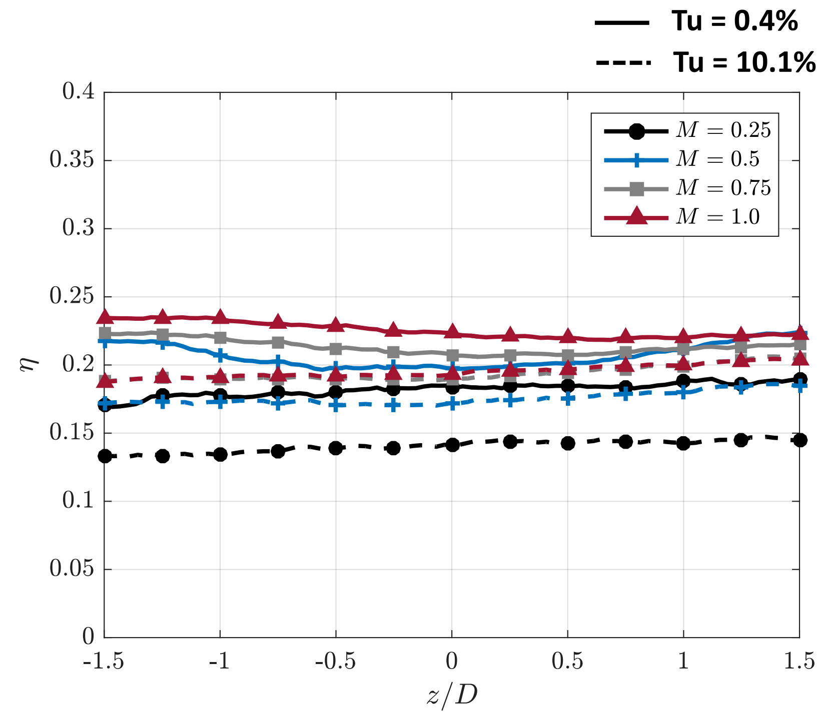

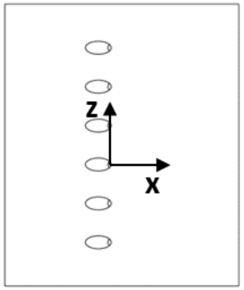

Reverse Film Cooling: Thermal Field

- Thermal field obtained in lateral crossplanes at various streamwise locations
- Measurements acquired by traversing a rake of 1mm diameter K-type thermocouples (spaced 15mm apart) in a 2D grid
- Near-exit measurements at the windward edge show a portion of the jet penetrating upstream of the hole exit
- Regions of high non-dimensional temperature correspond to lobes of high effectiveness

$$\theta = \frac{T_\infty - T}{T_\infty - T_c}$$

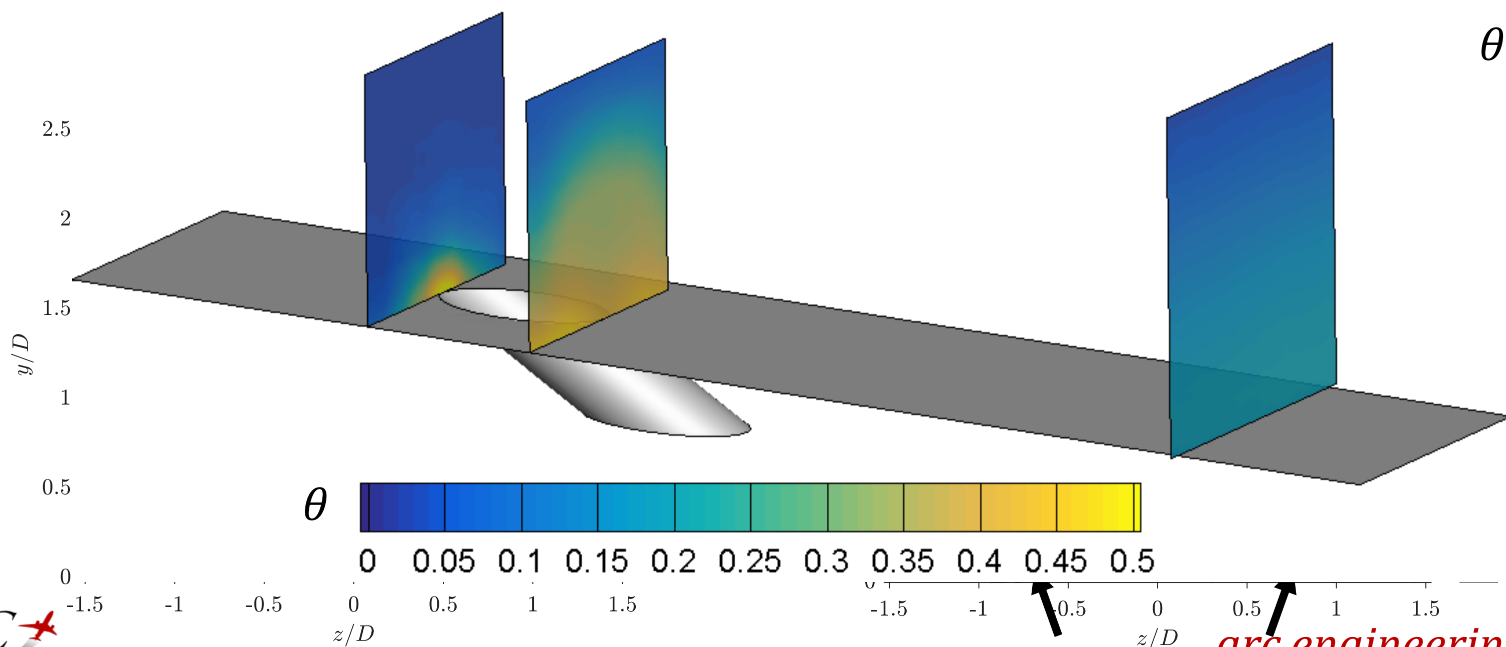

Reverse Film Cooling: Thermal Field

- Thermal fields at x/D = 8 are laterally uniform for all blowing ratios
- Vertical extent and magnitude of θ increases with blowing ratio

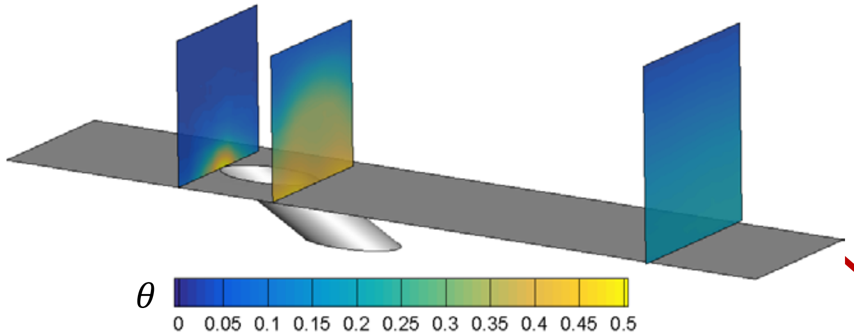

$$\theta = \frac{T_\infty - T}{T_\infty - T_c}$$

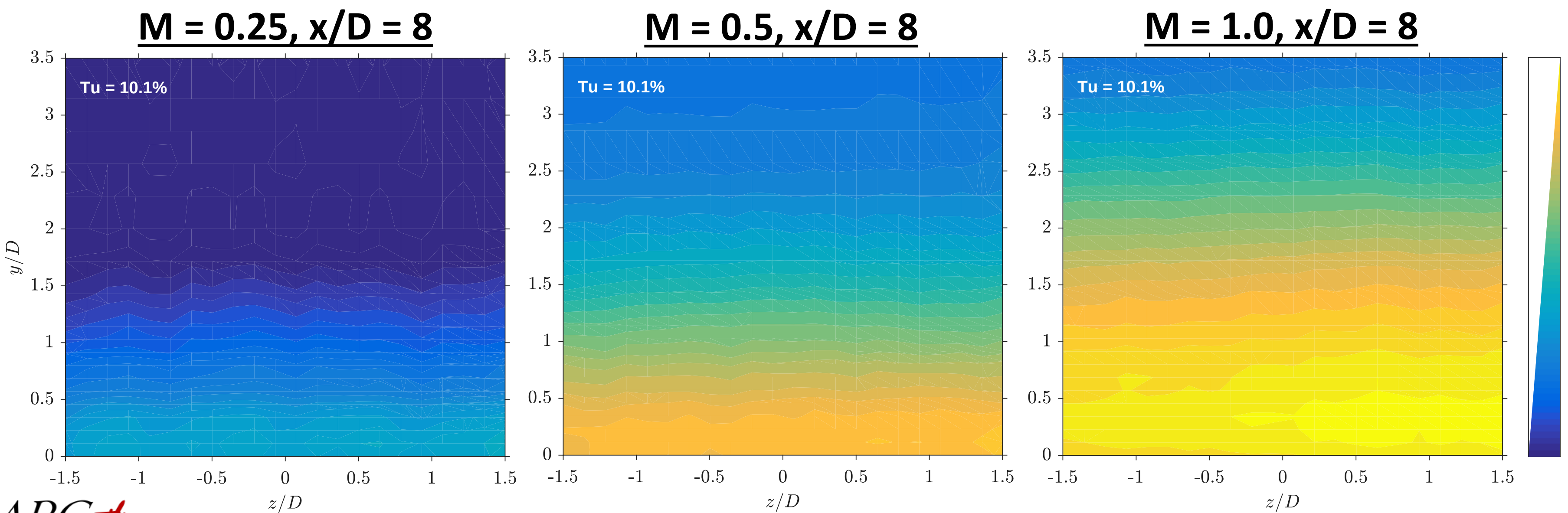

Reverse Film Cooling: Computational Details

- Computational domain consists of one hole pitch with periodic boundaries, and models a portion of the plenum.
- Domain discretized using structured hexahedral cells.
- Simulations performed using commercial package Star-CCM+ :
  - Unsteady – RANS
  - Implicit 2nd order unsteady solver
  - Star-CCM+'s "segregated solver" for flow and energy (SIMPLE)
  - 2nd order upwind scheme for convective terms
  - Turbulence modeled using *k*-ω-SST model

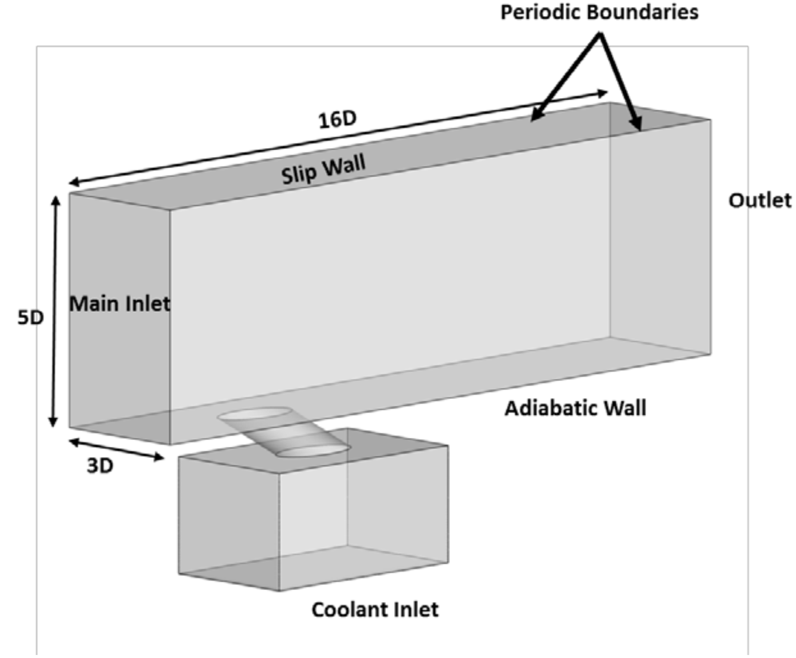

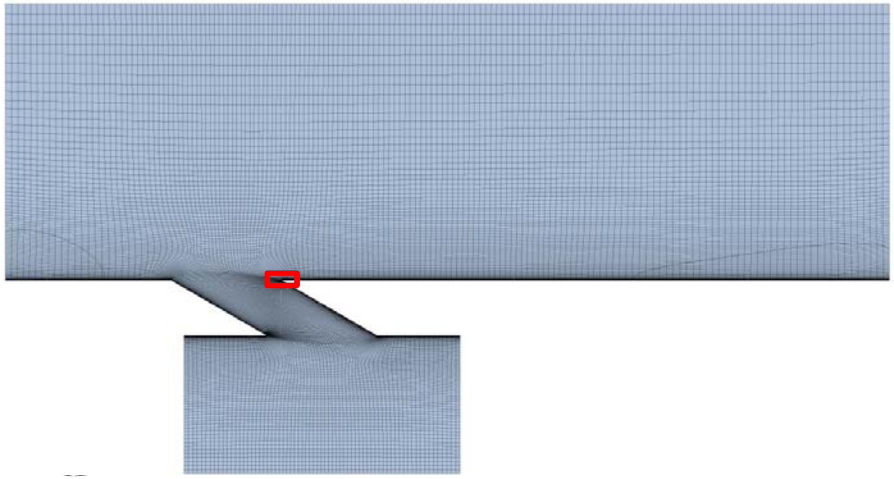

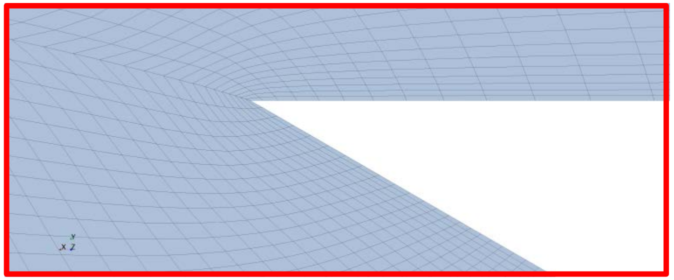

Reverse Film Cooling CFD: Grid Independence

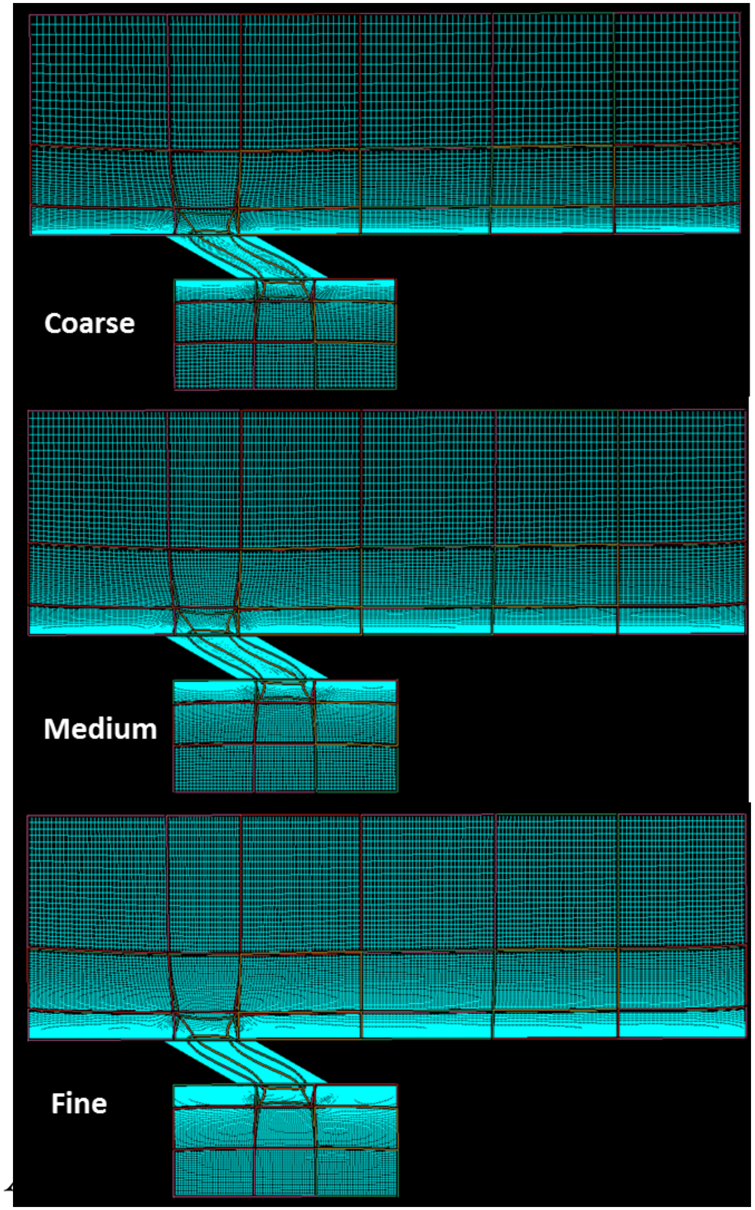

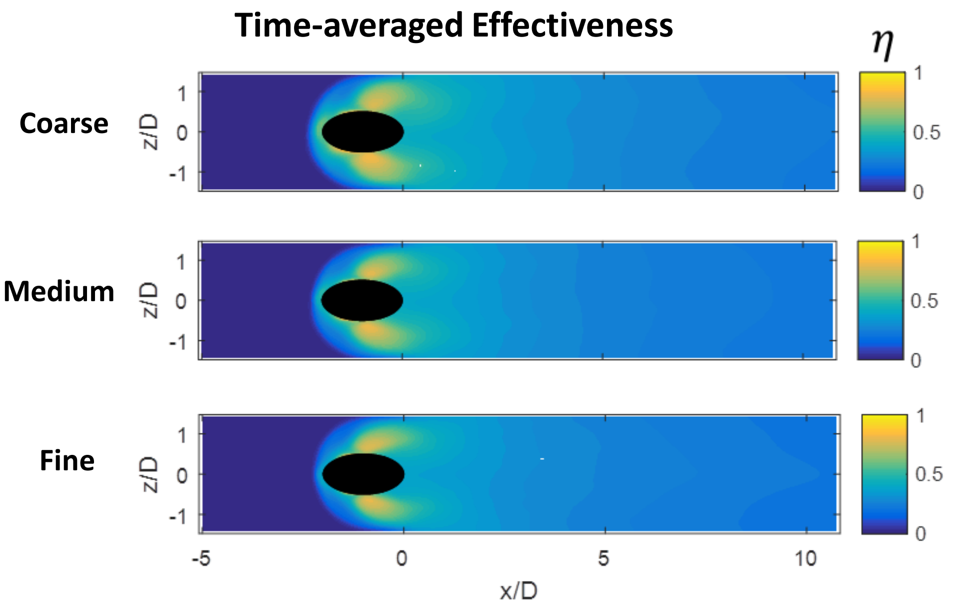

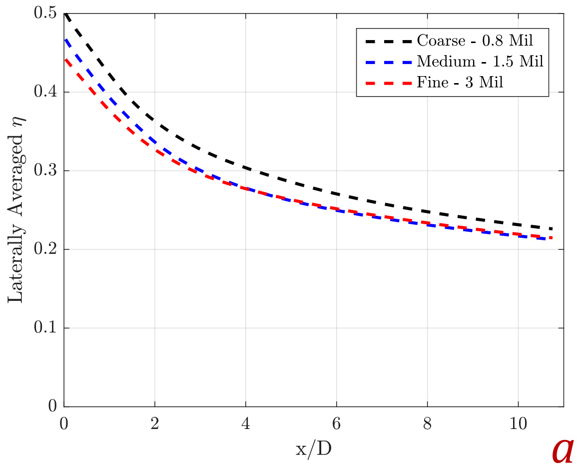

Grid Independence Study

Mesh	Cells	Wall y^+
Coarse	760,560	<1
Medium	1,528,080	<1
Fine	3,078,150	<1

Reverse Film Cooling CFD: Flowfield Comparison

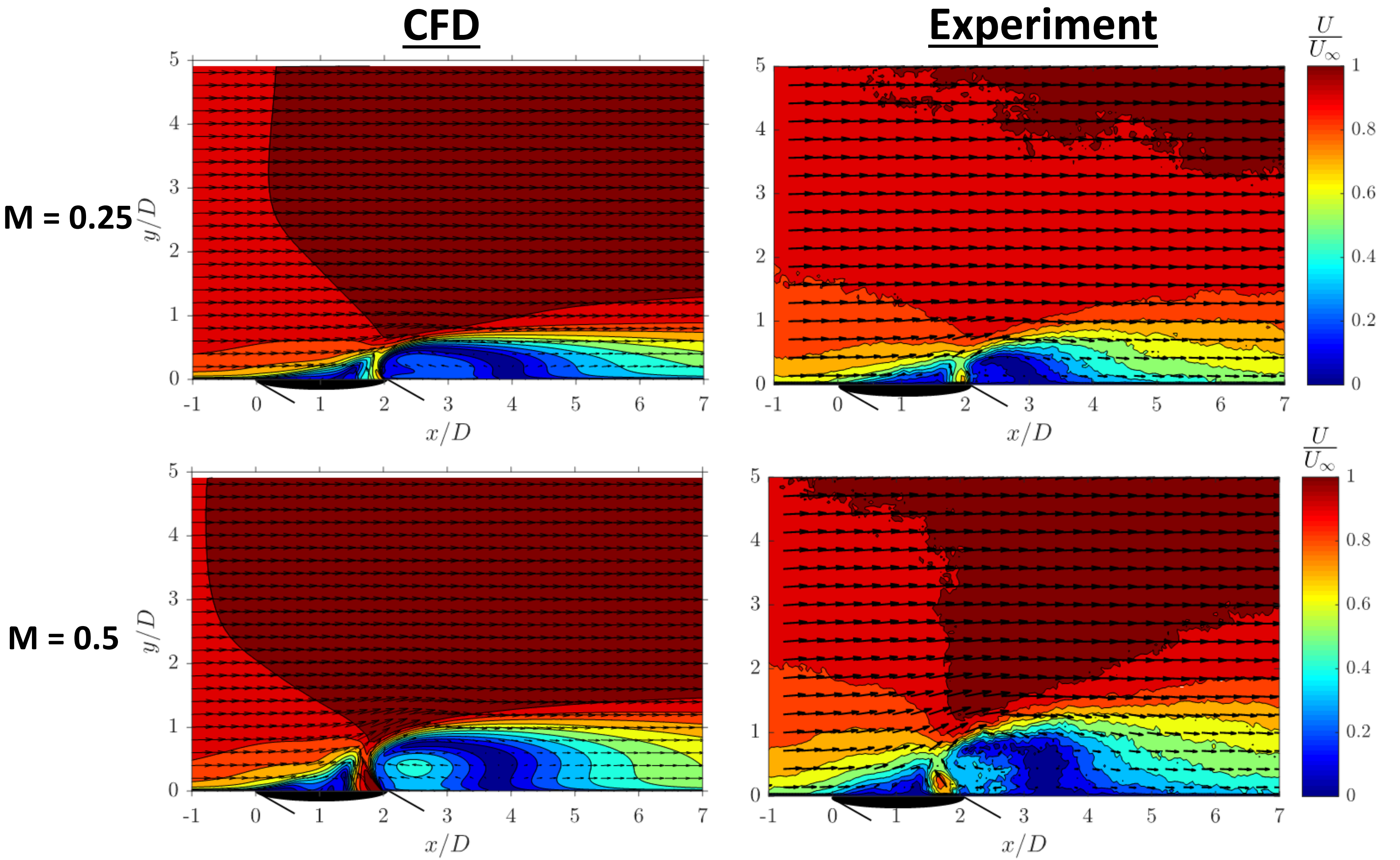

Reverse Film Cooling CFD: Unsteady Flow Field

Velocity Magnitude Contours in Bisecting Plane | **θ Contours in Bisecting Plane** | **Iso-surface of θ = 0.4**

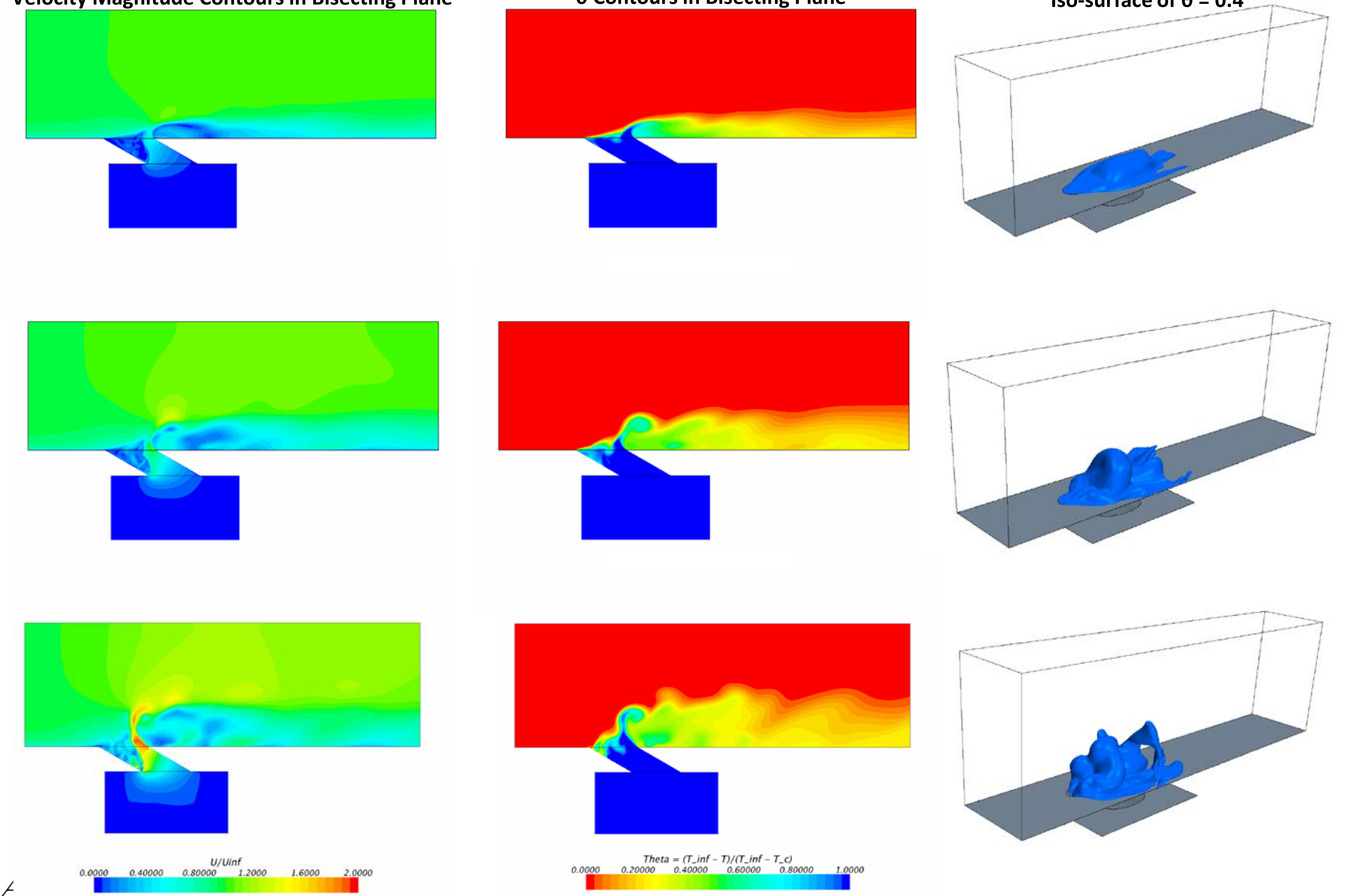

Looking Ahead

Manufacturing Oscillators with DMLS

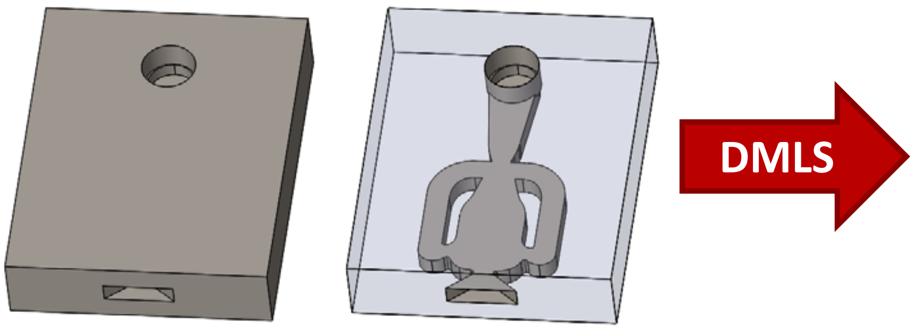

Inconel 718

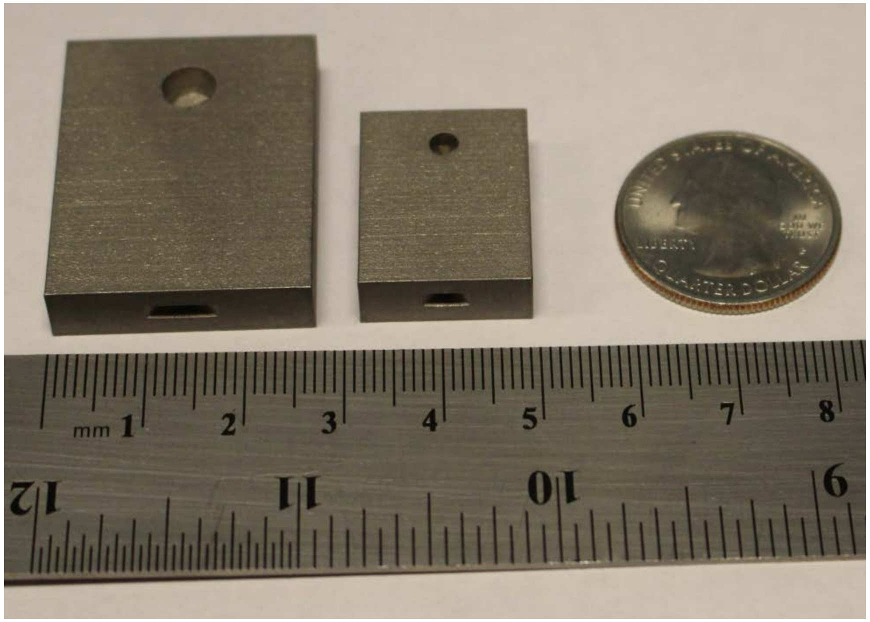

Freq. vs. Massflow of DMLS Oscillator

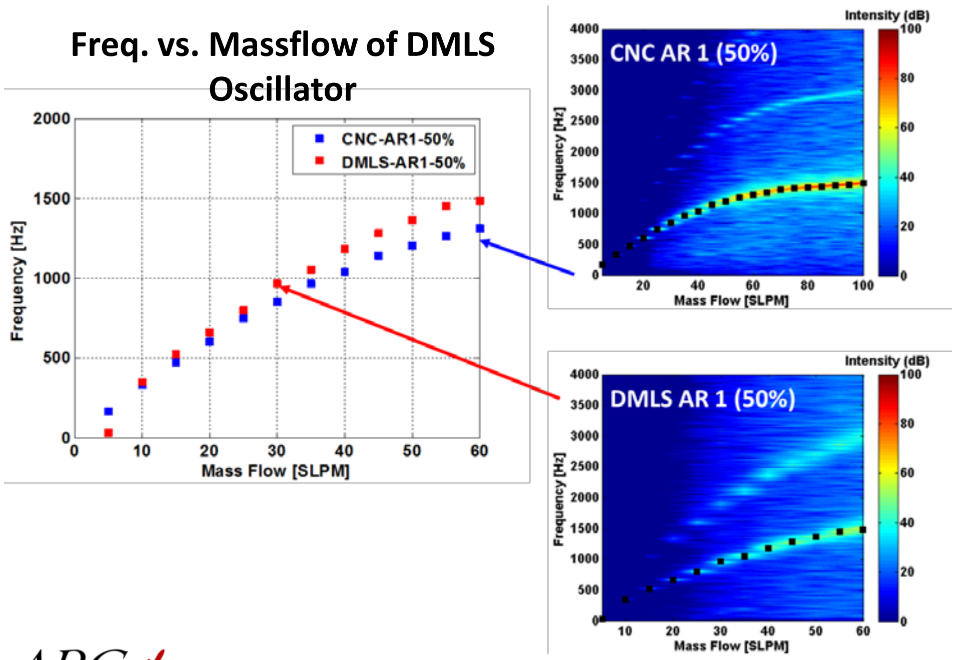

Schlieren of DMLS Oscillator

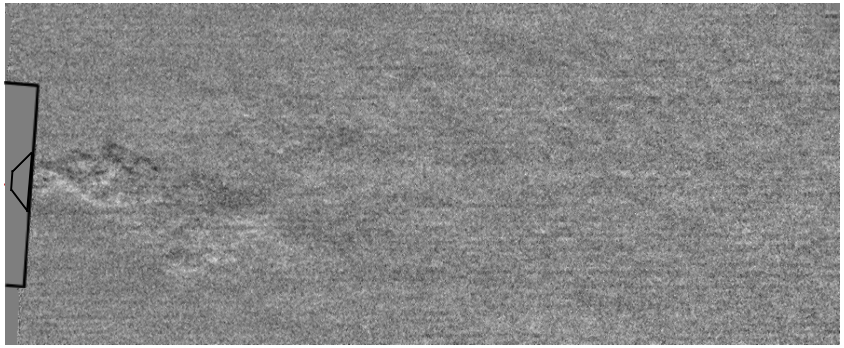

Fluidic Oscillators in Leading Edge Model

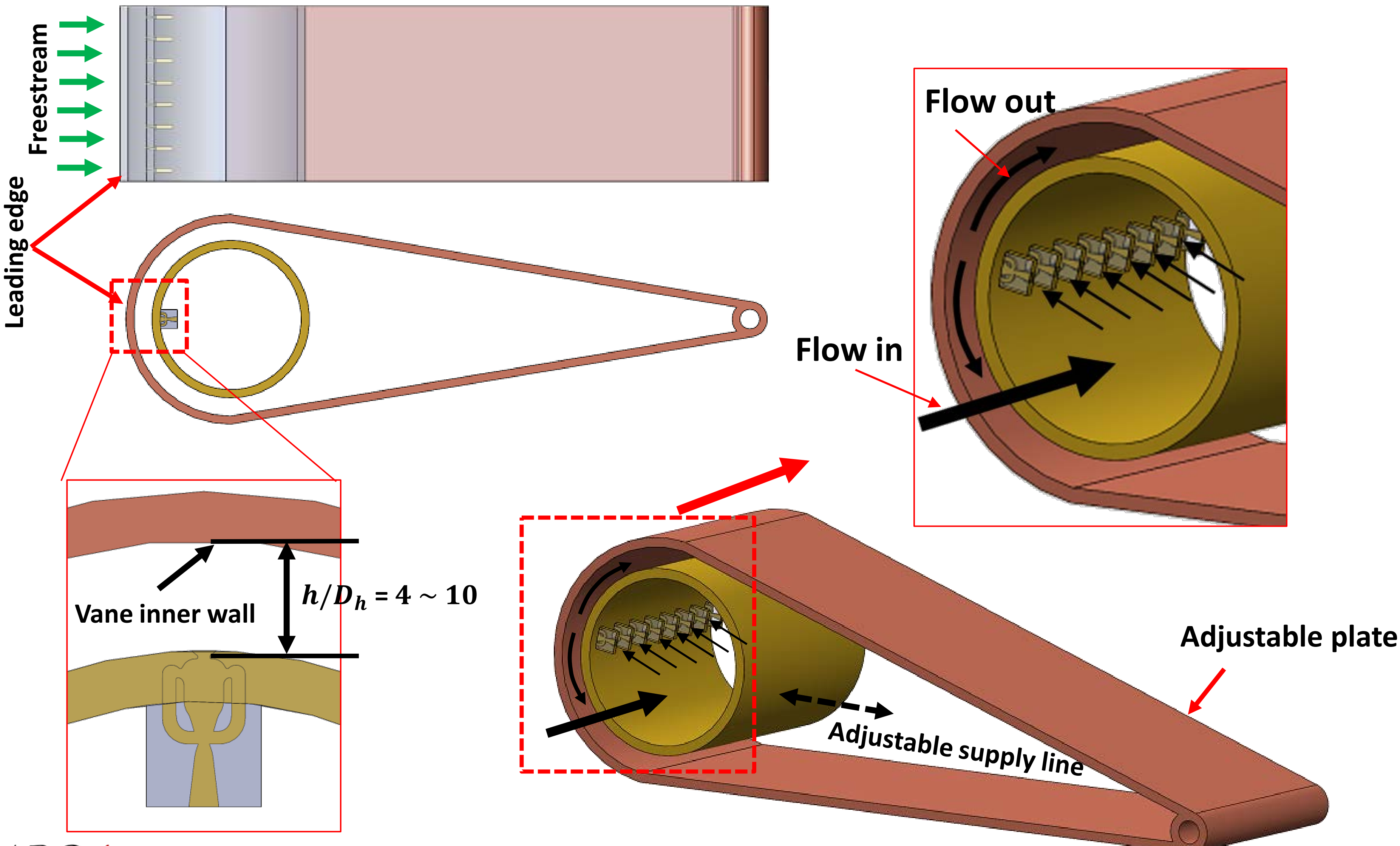

Fluidic Oscillator Nozzle Guide Vane Simulations

- A more uniform heat transfer performance would be advantageous in gas turbine applications.
- Currently, the fluidic oscillator impinging jet is being explored in a vane leading edge cooling application.

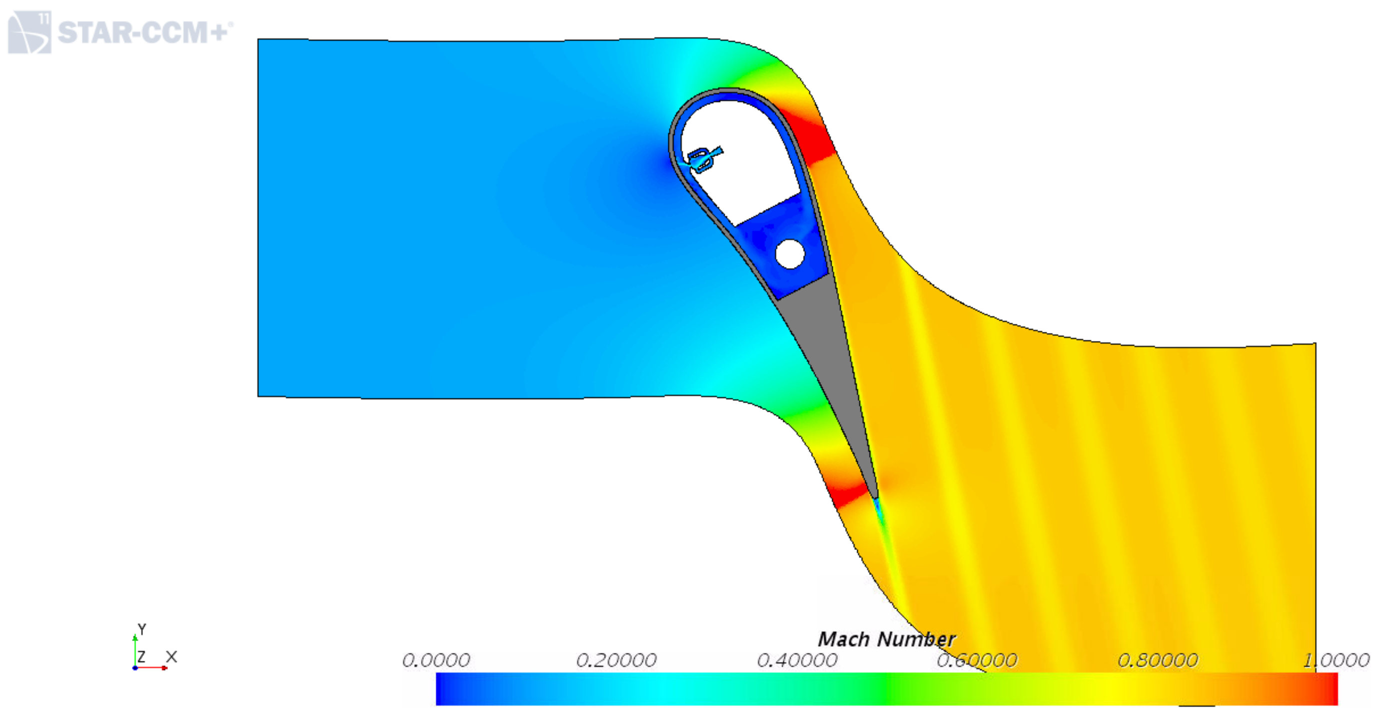

Fluidic Oscillator Film Cooling Vane Model

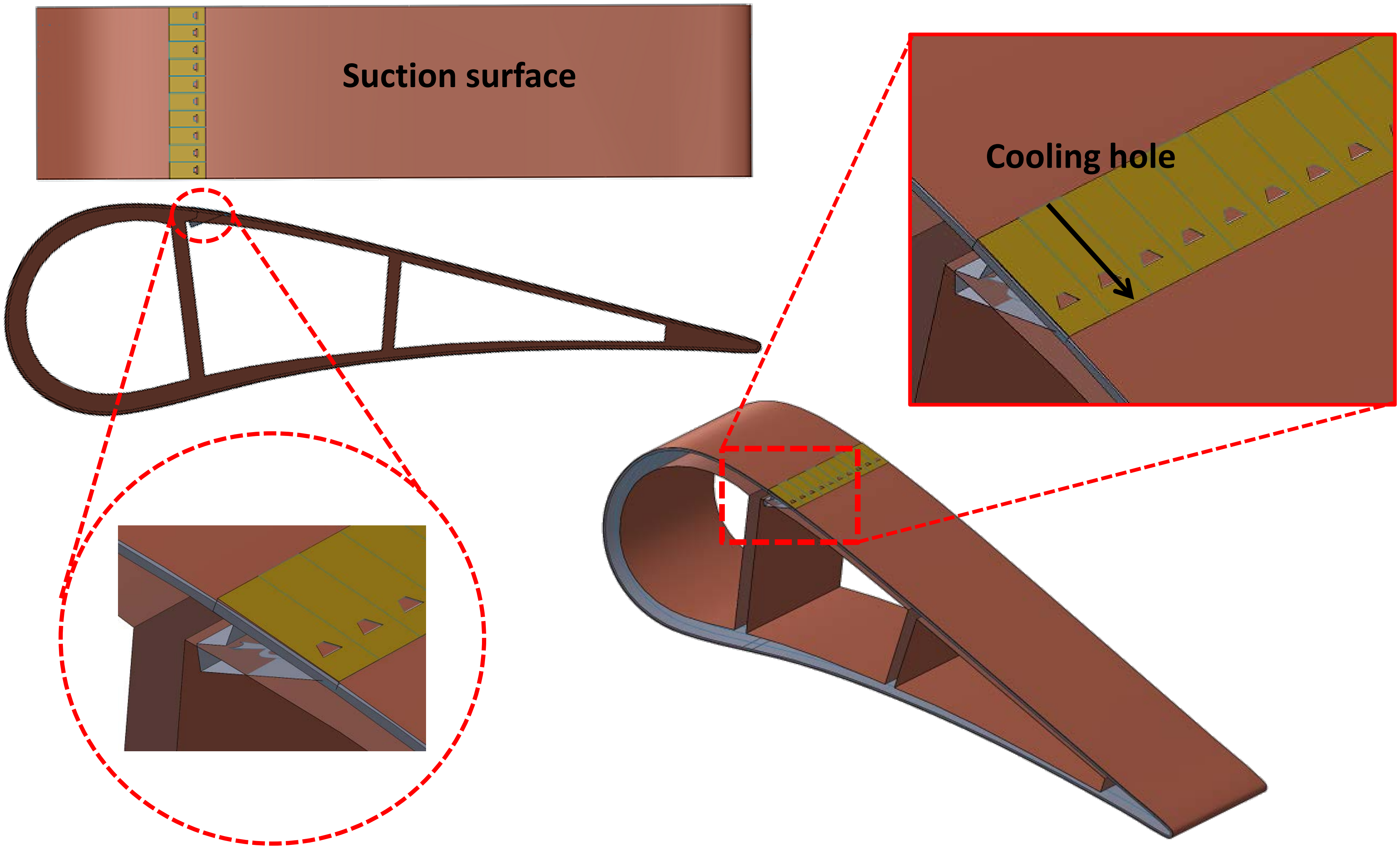

Reverse Film Cooling Vane Model and Simulations

Notional NGV Experimental Model

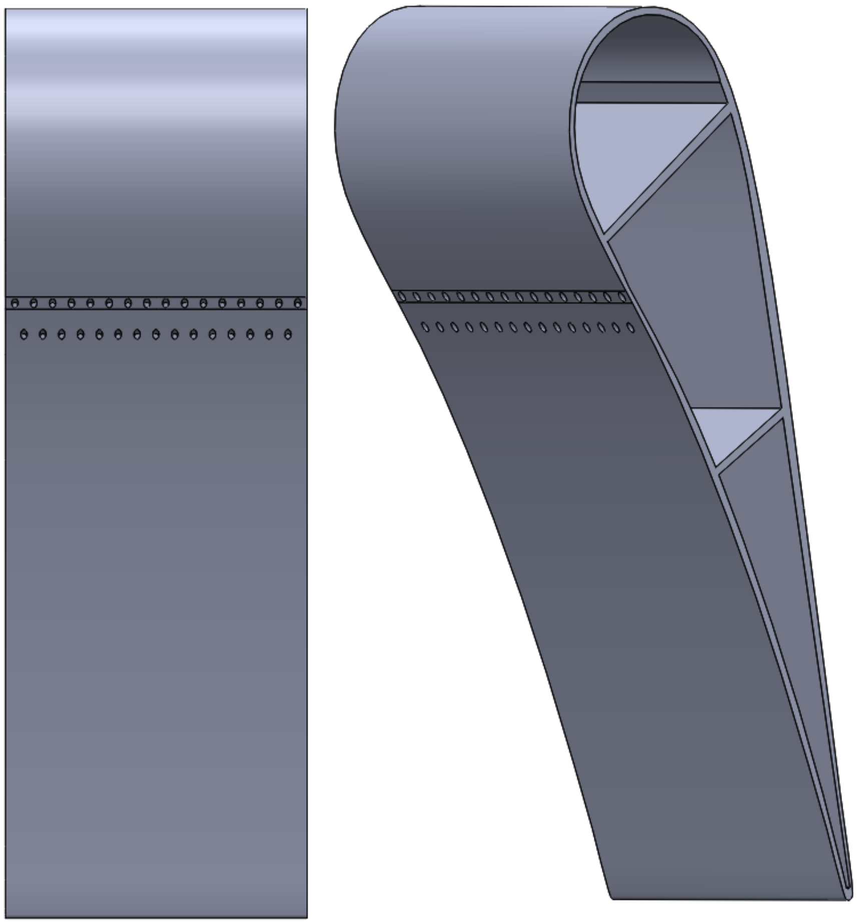

Simulation of NGV with reverse film cooling

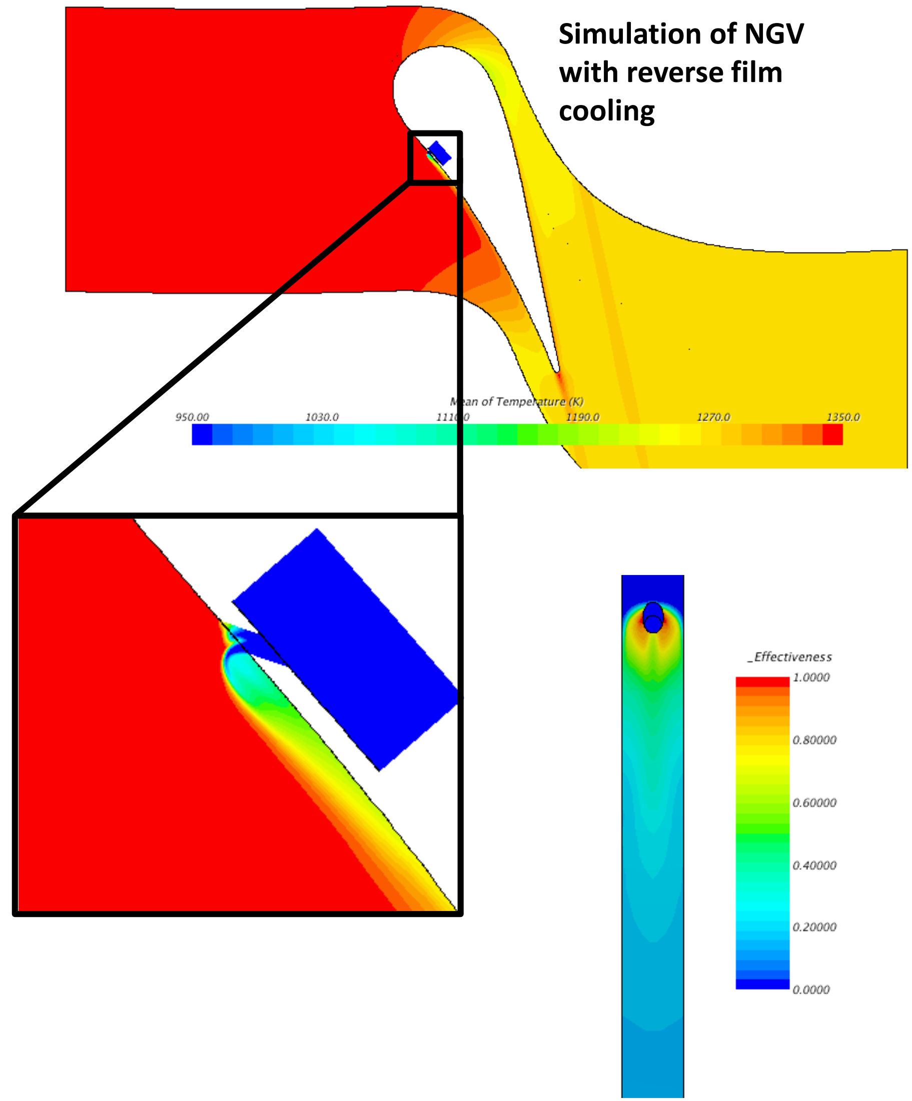

Trailing Edge Cooling with Microchannels

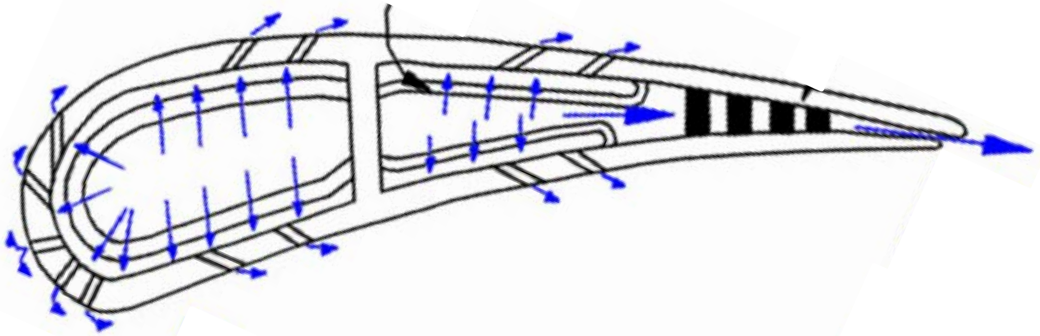

Adapted from: Han, J.-C., 2013, "Fundamental Gas Turbine Heat Transfer," *J. Therm. Sci. Eng. App.*, Vol. 5, 021007

Microchannel Surface Cooling

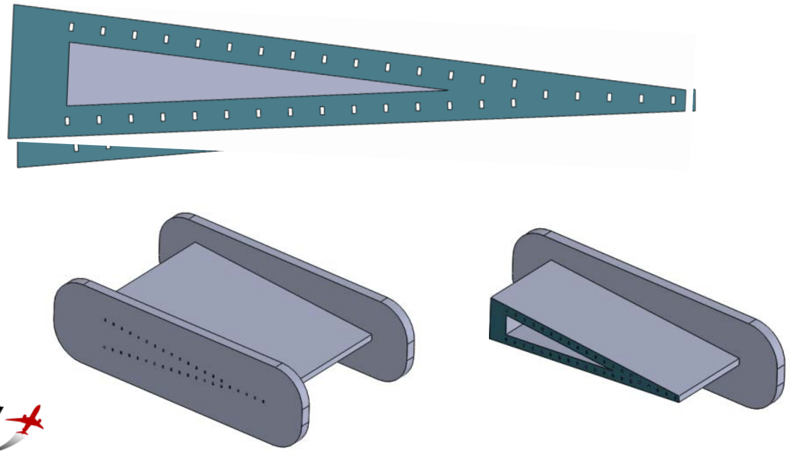

vs.

Conventional Cooling Methods

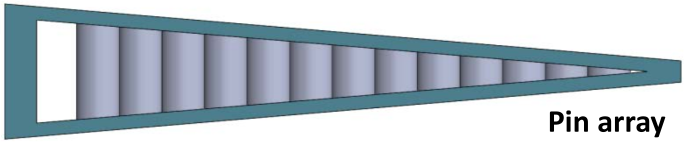

Pin array

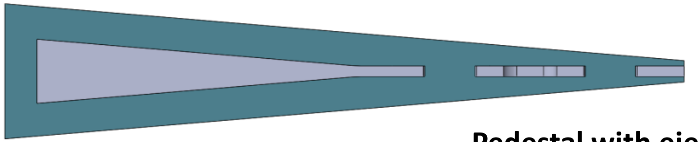

Pedestal with ejection

Gantt Chart

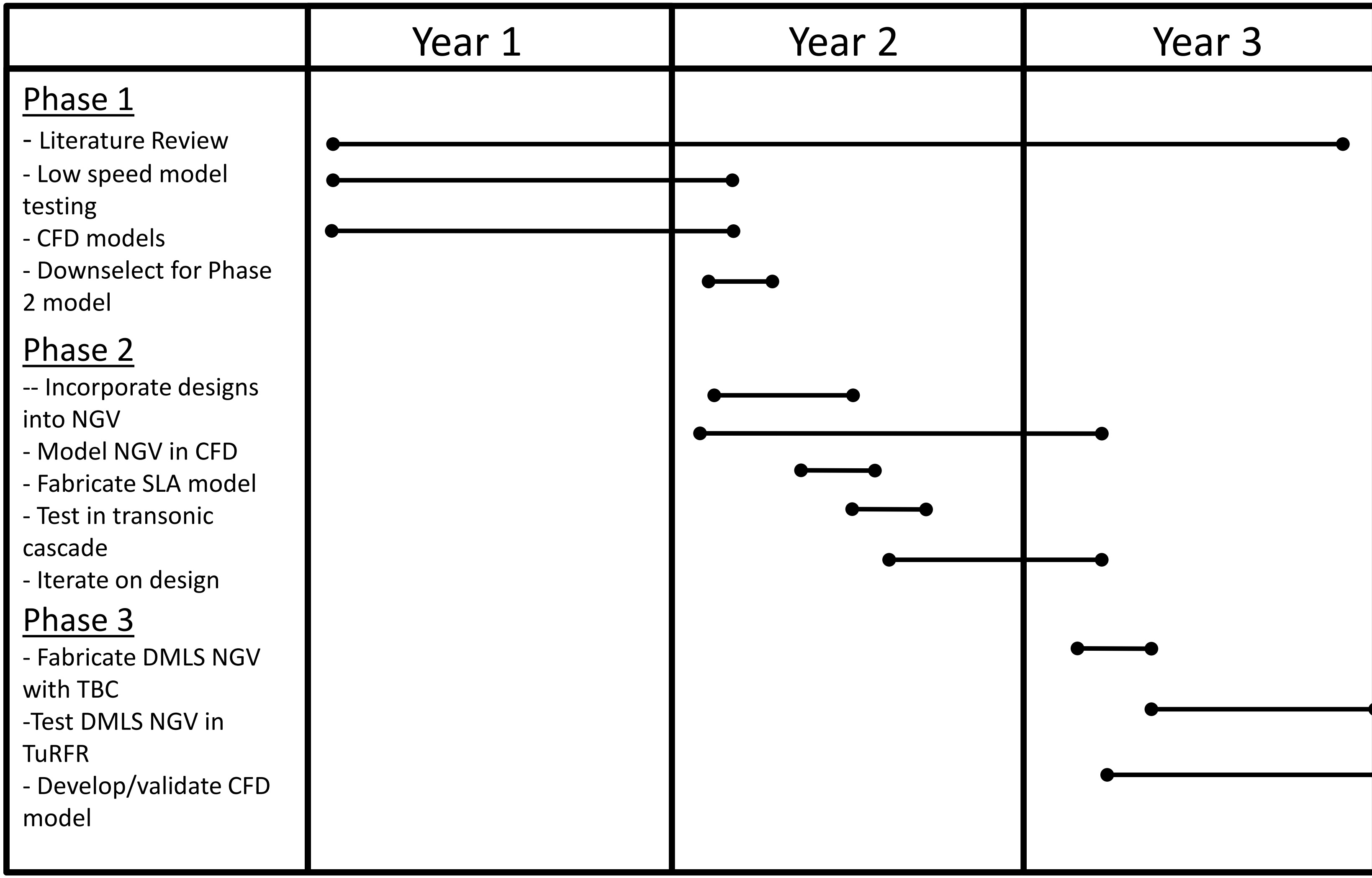
Year 1
Year 2
Year 3
Phase 1
- Literature Review
- Low speed model testing
- CFD models
- Downselect for Phase 2 model
Phase 2
-- Incorporate designs into NGV
- Model NGV in CFD
- Fabricate SLA model
- Test in transonic cascade
- Iterate on design
Phase 3
- Fabricate DMLS NGV with TBC
-Test DMLS NGV in TuRFR
- Develop/validate CFD model

Questions?

Reverse Film Cooling CFD: Flowfield

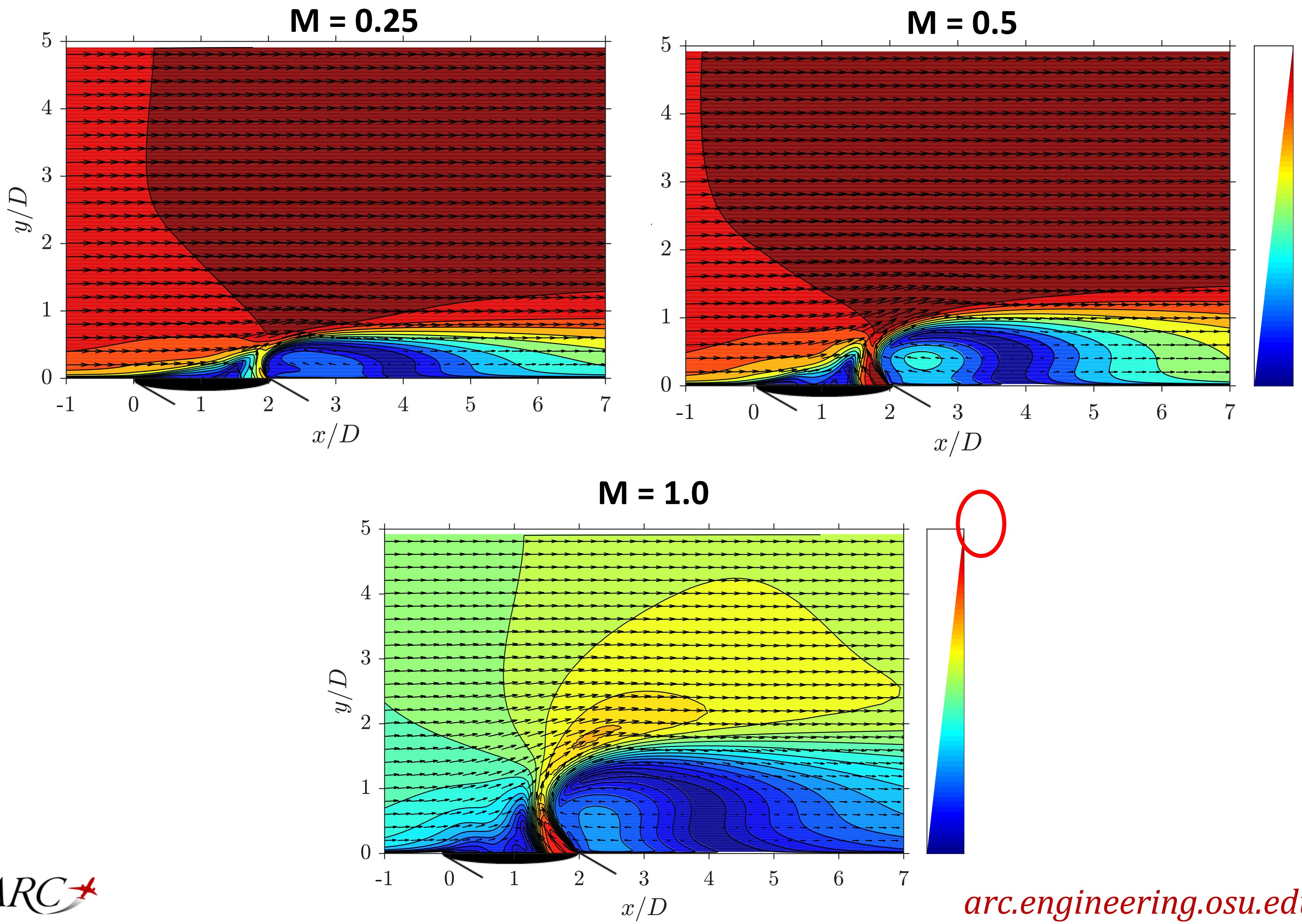

Reverse Film Cooling CFD: Film Cooling Effectiveness

- Simulations over predict effectiveness for all blowing ratios
  - Simulation (adiabatic wall) does not account for conduction and heating of coolant in the hole
- Similar "lobes" of high effectiveness observed in simulations, exaggerated over the experimental results
- Lateral uniformity predicted downstream of the hole

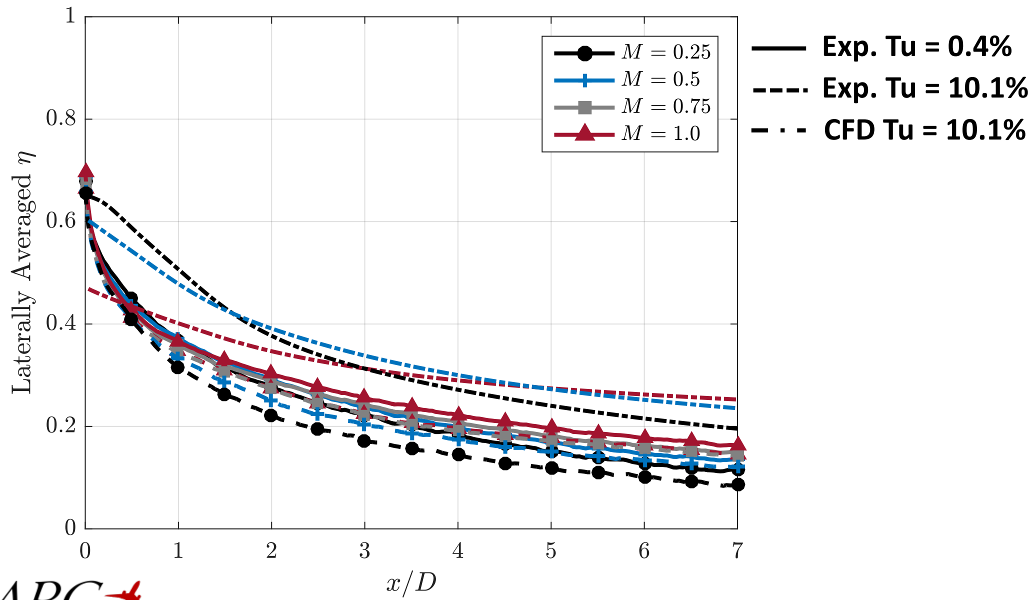

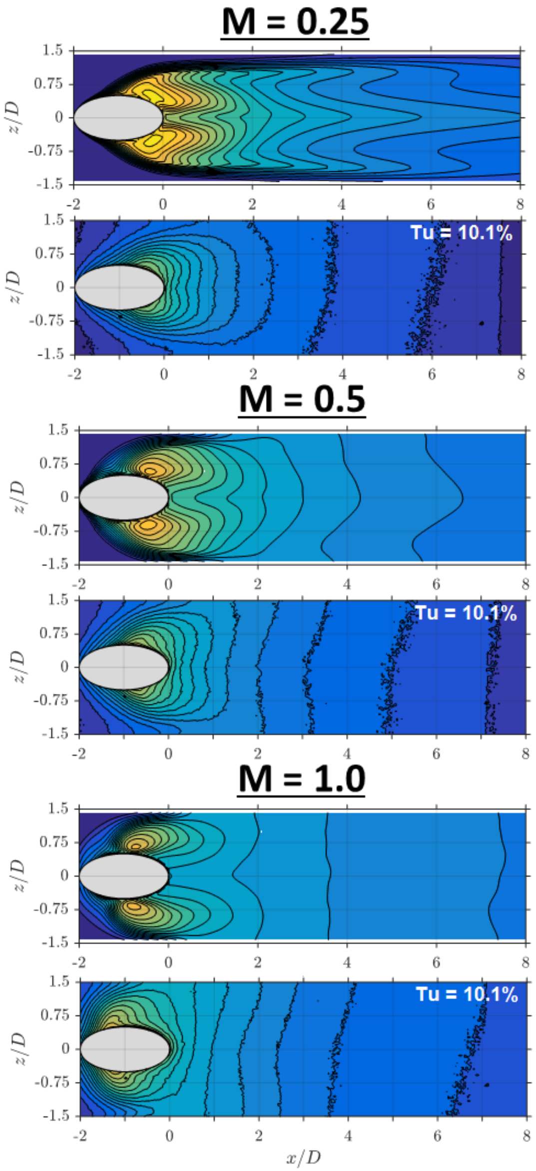

Reverse Film Cooling CFD: Conjugate Model

- Created a conjugate model to investigate the conduction due to upstream injection
- Solid is meshed using an unstructured polyhedral mesh, with a non-conformal interface between the fluid and solid
- **Struggling to get converged, symmetric solutions for M = 0.5 and 1.0. Suspect it may be the thermal time scale difference between fluid and solid?**

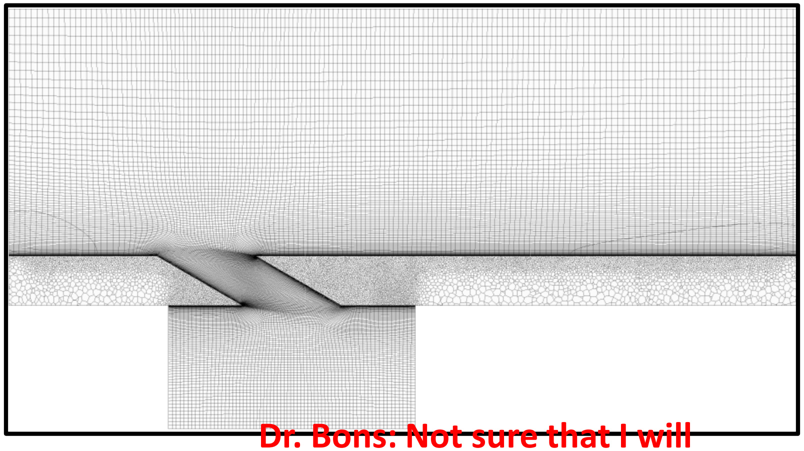

Dr. Bons: Not sure that I will have something definitive on this for the talk. Could just say that we are working on a conjugate model.

M = 0.25 **M = 0.5**

Adiabatic Wall

Conjugate